REMOVAL OF PARAQUAT AND OTHER POLLUTANTS BY ADSORPTION AND PHOTOCATALYSIS

Wina Rongchapo

A Thesis Submitted in Partial Fulfillment of the Requirements for the Degree of Doctor of Philosophy in Chemistry

Suranaree University of Technology

Academic Year 2015

การกำจัดพาราควอทและสารมลพิษอื่นด้วยการดูดซับและการเร่งปฏิกิริยาเชิงแสง

นางสาววีณา รองจะโปะ

วิทยานิพนธ์นี้เป็นส่วนหนึ่งของการศึกษาตามหลักสูตรปริญญาวิทยาศาสตรดุษฎีบัณฑิต

สาขาวิชาเคมี

มหาวิทยาลัยเทคโนโลยีสุรนารี

ปีการศึกษา 2558

REMOVAL OF PARAQUAT AND OTHER POLLUTANTS BY ADSORPTION AND PHOTOCATALYSIS

Suranaree University of Technology has approved this thesis submitted in partial fulfillments of the requirement for the Degree of Doctor of Philosophy.

Thesis Examining Committee

_____
(Asst. Prof. Dr. Sanchai Prayoonpokarach)
Chairperson

_____
(Assoc. Prof. Dr. Jatuporn Wittayakun)
Member (Thesis Advisor)

_____
(Prof. Dr. Wonyong Choi)
Member

_____
(Asst. Prof. Dr. Kunwadee Rangsriwatananon)
Member

_____
(Dr. Sirinuch Loiha)
Member

_____
(Prof. Dr. Sukit Limpijumnong)
Vice Rector for Academic Affairs and Innovation

_____
(Prof. Dr. Santi Maensiri)
Dean of Institute of Science

วีณา รองจะโปะ : การกำจัดพาราควอทและสารมลพิษอื่นด้วยการดูดซับและการเร่งปฏิกิริยาเชิงแสง (REMOVAL OF PARAQUAT AND OTHER POLLUTANTS BY ADSORPTION AND PHOTOCATALYSIS) อาจารย์ที่ปรึกษา : รองศาสตราจารย์ ดร. จตุพร วิทยาคุณ, 167 หน้า.

เป้าหมายหลักของงานวิทยานิพนธ์นี้คือการศึกษาการกำจัดสารกำจัดศัตรูพืชที่ใช้อย่างแพร่หลายในจังหวัดนครราชสีมา ได้แก่ พาราควอทและอิมิดาคลอพริด จากสารละลายโดยการดูดซับและการเร่งปฏิกิริยาเชิงแสง นอกจากนี้ ได้ขยายขอบเขตการศึกษาไปยังการกำจัดของสารมลพิษอื่น ๆ ที่มีประจุบวกคล้ายกับพาราควอท สารที่มีประจุลบและสารประกอบที่เป็นกลางโดยใช้ไททาเนียมไดออกไซด์ (TiO_2) ที่รองรับด้วยรีดิวซ์กราฟีนออกไซด์ (rGO)

ซิลิกาจากแกลบ (RHS) ซีโอไลต์ NaY ซีโอไลต์ NaX ซีโอไลต์ NaBEA MCM-41 และ Al-MCM-41 เป็นตัวดูดซับในการดูดซับของพาราควอทและอิมิดาคลอพริด การดูดซับของพาราควอทเกิดผ่านการแลกเปลี่ยนของไอออนบวก ค่าความจุในการดูดซับอยู่ในลำดับต่อไปนี้: NaY > NaBEA > MCM-41 > RHS เพื่อเพิ่มขีดความสามารถในการดูดซับ โดยใช้ตัวดูดซับที่มีปริมาณของ Al ในโครงสร้างที่สูงขึ้น ได้ศึกษาทั้งการดูดซับบนซีโอไลต์ NaX ซึ่งมีปริมาณของ Al ในโครงสร้างที่สูงกว่าในซีโอไลต์ NaY และ Al-MCM-41 ผลเป็นไปตามคาดหวังคือ การดูดซับบน Al-MCM-41 สูงกว่า MCM-41 อย่างไรก็ตาม ค่าความจุการดูดซับของ NaX ยังต่ำกว่าของ ซีโอไลต์ NaY จากการวิเคราะห์ลักษณะของ NaY และ NaX ทั้งก่อนและหลังดูดซับด้วยเทคนิคต่างๆ พบว่าโซเดียมไอออนในซีโอไลต์ NaX มีอันตรกิริยาที่แข็งแรงกับประจุลบที่อยู่ในโครงข่ายทำให้แลกเปลี่ยนไอออนได้น้อยลง

ในการสลายตัวด้วยการเร่งปฏิกิริยาเชิงแสงของพาราควอท ซีโอไลต์ NaY และ RHS เป็นตัวรองรับสำหรับตัวเร่งปฏิกิริยา TiO_2 และมีปริมาณ TiO_2 10 และ 30% โดยน้ำหนัก โดยเตรียมจากการใช้โซลของ TiO_2 ตัวเร่งปฏิกิริยาเชิงแสง TiO_2/NaY มีประสิทธิภาพต่ำ เนื่องจากดูดซับพาราควอทได้มาก ส่วนตัวเร่งปฏิกิริยาเชิงแสงที่มี RHS เป็นตัวรองรับสามารถสลายพาราควอทได้ดี ความสามารถในการสลายลดลงตามลำดับต่อไปนี้: 30 %TiO_2/RHS > TiO_2 > 10 %TiO_2/RHS

การศึกษาการกำจัดอิมิดาคลอพริดด้วยการดูดซับของ RHS NaY และ Al-MCM-41 และการสลายด้วยตัวเร่งปฏิกิริยาเชิงแสงของ 30 %TiO_2/NaY และ 30 %TiO_2/RHS การดูดซับไม่ได้เป็นวิธีการกำจัดที่เหมาะสม เนื่องจากอิมิดาคลอพริดจากตัวดูดซับ ถูกเคลื่อนย้ายกลับไปในสารละลายหลังจากเวลา 30 นาที สำหรับการสลายอิมิดาคลอพริดพบว่า อิมิดาคลอพริดถูกสลายได้ด้วยแสงและตัวเร่งปฏิกิริยาเชิงแสง โดยที่ TiO_2/NaY และ TiO_2/RHS มีประสิทธิภาพใกล้เคียงกัน

อีกส่วนหนึ่งของงานวิจัยนี้คือการปรับปรุงการเร่งปฏิกิริยาเชิงแสงของ TiO_2 ทางการค้า (P25) ด้วย rGO สำหรับการสลายสารมลพิษอินทรีย์ การศึกษาแบ่งออกเป็นสองส่วน ในส่วนแรกศึกษาผลการเร่งปฏิกิริยาเชิงแสงของ 1%rGO/P25 ในสารมลพิษอินทรีย์สามกลุ่ม ได้แก่ กลุ่มของประจุลบ ประจุบวก และสารมลพิษที่เป็นกลาง rGO/P25 ทั้งหมด มีผลการเร่งปฏิกิริยาสำหรับออกซิเดชันเชิงแสงไม่ดีเท่า P25 ในส่วนที่สองทำการศึกษาประสิทธิภาพของ rGO/P25 โดยปริมาณ rGO แตกต่างกัน (1-10% โดยน้ำหนัก) ในการสลาย CCl_4 และการผลิต H_2 ผ่านปฏิกิริยารีดักชันและการสลายเมทิลีนบลู ผ่านปฏิกิริยาออกซิเดชัน rGO/P25 ทั้งหมดเป็นตัวเร่งปฏิกิริยาที่ดีกว่า P25 สำหรับปฏิกิริยารีดักชัน อย่างไรก็ตาม P25 เป็นตัวเร่งปฏิกิริยาเชิงแสงที่เป็นออกซิเดชันที่ดีที่สุดสำหรับการสลายเมทิลีนบลู ที่ความเข้มข้นเมทิลีนบลูสูง เนื่องจากการแข่งขันการใช้อนุมูลอิสระไฮดรอกซิล ระหว่างการสลายเมทิลีนบลู และ rGO

สาขาวิชาเคมี ลายมือชื่อนักศึกษา_____

ปีการศึกษา 2558 ลายมือชื่ออาจารย์ที่ปรึกษา_____

WINA RONGCHAPO : REMOVAL OF PARAQUAT AND OTHER POLLUTANTS BY ADSORPTION AND PHOTOCATALYSIS
THESIS ADVISOR : ASSOC. PROF. JATUPORN WITTAYAKUN, Ph.D. 167 PP.

ZEOLITE NaY/ZEOLITE NaX/RHS/MCM-41/Al-MCM-41/TITANIUM DIOXIDE/ PARAQUAT/ADSORPTION/PHOTOCATALYSIS

The main goal of this thesis was to study removal of pesticides from aqueous solution including paraquat and imidachloprid which are widely used in Nakhon Ratchasima by adsorption and photocatalysis. The study was also extended to the removal of other pollutants with positive charge similar to paraquat, negative charge and neutral compounds using titanium dioxide (TiO_2) supported on reduce graphene oxide (rGO).

On the adsorption of paraquat and imidacloprid, the adsorbents were rice husk silica (RHS), zeolite NaY, NaX, NaBEA, MCM-41 and Al-MCM-41. The adsorption of paraquat occurred through cation exchange. The adsorption capacities were in the following order: NaY > NaBEA > MCM-41 > RHS. To increase the adsorption capacity, adsorbents with higher Al contents were studied including NaX which had a higher Al content than NaY and Al-MCM-41. As expected, the adsorption on Al-MCM-41 was higher than MCM-41 but the capacity on NaX was lower than NaY. The bare and paraquat containing zeolites (NaY and NaX) were characterized by several techniques. Sodium ion in NaX had a stronger interaction with the framework negative charge, making it less exchangeable with paraquat.

On the photocatalytic degradation of paraquat, TiO_2 was dispersed on zeolite NaY and RHS with 10 and 30 wt. % by grafting with TiO_2 sol. The NaY-supported catalysts showed low activity due to paraquat high adsorption. The degradation ability on RHS-supported ones decreased in the following order: 30 %TiO_2/RHS > un-supported TiO_2 > 10 %TiO_2/RHS.

The removal of imidacloprid was studied by adsorption on RHS, NaY and Al-MCM-41 and photocatalysis with 30%TiO_2/NaY and 30%TiO_2/RHS. The adsorption was not the appropriate removal method because imidacloprid from the adsorbent was transferred back to the solution after 30 min. Imidacloprid was degradable under light and photocatalysts where TiO_2/NaY and TiO_2/RHS showed similar activity.

The last part focused on improvement of commercial TiO_2 (P25) by rGO for photocatalytic degradation of organic pollutants. The study was divided into two parts. In the first part, rGO/P25 with 1 wt. % of rGO was tested for three groups of organic pollutants including anionic, cationic and neutral pollutants. The rGO/P25 did not show higher photooxidation than P25. In the second part, the activity of rGO/P25 was investigated with varying the rGO content (1-10 wt. %) for CCl_4 degradation and H_2 production via reduction and the methylene blue degradation via oxidation. All rGO/P25 catalysts exhibited higher performance than P25 for the reduction. However, P25 was the best oxidation photocatalyst at high methylene blue concentration probably due to competition to use OH• between degradation of methylene blue and rGO.

School of Chemistry Student's Signature_____

Academic Year 2015 Advisor's Signature_____

ACKNOWLEDGEMENT

I would like to express my sincere gratitude to my thesis advisor Assoc. Prof. Dr. Jatuporn Wittayakun for his support, patience and motivation during my Ph.D. Besides, I would like to thank Asst. Prof. Dr. Sanchai Prayoonpokarach for his support and guidance from the beginning of my graduated study.

My sincere thanks also go to supervisors, Prof. Dr. Wonyong Choi from Pohang University of Science and Technology (POSTECH), South Korea, Prof. Dr. Georgi Nikolov Vayssilov, Prof. Dr. Hristiyan Alexandrov Alexandrov from Sofia University "St. Kliment Ohridski", Bulgaria, and Assoc. Prof. Dr. Nurak Grisdanurak from Thammasat University (TU), Thailand. They gave me an opportunity to join their team as an exchange student and use research facilities. Their support made my thesis complete. I also thank Dr. Sirinuch Loiha from Khon Kaen University, Thailand, Dr. Pummarin Khamdahsag from TU and Dr. Gun-Hee Moon from POSTECH for their help and suggestion in several research procedures including adsorbent or catalyst preparation and reaction. I am also very thankful to the thesis examining committee for their helpful suggestions.

Thanks to all group members at Suranaree University of Technology (SUT) for their help, nice conversation and discussion. Also thank to all members outside SUT for help, nice atmosphere, parties and beautiful time.

Particularly, I would like to thank my family for their love, support, and continual encouragement during my education.

I would like to thank my colleagues at SUT who have shared my working experience and gave me tremendous useful suggestions and encouragements.

Finally, my Ph.D. study was supported by the Royal Golden Jubilee Ph.D. Program from Thailand Research Fund and Suranaree University of Technology (contract number PHD/0163/2552).

Wina Rongchapo

CONTENTS

Page

CONTENTS (Continued)

Page

CONTENTS (Continued)

Page

CONTENTS (Continued)

Page

CONTENTS (Continued)

Page

CONTENTS (Continued)

Page

CONTENTS (Continued)

Page

LIST OF FIGURES

LIST OF FIGURES (Continued)

LIST OF FIGURES (Continued)

LIST OF FIGURES (Continued)

LIST OF TABLES

CHAPTER I

INTRODUCTION

1.1 Introduction

Nakhon Ratchasima is a province In Thailand with the largest area of cassava cultivation. Pesticides commonly used in this agricultural activity include paraquat (1,1´-dimethyl-4,4´-dipyridinium dichloride) which is a herbicide and imidacloprid (1[(6-chloro-3-pyridinyl)methyl]-N-nitro-2- imidazolidinimine) which is an insecticide. Their structures are shown in Figure 1.1. Paraquat is a dication compound whereas imidacloprid is a neutral compound.

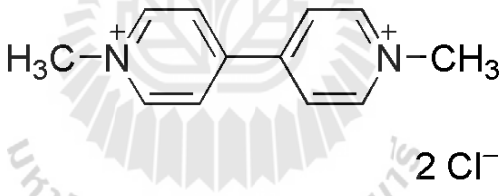

paraquat

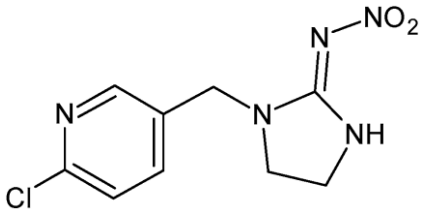

imidacloprid

Figure 1.1 Structures of paraquat and imidaloprid (Fossen, www, 2006; Pateiro-Moure, Estévez, and Gándara, 2010).

Paraquat, also known as methyl viologen, is hydrophilic in nature. Its solubility in water is as high as 620 g/L (Nur, Manan, Wei, Muhid, and Hamdan, 2005; Pateiro-Moure et al., 2010). It is widely used to control broadleaf weeds and grasses in both agricultural and non-agricultural areas. Its hydrolysis half-life is 161 days (USEPA, 1997). Paraquat is toxic to human and animals when exposed via ingestion, skin contact, or splash to eyes (Suntres, 2002). Ingestion of paraquat causes gastrointestinal irritation, abdominal pain, nausea, vomiting and diarrhea. Direct skin contact results in skin burns and dermatitis. If splashed to eyes, it causes irritation, burns, corneal damage and scarring of the eyes. Moreover, high accumulation of paraquat can cause injury to lungs as well as other organs. According to Information on Hazardous Chemicals and Occupational Diseases in Thailand, the concentration of paraquat which is immediately dangerous to life or health is 1 ppb (Thailand chemtrack, www, 2001). Therefore, paraquat removal is necessary.

Imidacloprid is in chloronicotinyl nitroguanidine class. It is used as an insecticide and a seed treatment. Imidacloprid may cause minimal redness to eyes and affected organs including the liver, kidney, heart and lung in animals. Its solubility in water is 0.51 g/L. Imidacloprid is stable to breakdown in low pH water but it is degraded by water at high pH solution; its half-life of 355 days. It can be degraded in water when exposed to light (USEPA, 1994).

Because paraquat and imidacloprid are used in a large amount each year, they can accumulate in the environment and contaminate water reservoirs. Two methods to remove both compounds are proposed including adsorption and photocatalysis in the presence of a catalyst.

1.2 Removal of pesticides in water

Adsorption was selected for pesticides removal because the method is efficient, simple, fast and not expensive. The first part of this thesis focused on adsorption of paraquat on materials with high surface area i.e., rice husk silica (RHS) and high porous materials synthesized from RHS including mesoporous silica (MCM-41) and zeolite (Y and BEA) in sodium form. Chapter III includes synthesis, characterization and paraquat adsorption. In addition, adsorption of blue dye in a commercial grade paraquat on all adsorbents was studied. Chapter IV involves paraquat adsorption by adsorbents with a higher Al content including zeolite NaX and Al-MCM-41. Zeolite NaX has the same faujasite (FAU) framework as NaY but higher Al content. For MCM-41 which has high surface area, Al was added to the structure in various content (10, 15, 20 and 25 wt. %). In Chapter V, NaY and NaX before and after paraquat adsorption were characterized by several techniques to explain the different capacities.

Another method to remove paraquat is photocatalytic degradation in aqueous solution by UV light in the presence of catalysts i.e., titanium dioxide powder (TiO_2) (Florêncio et al., 2004). The process decomposes a complex molecule to small molecules i.e., CO_2 and NH_3 which decreases its toxicity. However, this method is complicate because a specific range and intensity of light is required to activate electrons in valence band of the catalyst to conduction band. Chapter VI photocatalysts containing 10 and 30 wt. % TiO_2 on RHS and NaY were prepared, characterized and tested in photocatalytic degradation of paraquat.

For the removal of imidacloprid, both adsorption and photocatalytic degradation were investigated in Chapter VII. Chapter VIII involves catalytic

performance of hybrid material between reduced graphene oxide (rGO) and TiO_2, P25 (rGO/P25) for photocatalytic degradation of organic pollutants. The rGO/P25 was prepared by Gun-hee Moon, a collaborator in Korea (Moon, D. Kim, H. Kim, Bokare, and Choi, 2014). In Chapter VIII, organic pollutants were divided into three types including anionic (acid orange 7 and 2,4 dichlorophenoxyacetic acid), cationic (methylene blue and rhodamine B) and neutral pollutants (4-chlorophenol). The rGO/P25 with one wt. % of rGO was tested for all groups of pollutants. Moreover, the activity of rGO/P25 was investigated with varying the rGO content (1, 2, 4, 6, 8 and 10 wt. %) for the degradation of photooxidative reduction and oxidation in Chapter IX. Carbon tetrachloride (CCl_4) degradation and hydrogen (H_2) production were studied via reduction process and the degradation of methylene blue was studied via oxidation process.

1.3 Research objectives

1.3.1 To prepare and characterize RHS as an adsorbent and silica source for the synthesis of other adsorbents including zeolite NaY, NaX, NaBEA, MCM-41 and Al-MCM-41.

1.3.2 To prepare and characterize TiO_2/RHS and TiO_2/NaY by grafting the supports with TiO_2 sol.

1.3.3 To study adsorption and photocatalytic degradation of paraquat and imidacloprid in aqueous solution.

1.3.4 To investigate the photocatalytic degradation of other pollutants on rGO/P25.

1.4 Scope and limitations of study

1.4.1 Silica from rice husk was extracted by a method from the literature (Khemthong, Prayoonpokarach, and Wittayakun, 2007).

1.4.2 The adsorbents for paraquat in this work were NaY, NaBEA, MCM-41 and Al-MCM-41. All of them were synthesized with a method from the literature using rice husk silica source (Chen, Huang, Ding, and Li, 1997; Khemthong et al., 2007; Loiha, Prayoonpokarach, Songsiriritthigun, and Wittayakun, 2009; Preethi et al., 2008; Rintramee, Föttinger, Rupprechter, and Wittayakun, 2012; Robson, www, 2001; Wittayakun, Khemthong, and Prayoonpokarach, 2008).

1.4.3 TiO_2, TiO_2/RHS and TiO_2/NaY photocatalysts were prepared by grafting method and titanium tetrabutoxide ($C_{16}H_{36}O_4Ti$) was used as a titanium source described in the literature (Artkla et al., 2009).

1.4.4 rGO was prepared by Gun-Hee Moon (POSTECH).

1.5 References

Artkla, S., Wantala, K., Srinameb, B., Grisdanurak, N., Klysubun, W., and Wittayakun, J. (2009). Characteristics and photocatalytic degradation of methyl orange on Ti-RH-MCM-41 and TiO_2/RH-MCM-41. **Korean Journal of Chemical Engineering**. 26: 1556-1562.

Chen, X., Huang, L., Ding, G., and Li, Q. (1997). Characterization and catalytic performance of mesoporous molecular sieves Al-MCM-41 materials. **Catalysis Letters**. 44: 123-128.

Florêncio, M. H., Pires, E., Castro, A. L., Nunes, M. R., Borges, C., and Costa, F. M. (2004). Photodegradation of diquat and paraquat in aqueous solutions by titanium dioxide: evolution of degradation reactions and characterization of intermediates. **Chemosphere**. 55: 345-355.

Fossen, M. (2006). Environmental Fate of Imidacloprid. **Environmental Monitoring Department of Pesticide Regulation**. [On-line] Available: http://www.cdpr.ca.gov/docs/emon/pubs/enfate.htm.

Khemthong, P., Prayoonpokarach, S., and Wittayakun, J. (2007). Synthesis and characterization of zeolite LSX from rice husk. **Suranaree Journal of Science and Technology**. 14: 367-379.

Loiha, S., Prayoonpokarach, S., Songsiriritthigun, P., and Wittayakun, J. (2009). Synthesis of zeolite beta with pretreated rice husk silica and its transformation to ZSM-12. **Materials Chemistry and Physics**. 115: 637-640.

Moon, G., Kim, D., Kim, H., Bokare, A. D., and Choi., W. (2014). Platinum-like behavior of reduced graphene oxide as a cocatalyst on TiO_2 for the efficient photocatalytic oxidation of arsenite. **Environmental Science & Technology Letters**. 1: 185-190.

Nur, H., Manan, A. F. N. A., Wei, L., Muhid, M. N. M., and Hamdan, H. (2005). Simultaneous adsorption of a mixture of paraquat and dye by NaY zeolite covered with alkylsilane. **Journal of Hazardous Materials**. B117: 35-40.

Pateiro-Moure, M. P., Estévez, M. A., and Gándara, J. S. (2010) Competitive and non-competitive adsorption/desorption of paraquat, diquat and difenzoquat in vineyard-devoted soils. **Journal of Hazardous Materials**. 178: 194-201.

Preethi, M. E. L., Revathi, S., Sivakumar, T., Manikandan, D., Divakar, D., Rupa, A. V., and Palanichami, M. (2008). Phenol hydroxylation using Fe/Al-MCM-41 catalysts. **Catalysis Letters**. 120: 56-64.

Rintramee, K., Föttinger, K., Rupprechter, G., and Wittayakun, J. (2012). Ethanol adsorption and oxidation on bimetallic catalysts containing platinum and base metal oxide supported on MCM-41. **Applied Catalysis B: Environmental**. 115: 225-235.

Robson, H. (ed) (2001). **Verified Syntheses of Zeolitic Materials 2nd Revised Edition**. [On-line] Available: http://www.iza-online.org/synthesis.

Suntres, Z. E. (2002). Role of antioxidants in paraquat toxicity. **Toxicology**. 180: 65-77.

Thailand Chem Track. (2001). Information on Hazardous Chemicals and Occupational Diseases. **Paraquat dichloride** [On-line] Available: http://www.chemtrack.org/ HazMap-Agent-Info.asp?ID=1125.

United States Environmental Protection Agency. (1997). Paraquat dichloride, **R.E.D Facts Environmental Protection Agency, office of prevention pesticides, and toxic substances**. Washington DC.

United States Environmental Protection Agency. (1994). Imidacloprid Pesticide Fact Sheet, **U.S. Environmental Protection Agency**. Washington DC.

Wittayakun, J., Khemthong, P., and Prayoonpokarach, S. (2008). Synthesis and characterization of zeolite NaY from rice husk silica. **Korean Journal of Chemical Engineering**. 25: 861-864.

CHAPTER II

LITERATURE REVIEW

2.1 Adsorption of paraquat

Paraquat can be adsorbed on various kinds of materials, especially SiO_2–based compounds. It could be adsorbed strongly on clay minerals such as sepiolite (S), bentonite (B), and illite (I) (Seki and Yurdakoç, 2005). The adsorption occurred through ion-exchange with clay cations. Other adsorbents are activated bleaching earth (Tsai, Lai, and Hsien, 2004), diatomaceous earth (Tsai, Hsien, Chang, and Lo, 2005) and phillipsite faujasite tuff (Ibrahim and Jbara, 2009). Comparison of those adsorbents in terms of adsorbate to solution volume, range of paraquat concentration and maximum capacity are shown in Table 2.1.

Ibrahim and Jbara (2009) studied paraquat adsorption on natural phillipsite–faujasite tuff from Jordan. This material included 65% of zeolites (45% faujasite and 20% phillipsite), 30% palagonite and 5% of calcite. Paraquat was readily ion exchanged into the faujasite. When the faujasite tuff was activated by Na^+, K^+, Ca^{2+} and Mg^{2+}, the paraquat adsorption capacities were the highest on the tuff in Na^+ and K^+ form due to a rapid exchange (Table 2.1). A well-known type of faujasite is zeolite Y.

Table 2.1 Comparisons of maximum adsorption capacity on various adsorbents.

adsorbent	Adsorbent weight and paraquat solution volume	Range of paraquat concentration (ppm)	Maximum capacity [a] (mg/g-adsorbent)	Reference
- Sepiolite - Bentonite - Illite	0.1 g in 20 mL (5.0 g/L)	25-250	12.3 42.4 54.5	Seki and Yurdakoç, 2005
Hydrolyzed graft copolymer of PMAA-rice husk	0.2 g in 1 L (0.2 g/L)	36-180	292.5	Hsu et al., 2009
Rice husk graft polymer of PMANa	0.2 g in 1 L (0.2 g/L)	36-120	317.7	Hsu and Pan, 2007
- Tire-derived activated carbon - Commercial activated carbon	1 g in 200 mL (5.0 g/L)	10-40	33.7 75.8	Hamadi, Swaminatha, and Chen, 2004

[a] calculated from Langmuir model

Table 2.1 Comparisons of maximum adsorption capacity on various adsorbents (Continued).

adsorbent	Adsorbent weight and paraquat solution volume	Range of paraquat concentration (ppm)	Maximum capacity [a] (mg/g-adsorbent)	Reference
- Phillipsite-faujasite tuff	0.25 g in 50 mL (5.0 g/L)	150-500	4.67	Ibrahim and Haneen, 2009
- Na form			7.02	
- K form			6.96	
- Ca form			3.67	
- Mg form			3.49	
Clay mineral from spent bleaching earth	0.5 g in 2 L (0.25 g/L)	30	24.8[b]	Tsai and Lai, 2006
Treated diatomaceous earth	1 g in 2 L (0.5 g/L)	30	17.06 [b]	Tsai et al., 2005

[a] calculated from Langmuir model

[b] calculated from kinetic study

Nur et al. (2005) used a commercial NaY zeolite with surface area of 900 m^2/g as an adsorbent for paraquat adsorption. With 25 mL of paraquat with concentration of 300 ppm and 0.4 g of NaY, a complete removal was achieved in less than 10 min. When NaY particles were covered with alkylsilane, the zeolite hydrophillicity decreased. The paraquat adsorption slightly decreased (but still more than 95%) and blue dye (Cibacron Blue 35A) could be removed. However, the effect of initial concentration and pH of paraquat were not reported. These parameters are fundamental information which could be helpful for a further application such as paraquat removal from real sites with variation of paraquat concentration.

In this work, NaY zeolite was synthesized from rice husk silica (RHS) and used as an adsorbent and supporting material. Besides, zeolite bata (BEA) was interesting as an adsorbent because it has high surface area and large cavity size. Zeolite BEA is large pore zeolite with 12 membered-ring similar to zeolite Y. Loiha et al. (2009) reported that surface area of BEA synthesized with RHS was 670 m^2/g.

Another potential adsorbent for paraquat was a siliceous material. Brigante and Schulz (2011) studied the adsorption of paraquat on SiO_2 synthesized from tetraethyl orthosilicate (TEOS) and SiO_2 modified with TiO_2 (TiO_2-SiO_2) by an inverse microemulsion method. Adsorption of paraquat on bare SiO_2 was lower than TiO_2-SiO_2 at pH 9.5. This is because bare SiO_2 has a neutral framework which lacks of acidity (negative site) for adsorption of paraquat dication. In contrary to TiO_2-SiO_2, the acidity of TiO_2 was enhanced by dispersion on SiO_2 and the particle agglomeration was avoided. In this work the adsorption on mesoporous siliceous material synthesized from rice husk silica (MCM-41) was also studied. MCM-41 has a larger surface area than zeolite but only consists of silica. Thus, the lack of acid sites

which could be a limitation as an adsorbent. Addition of Al to MCM-41 could increase acid site. Chumee, Grisdanurak, Neramittagapong, and Wittayakun (2009) reported that MCM-41 grafted with Al had surface area more than 700 m^2/g. In this work Al-containing MCM-41 (Al-MCM-41) was synthesized and tested for paraquat adsorption.

2.2 Adsorption of imidacloprid

Imidacloprid is very hydrophilic and has a high tendency to migrate from soil to ground water. Thus, it is necessary to find an adsorbent to remove it from water. Sorption of imidacloprid and other pesticides was studied by Nemeth-Konda, Fuleky, Morovjan, and Csokan (2002) on Hungarian agricultural soil containing 1.16% organic matter, 21.8% silt, 15.4% clay and 62.8% sand with cation exchange capacity of 16.8 meg/100 g of soil. The studied concentrations were ranged between 0.04 and 5.00 ppm and the experiment was done by mixing 5 g of soil with 25 mL of the pesticides. The sorption isotherm was described by Freudlich model which is suitable for adsorbents with heterogeneous sites and multilayer adsorption, with non-uniform distribution of adsorption heat.

Flores-Céspedes, Fernández-Pérez, Villafranca-Sánchez, and González-Pradas (2006) studied effect of dissolved organic matter (DOM) on sorption of imidacloprid and other pesticides on Luvic Xerosol soil containing 0.27% organic carbon, 35.35% silt, 59.73% Clay and 4.92% sand with cation exchange capacity of 15.51 meg/100 g of soil. The concentrations were ranged between 2 and 25 ppm and the experiment was done by mixing 3 g of soil with 25 mL of the pesticides for 24 h. The sorption isotherm was described by Freudlich equation. Imidacloprid had the lowest soil

sorption capacity when compared other pesticides. From the results of co-sorption of imidacloprid with DOM, imidacloprid sorption on soil was reduced by competition of DOM. It showed the hydrophilic properties in agreement with the above literature. Thus, the improvement of imidacloprid removal base on the adsorption might be possible on hydrophilic adsorbent.

Zeolite presents hydrophilic properties because of the negative charge in the zeolite framework generated from Al. Thus, various zeolites were used in this work along with MCM-41 and Al-MCM-41.

2.3 Background of adsorbents

2.3.1 Siliceous materials

SiO_2-based materials with high surface area and acid sites are potential adsorbents. Examples are rice husk silica (RHS) and some porous compounds derived from RHS including Mobil Composition of Matter No. 41 (MCM-41) and MCM-41 modified by Al (Al-MCM-41). RHS was prepared by a procedure described in the literature (Wittayakun et al., 2008). The dried rice husk was refluxed in 3 M HCl solution at 85 °C for 6 h. Finally, the refluxed rice husk was pyrolyzed in a muffle furnace at 550 °C for 6 h to remove the carbon content. RHS has potential as a silica source (purity silica ~ 98 wt. %) for the production of silicon-based inorganic materials such as mesoporous silica including MCM-41 and zeolites (Khemthong et al., 2007).

MCM-41

MCM-41 is a uniform mesoporous material (2–50 nm, higher than zeolites) with high surface area (>700 m^2/g) (Yang, Gaib, and Lin, 2012). MCM-41 is rich in silanol groups (Si-OH). The silanol groups on RHS and MCM-41 can interact with other molecules via hydrogen bonding (Braga et al., 2011). However, surface area of RHS is much lower than MCM-41 (Artkla, Grisdanurak, Neramittagapong, and Wittayakun, 2008).

2.3.2 Zeolites

Zeolites are microporous aluminosilicate materials. Structures of zeolites are crystalline polymers based on arrangement of $[SiO_4]$ or $[AlO_4^-]$ tetrahedral linked to each other by sharing all the oxygen atoms to form a framework of cavities and channels. Framework oxygens connecting tetrahedral Si and Al atoms are attached with hydroxyl groups and cations. Amount of cationic sites is parallel to the amount of aluminum atoms (Guisnet and Gilson, 2002). Therefore, zeolites have cationic sites for ion-exchange.

Zeolite Y and X

Structure of zeolite Y and X is classified in a faujasite (FAU) type framework as shown in Figure 2.1. It contains units of double 6-ring (D6R), sodalite units (SOD), a very large cavity with four 12-oxygen ring windows known as a supercage with diameter of 1.3 nm and four apertures with dimension of 0.74 × 0.74 nm (Roland and Kleinschmit, 2003). Si/Al ratio of zeolite X and Y are around 1.1-1. and 1.6-3.0, respectively. It was previously reported that zeolite Y could adsorb paraquat (Nur et al., 2005; Stratakis and Stavroulakis, 2001; Zhang, Kim, and Dutta, 2006).

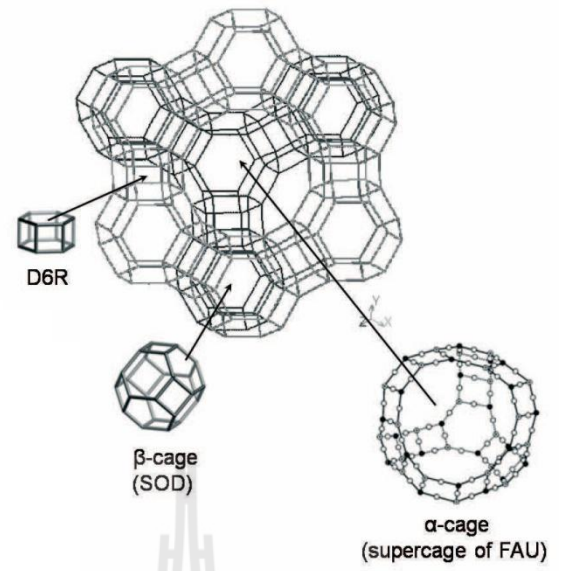

Figure 2.1 Structure of FAU framework (Ríos, Williams, and Castellanos, 2012).

Zeolite beta (BEA)

Zeolite beta is large pore zeolite with 12 membered-rings and its structure has large cavity size with 0.66 × 0.67 nm. The Si/Al ratio could be ranged from 8 to 20 (Roland and Kleinschmit, 2003). The structure of zeolite BEA is shown in Figure 2.2. Zeolite (BEA) is also interesting as an adsorbent because it has high surface area and its structure has large cavity size. Loiha et al. (2009) reported surface area of BEA synthesized with RHS to be 670 m^2/g. The paraquat adsorption on NaY and NaBEA was compared in this work because they have large pore channel but different Si/Al ratio and surface area (Roland and Kleinschmit, 2003).

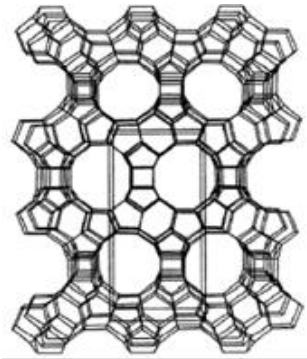

Figure 2.2 Structure of BEA framework (Baerlocher and McCusker, www, 2001).

2.4 Photocatalytic degradation of paraquat

Photocatalysis involves a chemical reaction in the presence of a catalyst that is influenced by radiation energy. The principle of the photocatalytic reaction is shown in Figure 2.3. The reaction is initiated by light absorption of the photocatalyst. The absorbed energy excites electrons in a valence band (VB) to a conduction band (CB) that results in the formation of excited electrons (e^-) and positive holes (h^+) pairs. Positive holes in VB act as an oxidizer and electrons in CB act as a reducer. In general, radicals can be produced from their reaction with water or oxygen. The radicals then react with a pollutant molecule and cause degradation. However, the redox process has to compete with the recombination of the e^- and h^+. Therefore, bringing a target compound closer to the surface of the photocatalyst through adsorption process would improve photocatalysis efficiency. Photocatalysis efficiency can be improved by collecting pollutant in the solution to the surface of photocatalyst. Activated carbon, silica and zeolite were used to adsorb pollutants which promoted the photocatalytic activity (Kaneko and Okura, 2002).

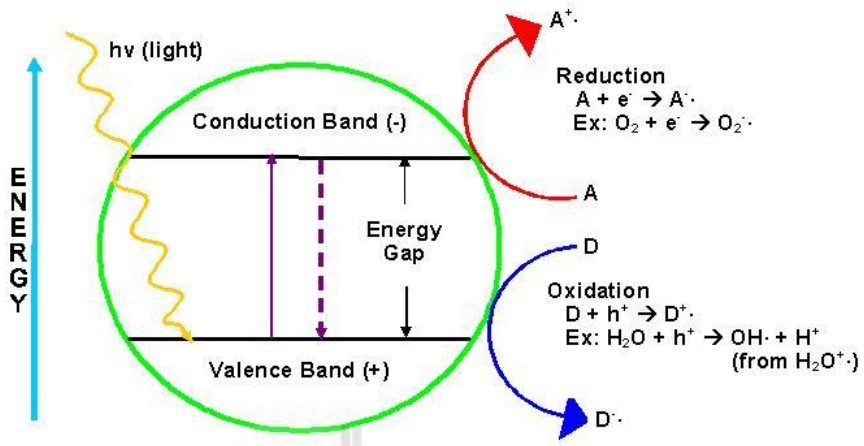

Figure 2.3 Mechanism of photocatalysis (NSTA, www, 2005).

Paraquat can be degraded by microbiological and photochemical processes to different intermediate products such as: monoquat monopyridone, picolinic acid and succinic acid (Moctezuma, Leyva, Monreal, Villegas, and Infante, 1999). However, the degradation by microbiological processes takes a long time. The faster degradation can be accomplished by photochemical processes in the presence of a catalyst.

Moctezuma et al. (1999) used a commercial titanium dioxide (TiO_2, P25) as a photocatalyst for paraquat degradation. The reaction was carried out in a Pyrex glass tube reactor which was illuminated with six UV light lamps. The paraquat solution with concentrations 20 and 40 ppm was mixed with 0.2 g of P25 and bubbled with pure oxygen. P25 enhanced the rate of degradation leading to a complete removal in about 2 h. P25 was effective in acidic, neutral and basic condition. Three unidentified intermediates were detected with high performance liquid chromatography analysis at the beginning of the reaction and the amount of the intermediates decreased towards the end of the reaction.

Florêncio et al. (2004) investigated intermediates and products from photodegradation of paraquat by various catalysts including synthesized TiO_2, $Ti_{1-x}Fe_xO_{2-\infty}$ (x = 0% and 4%) and P25. P25 provided the highest catalytic activity, whereas $Ti_{1-x}Fe_xO_{2-\infty}$ was not active. The synthesized TiO_2 showed a lower catalytic activity than P25 because it had a larger particle size and lower surface area. Reaction intermediates and products from the reaction with P25 and UV irradiation for the time less than 90 min were identified by mass spectrometry as shown in Figure 2.4. Nevertheless, paraquat was completely degraded within 12 h.

Vohra and Tanaka (2003) used silica-coated titanium dioxide (SiO_2-TiO_2) as a catalyst for photocatalytic degradation of various pollutants including paraquat with a 6 W black light UV source. Coating TiO_2 with SiO_2 resulted in the increase in surface area and change in surface charge characteristics that is the pH at point of zero charge was ~ 3.2 compared to that of TiO_2, which was ~ 6.4. When the reaction was conducted at pH 6, the surface of SiO_2-TiO_2 was negatively charged and could attract a positive charge of paraquat resulting in more adsorption of the compound compared to plain TiO_2. This also enhanced the degradation rate for paraquat. For 2×10^{-5} M paraquat (500 mL solution and 2 g catalyst), paraquat degradation was complete in less than 20 min.

Lee, M. Kim, and D. Kim (2002) prepared TiO_2 using a sol-gel method and hydrothermal method with titanium tetraisopropoxide and used as catalysts for degradation of paraquat. TiO_2 prepared from each method was immobilized onto a glass tube using a dip-coating method. The same procedure was also conducted with P25. A 6 W low-pressure mercury UV lamp was inserted into the dip-coated glass tube and the tube was immersed into a reactor containing paraquat solution where air

was sparged into the solution at flow rate of 1 L/min. For 100 mg/L paraquat, 99%, 75% and 65% removal in 12 h were obtained with hydrothermal synthesized TiO_2, P25 and sol-gel synthesized TiO_2, respectively. Immobilization of the catalysts onto the solid support provides a uniform distribution of UV light compared to a system using a catalyst suspended in a solution and makes ease of catalyst separation and recycling.

From the previous works, photocatalysis of paraquat with TiO_2 was investigated at low concentration and the degradation was slow, completed within 12 h. Therefore, TiO_2 photocatalyst has designed to degrade paraquat at high concentration in a short time. Artkla et al. (2009) reported that RH-MCM-41grafted TiO_2 using titanium tetrabutoxide had anatase phase which was active in photocatalytic degradation of methyl orange. In this work, TiO_2 was prepared from titanium tetrabutoxide to produce a pure anatase TiO_2. TiO_2 precursor was incorporated with adsorbents. The particle size of TiO_2 was decreased to promote photocatalysis of paraquat.

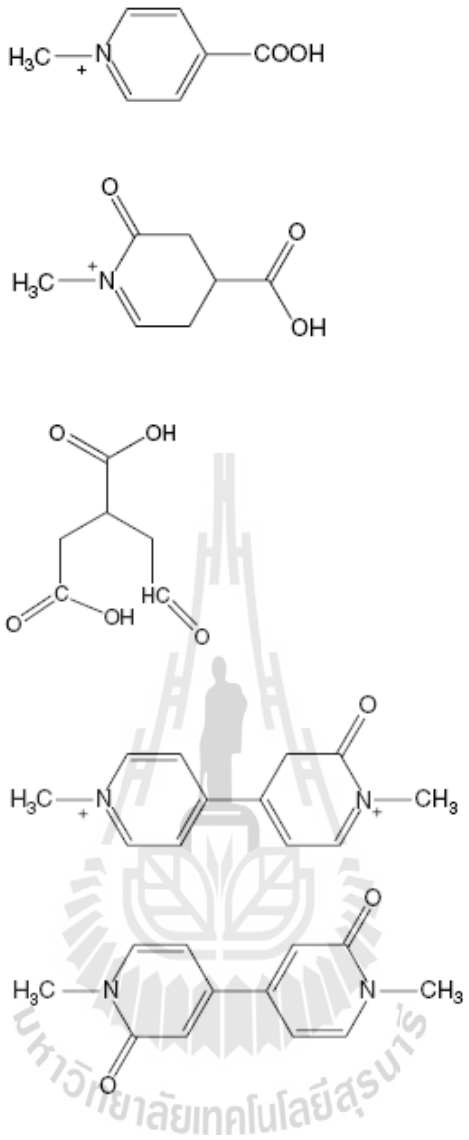

Figure 2.4 Intermediates or reaction products of paraquat photocatalytic degradation (Florêncio et al., 2004).

2.5 Photocatalytic degradation of imidacloprid

Imidacloprid can be degraded by light in water (USEPA, 1994) but the process is slow. Thus, it is interesting to investigate its degradation by photocatalysis to decrease the degradation time. The primary degradation products from photolysis are

imidacloprid urea, 6-chloronicotinic aldehyde, 6-chloro-N-methylnicotinacidamide, 6-chloro-3-pyridyl-methylethylene diamine (Fossen, www, 2006).

Malato et al. (2002) employed solar technology to degrade imidacloprid by TiO_2 slurry (200 mg/L of P25). Imidacloprid can be degraded spontaneously up to 55% by solar illumination in 48 h. When using TiO_2, imidacloprid was degraded completely in 120 min.

Kitsiou, Filippidis, Mantzavinos, and Poulios (2009) studied heterogonous photocatalytic degradation of imidacloprid in aqueous solution and determined by-products during the photocatalysis. At an initial concentration of 20 ppm with the catalyst loading of 0.5 g/L, the photocatalytic activity after 60 min radiation increased in order: anatase TiO_2 with UV-100 < P25 < ZnO, with degradation efficiency of 26, 64 and 76%, respectively. ZnO has a similar band energy to TiO_2 but TiO_2 had a faster recombination than ZnO. Therefore, they improved photocatalytic activity of P25. P25 modified with Fe^{3+} and H_2O_2 showed degradation efficiency 75% after 30 min of radiation. By-products formed during the photocatalytic degradation are shown in Figure 2.5.

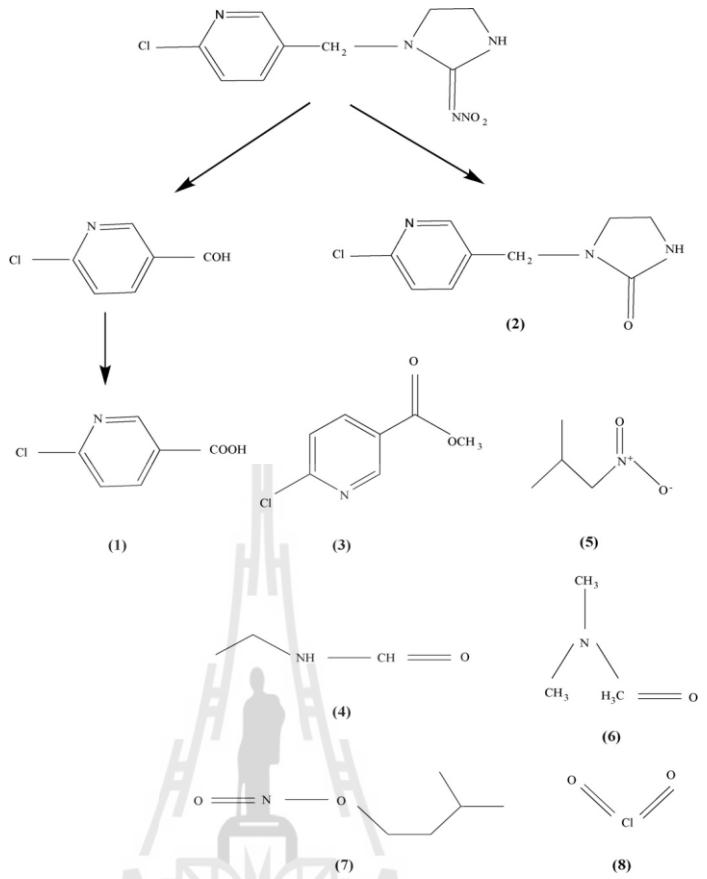

Figure 2.5 By-products formed during the photocatalytic degradation: 6-chloronicotic acid (1), 1-(6-chloro-3-pyridinyl) methyl-2-imidazolidinone (2), methyl-6-chloronicotinate (3), N-ethylformamide (4), 2-methyl-1-nitropropane (5), dimethyl formamide (6), amyl nitrite (7) and chlorine dioxide (8) (Kitsiou et al., 2009).

2.6 Background of photocatalysts

2.6.1 Titanium dioxide (TiO_2)

Photocatalyst is a semiconductor which has narrow band gap energy and can be activated by light such as ultraviolet and sunlight. The best known photocatalyst for environmental application at the present is titanium dioxide (TiO_2)

(Keneko and Okura, 2002). TiO_2 occurs in nature in rutile and anatase. Their band gap energies are about 3.2 and 3.0 eV, respectively (Sobczyński and Dobosz, 2001). Anatase transforms to rutile at temperatures above 700 ^oC. The anatase phase showed better photocatalytic efficiency than the other phases (Diebold, 2003). The rutile form was claimed to be catalytically inactive or a much less active form. Commercial P25 which has both anatase and rutile forms with the ratio of anatase to rutile equal to 3–4:1, is one of the best TiO_2 photocatalysts and used frequently as a benchmark in photocatalysis. Benefits of TiO_2 over other semicoductors are high activity, large stability to light illumination, low price and nontoxicity.

5

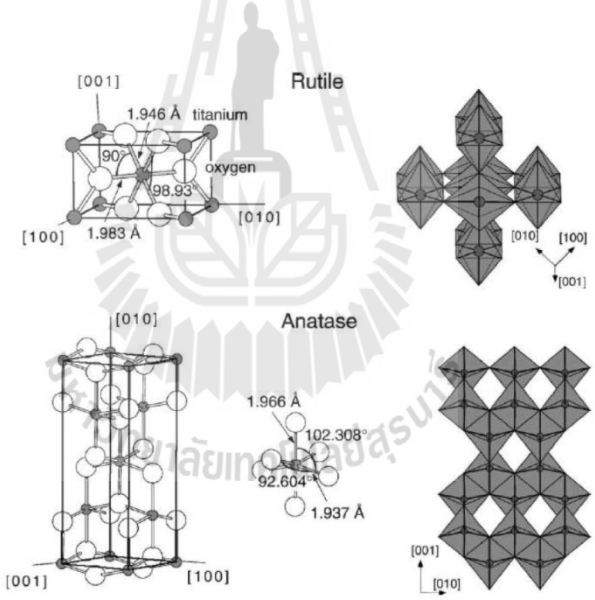

Figure 2.6 Crystal structures of rutile and anatase phases (Diebold, 2003).

2.6.2 Preparation of TiO_2 on NaY and RHS

Artkla et al. (2009) reported that TiO_2 grafted on RH-MCM-41 from titanium tetrabutoxide had anatase phase which was highly active for photocatalytic degradation of methyl orange. In this work, TiO_2 was prepared by the same

precursor, titanium tetrabutoxide to produce only the active anatase. The TiO_2 precursor was incorporated with adsorbents to increase paraquat interaction on the surface and improve dispersion of TiO_2, both cases, to promote photocatalysis of paraquat. The photocatalysts were prepared by grafting the support with TiO_2 sol from an acid catalyzed sol-gel formation method.

2.7 References

Artkla, S., Grisdanurak, N., Neramittagapong, S. and Wittayakun, J. (2008). Characterization and catalytic performance on transesterification of palm olein of potassium oxide supported on RH-MCM-41 from rice husk silica. **Suranaree Journal of Science and Technology**. 15: 133-138.

Artkla, S., Wantala, K., Srinameb, B., Grisdanurak, N., Klysubun, W., and Wittayakun, J. (2009). Characteristics and photocatalytic degradation of methyl orange on Ti-RH-MCM-41 and TiO_2/RH-MCM-41. **Korean Journal of Chemical Engineering**. 26: 1556-1562.

Baerlocher, Ch. and McCusker, L. B. (2001). Framework Types. **Database of Zeolite Structures**. [Online] Available: http://www.iza-structure.org/databases/

Braga, P. R. S., Costa, A. A., de Macedo, J. L., Ghesti, G. F., de Souza, M. P., Dias, J. A. and Dias, S. C.L. (2011). Liquid phase calorimetric-adsorption analysis of Si-MCM-41: Evidence of strong hydrogen-bonding sites. **Microporous and Mesoporous Materials**. 139: 74-80.

Brigante, M., and Schulz, P. C. (2011). Adsorption of paraquat on mesoporous silica modification with titania: Effects of pH, ionic strength and temperature. **Journal of Colloid and Interface Science**. 363: 355-361.

Chumee, J., Grisdanurak, N., Neramittagapong, S., and Wittayakun, J. (2009). Characterization of AlMCM-41 synthesized with rice husk silica and utilization as supports for platinum-iron catalysts. **Brazilian Journal of Chemical Engineering**. 26: 367-373.

Diebold, U. (2003). The surface science of titanium dioxide. **Surface Science Report**. 48: 53-229.

Florêncio, M. H., Pires, E., Castro, A. L., Nunes, M. R., Borges, C., and Costa, F. M. (2004). Photodegradation of diquat and paraquat in aqueous solutions by titanium dioxide: evolution of degradation reactions and characterization of intermediates. **Chemosphere**. 55: 345-355.

Flores-Céspedes, F., Fernández-Pérez, M., Villafranca-Sánchez, M., and González-Pradas, E. (2006). Cosorption study of organic pollutants and dissolved organic matter in a soil. **Environmental Pollution**. 142: 499-456.

Fossen, M. (2006). Environmental Fate of Imidacloprid. **Environmental Monitoring Department of Pesticide Regulation**. [On-line] Available: http://www.cdpr.ca.gov/docs/emon/pubs/enfate.htm.

Guisnet, M., and Gilson, J. P. (2002). **Zeolites for cleaner technologies**. Imperial College Press, London.

Hamadi, N. K., Swaminathan, S., and Chen, X. (2004). Adsorption of Paraquat dichloride from aqueous solution by activated carbon derived from used tires. **Journal of Hazardous Materials**. 112: 133-141.

Hsu, S., Chen, L., Lee, C., Pan, T., You, B., and Yan, Q. (2009). Preparation of methacrylic acid-modified rice husk improved by an experimental design and

application for paraquat adsorption. **Journal of Hazardous Materials**. 171: 465-470.

Hsu, S., and Pan, T. (2007). Adsorption of paraquat using methacrylic acid-modified rice husk. **Bioresource Technology**. 98: 3617-3621.

Ibrahim, K. M., and Jbara, H. A. (2009). Removal of paraquat from synthetic wastewater using phillipsite–faujasite tuff from Jordan. **Journal of Hazardous Materials**. 163: 82-86.

Kaneko, M., and Okura, I. (2002). **Photocatalysis : Science and Technology**. New York: Springer.

Khemthong, P., Prayoonpokarach, S., and Wittayakun, J. (2007). Synthesis and characterization of zeolite LSX from rice husk. **Suranaree Journal of Science and Technology**. 14: 367-379.

Kitsiou, V., Filippidis, N., Mantzavinos, D., and Poulios, I. (2009). Heterogeneous and homogeneous photocatalytic degradation of the insecticide imidacloprid in aqueous solutions. **Applied Catalysis B: Environmental**. 86: 27-35.

Lee, J., Kim, M., and Kim, B. (2002). Removal of paraquat dissolved in a photoreactor with TiO_2 immobilized on the glass-tubes of UV lamps. **Water Research**. 36: 1776-1782.

Loiha, S., Prayoonpokarach, S., Songsiriritthigun, P., and Wittayakun, J. (2009). Synthesis of zeolite beta with pretreated rice husk silica and its transformation to ZSM-12. **Materials Chemistry and Physics**. 115: 637-640.

Malato, S., Blanco, J., Cáceres, J., Alba, A. R. F., Agüera, A., and Rodriguez, A. (2002). Photocatalytic treatment of water-soluble pesticides by photo-Fenton and TiO_2 using solar energy. **Catalysis Today**. 76: 209-220.

Moctezuma, E., Leyva, E., Monreal, E., Villegas, N., and Infante, D. (1999). Photocatalytic degradation of the herbicide “paraquat”. **Chemophere**. 39: 511-517.

Nemeth-Konda, L., Fuleky, Gy., Morovjan, Gy., and Csokan, P. (2002). Sorption behaviour of acetochlor, atrazine, carbendazim, diazinon, imidacloprid and isoproturon on Hungarian agricultural soil. **Chemosphere**. 48: 545-552.

Nur, H., Manan, A. F. N. A., Wei, L., Muhid, M. N. M., and Hamdan, H. (2005). Simultaneous adsorption of a mixture of paraquat and dye by NaY zeolite covered with alkylsilane. **Journal of Hazardous Materials**. B117: 35-40.

NSTA. (2005). Present Technology. **Photocatalysis**. [On-line] Available: http://dev.nsta.org/ evwebs/1952/photocatalysis.htm.

Ríos, C. A., Williams, C. D., and Castellanos, O. M. (2012). Crystallization of low silica Na-A and Na-X zeolites from transformation of kaolin and obsidian by alkaline fusion. **Ingeniería y Competitividad**. 14(2):125-137

Roland, E., and Kleinschmit, P. (2003). Zeolites. **Ullmann’s Encyclopedia of Industrial Chemistry.** Vol. 39. Weinheim: Wiley-VCH.

Seki, Y., and Yurdakoç, K. (2005). Paraquat adsorption onto clays and organoclays from aqueous solution. **Journal of Colloid and Interface Science**. 287: 1-5.

Sobczyński, A., and Dobosz, A. (2001). Water purification by photocatalysis on semiconductors. **Polish Journal of Environmental Studies**. 10: 195-205.

Tsai, W. T., Hsien, K. J., Chang, Y. M., and Lo, C. C. (2005). Removal of herbicide paraquat from an aqueous solution by adsorption onto spent and treated diatomaceous earth. **Bioresource Technology**. 96: 657-663.

Tsai, W. T., Lai, C. W., and Hsien, K. J. (2004). Adsorption kinetics of herbicide paraquat from aqueous solution onto activated bleaching earth. **Chemosphere**. 55: 829-837

Tsai, W., and Lai, C. (2006) Adsorption of herbicide paraquat by clay mineral regenerated from spent bleaching earth. **Journal of Hazardous Materials**. 134: 144-148.

United States Environmental Protection Agency. (1994). Imidacloprid Pesticide Fact Sheet, **U.S. Environmental Protection Agency**. Washington DC.

Vohra, M. S., and Tanaka, K. (2003). Photocatalytic degradation of aqueous pollutants using silica-modified TiO_2. **Water Research**. 37: 3992-3996.

Wittayakun, J., Khemthong, P., and Prayoonpokarach, S. (2008). Synthesis and characterization of zeolite NaY from rice husk silica. **Korean Journal of Chemical Engineering**. 25: 861-864.

Yang, P., Gaib, S., and Lin, J. (2012). Functionalized mesoporous silica materials for controlled drug delivery. **Chemical Society Reviews**. 41: 3679-3698.

Zhang, H., Kim, Y., and Dutta, P. K. (2006). Controlled release of paraquat from surface-modified zeolite Y. **Microporous and Mesoporous Materials**. 88: 312-318.

CHAPTER III

PARQUAT ADSORPTION ON POROUS MATERIALS SYNTHESIZED FROM RICE HUSK SILICA

Abstract

This chapter focuses on the utilization of rice husk silica (RHS), MCM-41, zeolite NaY and NaBEA for adsorption of herbicide paraquat. In the real situation, a commercial paraquat containing blue dye is used by farmers. Thus, the blue dye adsorption was also studied on all adsorbents to find the adsorbent for both compounds. The adsorption of paraquat occurred through a cation exchange process. The adsorption capacities of the adsorbents decreased in the following order: NaY > NaBEA > MCM-41 > RHS, consistent with the amount of Al. The adsorption behavior fitted well with Langmuir model and the maximum adsorption capacity of 185.2 mg/g-adsorbent was obtained on NaY. The blue dye in the commercial grade paraquat did not interfere the paraquat adsorption. MCM-41 was the most efficient adsorbent for the blue dye but RHS was favorable in term of production cost. A mixture of NaY and RHS is recommended for simultaneous adsorption of paraquat and blue dye.

3.1 Introduction

Utilization of pesticides such as paraquat can lead to water pollution because some of those compounds degrade slowly and accumulate in the environment. Paraquat is highly soluble in water due to its cationic and hydrophilic nature (Pateiro-Moure et al., 2010). It is widely used to control broadleaf weeds and grasses (USEPA, 1997). Paraquat is highly toxic when exposed to human and animals by ingestion, skin contact or splash to eyes (Suntres, 2002). According to the Chemical Safety Database, the level which is immediately dangerous to humans is 1 ppb (Thailand chemtrack, www, 2001).

Various methods have been employed for the removal of paraquat in water samples. Adsorption is one of the viable methods because it is simple, efficient, and inexpensive. Siliceous compounds such as silica (SiO_2) (Brigante and Schulz, 2011), clay minerals (Seki and Yurdakoç, 2005), activated bleaching earth and diatomaceous earth (Tsai et al., 2004; Tsai et al., 2005; Tsai and Lai, 2006) were reported as adsorbents for paraquat. Adsorption of paraquat on SiO_2 was low because it lacks acidity (Brigante and Schulz, 2011).

From literature review, SiO_2-based materials with high surface area and acid sites are suitable for paraquat adsorption. Therefore, we employed rice husk silica (RHS) and some porous compounds derived from RHS including MCM-41and zeolite BEA in sodium form (NaBEA) as adsorbents for paraquat. RHS, which is amorphous silica with high purity and surface area, could be produced by acid leaching and used efficiently as a silica source for a synthesis of porous materials (Wittayakun et al., 2008; Loiha et al., 2009; Rintramee et al., 2012).

MCM-41 is a siliceous material with highly uniform mesopores and high surface area. Compared to RHS and zeolites, MCM-41 has the highest surface area. It is rich of silanol groups (Si-OH) which can interact with molecules with electronegative atoms via hydrogen bonding (Braga et al., 2011). Zeolites are microporous aluminosilicates containing [SiO_4] and [AlO_4^-] tetrahedral units linked to each other by sharing all the oxygen atoms to form a framework with uniform cavities and channels. Substitution of Si^{4+} by Al^{3+} generated negative charge in the zeolite framework and a cation is required to balance the charge. The balancing cation in zeolites resides in zeolite cavities and can be exchanged with other cation. The amount of cationic sites is parallel to the amount of aluminum atoms or Si/Al ratio of the zeolite (Guisnet and Gilson, 2002). In addition, surface of zeolites, especially in hydrated phase contains hydroxyl groups which can interact with other molecules by hydrogen bond. NaBEA which is one of zeolite has the Si/Al ratio in BEA is 8-20 and the cavity dimension is 0.66 × 0.67 nm (Roland and Kleinschmit, 2003).

Besides, zeolite Y in sodium form (NaY) which is in FAU family with higher surface area than those of RHS and NaBEA was employed in this work. The Si/Al ratio in zeolite Y is 1.5-3.0. This zeolite structure is formed by six sodalite cages creating a large cavity known as supercage with diameter of 1.3 nm and four apertures with dimension of 0.74 × 0.74 nm (Roland and Kleinschmit, 2003). It was reported that paraquat could be adsorbed on natural faujasite tuff in Na form (Ibrahim and Haneen 2009). Zhang et al. (2006) loaded paraquat on NaY by ion exchange and released by treating with NaCl solution. Nur et al. (2005) reported that NaY (0.4 g) could completely adsorb commercial paraquat (concentration of 300 ppm, volume 25 mL) but unable to adsorb blue dye. When NaY was covered with alkylsilane, the

adsorption of paraquat slightly decreased and the dye adsorption was significantly improved. However, they neither vary the paraquat concentration nor report paraquat adsorption capacity.

The objective of the work in this chapter is to investigate ability of porous materials derived from RHS including MCM-41, NaY and NaBEA for paraquat adsorption. The paraquat adsorption isotherms were fitted with Langmuir and Freundlich models. Adsorption of commercial grade paraquat containing blue dye and analytical reagent grade was compared on the adsorbent with the highest capacity. The adsorption of blue dye on all adsorbents was also compared.

3.2 Experimental

3.2.1 Materials

Adsorbents in this work were RHS-based porous materials including NaY, NaBEA, RH-MCM-41, and bare RHS. Chemicals for the preparation of the RHS and zeolite synthesis were hydrochloric acid (37% HCl, Carlo-Erba), sodium aluminate (~55 – 56% of $NaAlO_2$, Riedel-de Haën), sodium hydroxide (97% NaOH, Carlo-Erba), and rice husk (local rice mill near SUT, Nakhon Ratchasima, Thailand). Paraquat, analytical reagent grade (99.9 %w/w, Fluka) and commercial grade (27.6 %w/v, Masda) were used in the adsorption studies. The analytical reagent grade was used to obtain a calibration curve for the determination of paraquat concentration in aqueous samples.

3.2.2 Preparation of adsorbents

RHS and RHS-based porous materials including MCM-41, NaY, and NaBEA were used as adsorbents. RHS was prepared from rice husk by acid leaching (Khemthong et al., 2007). Dried rice husk was refluxed in 3 M HCl for 6 h, washed repeatedly with DI water until the filtrate was neutral, dried at 100 °C overnight and pyrolyzed in a muffle furnace at 550 °C for 6 h.

Zeolite NaY was synthesized from seed gel and feedstock gel by the procedure described in a previous work by Wittayakun et al. (2008). The seed gel was prepared by dissolving NaOH and $NaAlO_2$ in deionized water followed by the addition of Na_2SiO_3 solution and kept at room temperature for 24 h. The feedstock gel was prepared by a method similar to that of the seed gel except that it was used immediately without aging. In the synthesis, both gels were mixed to form overall gel, aged (kept undisturbed) at room temperature 24 h, and crystallized at 100 ^{o}C 24 h. After the crystallization step, the resulting white powder was separated by filtration, washed, and dried at 100 ^{o}C.

The MCM-41, and NaBEA were synthesized by methods described in the literature (Rintramee et al., 2012; Loiha et al., 2009).

3.2.3 Characterization of adsorbents

Si/Al ratios were determined using energy dispersive X-ray fluorescence (EDXRF) spectrometer (Oxford ED2000). Standards for EDXRF were prepared by fusing physical mixture of silica (SiO_2) and alumina (Al_2O_3, Fluka) at various ratios. Phase and structure were confirmed by powder X-ray diffraction (XRD) using Bruker axs diffractometer D5005 with Cu K_α radiation. The N_2

adsorption-desorption analysis was done at relative pressure from 0.01 to 0.99 on a Micromeritics ASAP 2010 analyzer. The samples were degassed at 300 ^{o}C under vacuum for 8 h before measurement. Surface area was obtained by BET method.

3.2.4 Adsorption of paraquat on porous materials

First, a screening test was done to choose the best adsorbent with the highest capacity for the subsequent studies. Paraquat adsorption was done in a 125 mL polypropylene bottle. The system comprised of 0.05 g of adsorbent sieved from 63 to 75 µm and 20 mL of 80 to 1000 ppm of paraquat solution (prepared from the analytical reagent grade). The mixture was stirred at room temperature for 60 min and the adsorbent was separated by a 0.45 µm nylon syringe filter. The paraquat concentration was determined by Ultraviolet-Visible spectrophotometer (Varian Cary 1E) at λ_{max} of 257 nm (Nur et al., 2005; Iglesias et al., 2010). The adsorption data were fitted with Langmuir and Freundlich isotherms.

Langmuir adsorption isotherm is applicable to chemisorptions to form a monolayer. In this model, the adsorbent surface composed of equivalent and dependent sites for adsorption. The rate of adsorption depends on concentration of adsorbate and fraction of bare sites. The rate of desorption depends on activation energy of adsorption. At equilibrium the rate of adsorption equals to that of desorption. It is assumed that there is no adsorbate – adsorbate interaction. In the Langmuir adsorption isotherm, a plateau is generally obtained.

The Langmuir adsorption isotherm is defined by equation (3.1).

$$q = q_m K_A X_e /(1+ K_A X_e) \quad \ldots(3.1)$$

where, q (mg/g) is the amount of the adsorbate adsorbed per gram of the adsorbent;

q_m (mg/g) is the amount of the adsorbate adsorbed to form a monolayer coverage;

K_A (L/mg) is the Langmuir adsorption equilibrium constant;

X_e (mg/L) is the amount of the adsorbate in a solution at equilibrium

Adsorption data can be fitted to the Langmuir isotherm in its linear form as in equation (3.2).

$$X_e/q = X_e/q_m + 1/K_A q_m \quad \ldots(3.2)$$

It is possible that there are deviations from Langmuir isotherm. Then other types of isotherm can be used to explain the adsorption behavior. For example, Freundlich adsorption isotherm is used for adsorbents with multisites.

The Freundlich adsorption isotherm is defined as shown in equation (3.3).

$$q = K_F * X_e^{1/n} \quad \ldots(3.3)$$

where, K_F and n are both Freundlich constant.

Adsorption data can be fitted to the Freundlich isotherm in its linear form as:

$$\log q = \log K_F + 1/n(\log X_E) \quad \ldots(3.4)$$

Adsorption isotherms of paraquat were acquired from solutions with concentrations in the range of 80-1000 ppm. Kinetic experiment was done with 0.05 g of NaY and 20 mL of 650 ppm of commercial paraquat at various times.

Influence of blue dye on the adsorption of paraquat prepared from the commercial grade paraquat was evaluated on the best adsorbent. The adsorption efficiency was determined at the λ_{max} of 629 nm (Nur et al., 2005).

3.3 Results and discussion

3.3.1 Characterization of adsorbents

XRD patterns of all adsorbents are shown in Figure 3.1. The patterns are used to confirm the phase of the adsorbents. The pattern of RHS (Figure 3.1a) shows a broad peak around 22 degree which is characteristic of amorphous silica (Khemthong et al., 2007). The pattern of MCM-41 (Figure 3.1b) consisted of a strong peak at 2.3 degree and weak peaks at 3.9 and 4.6 degree which are the characteristic of MCM-41 (Rintramee et al., 2012). The XRD patterns of NaY and NaBEA (Figure 3.1c) also confirmed the structure of each zeolite (Wittayakun et al., 2008; Loiha et al., 2009).

N_2 adsorption-desorption isotherm of all adsorbents are shown in Figure 3.2. The isotherm of RHS (Figure 3.2a) indicated that it had broad pore range with both micro- and mesopores. The isotherm of MCM-41 was type IV (Figure 3.2b), a characteristic of mesoporous materials with a type H1 hysteresis loop and a characteristic of an open-ended tubular pore (Rouquerol et al., 1999). The isotherm of NaY and NaBEA (Figure 3.2c) were type I, characteristic of microporous materials (Wittayakun et al., 2008; Loiha et al., 2009). The adsorption increased quickly at low pressure due to adsorption in micropores and on external surface. Then, the adsorbed volume was nearly constant as a monolayer was formed.

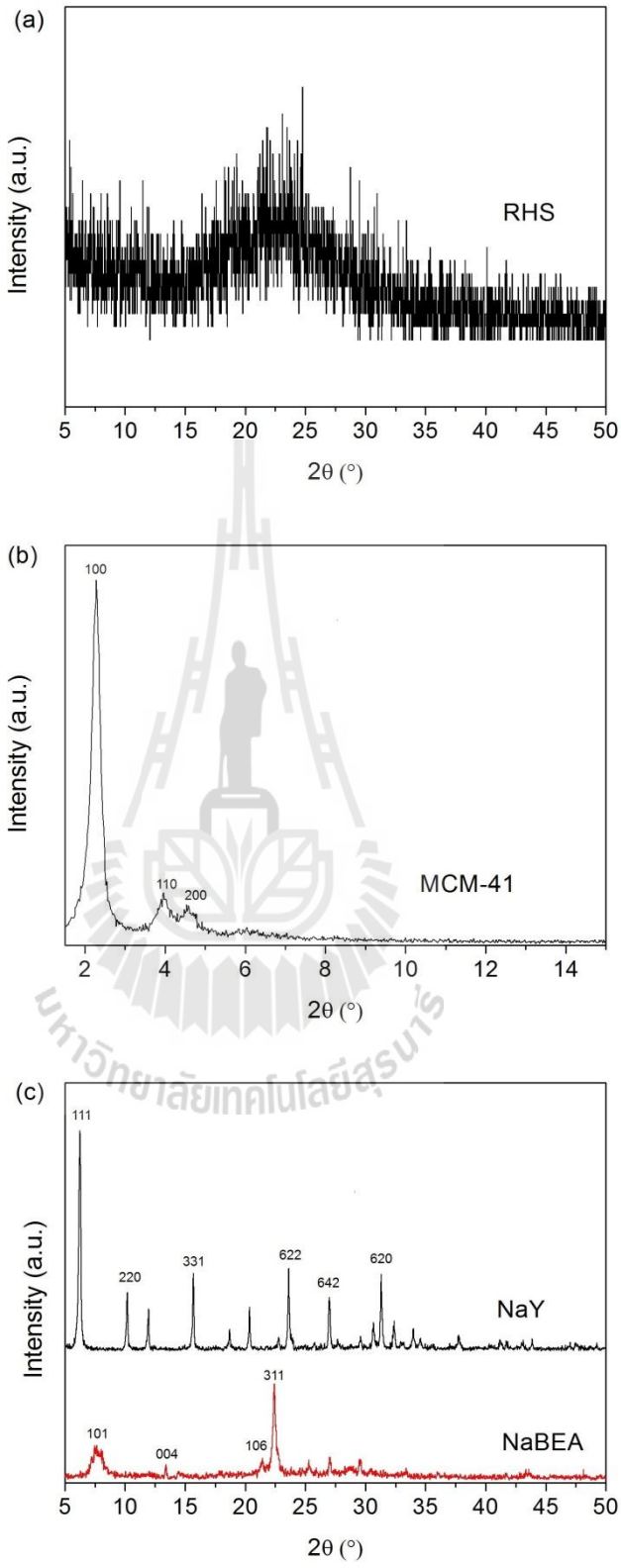

Figure 3.1 XRD patterns of RHS (a), MCM-41 (b), and zeolites NaY and NaBEA (c).

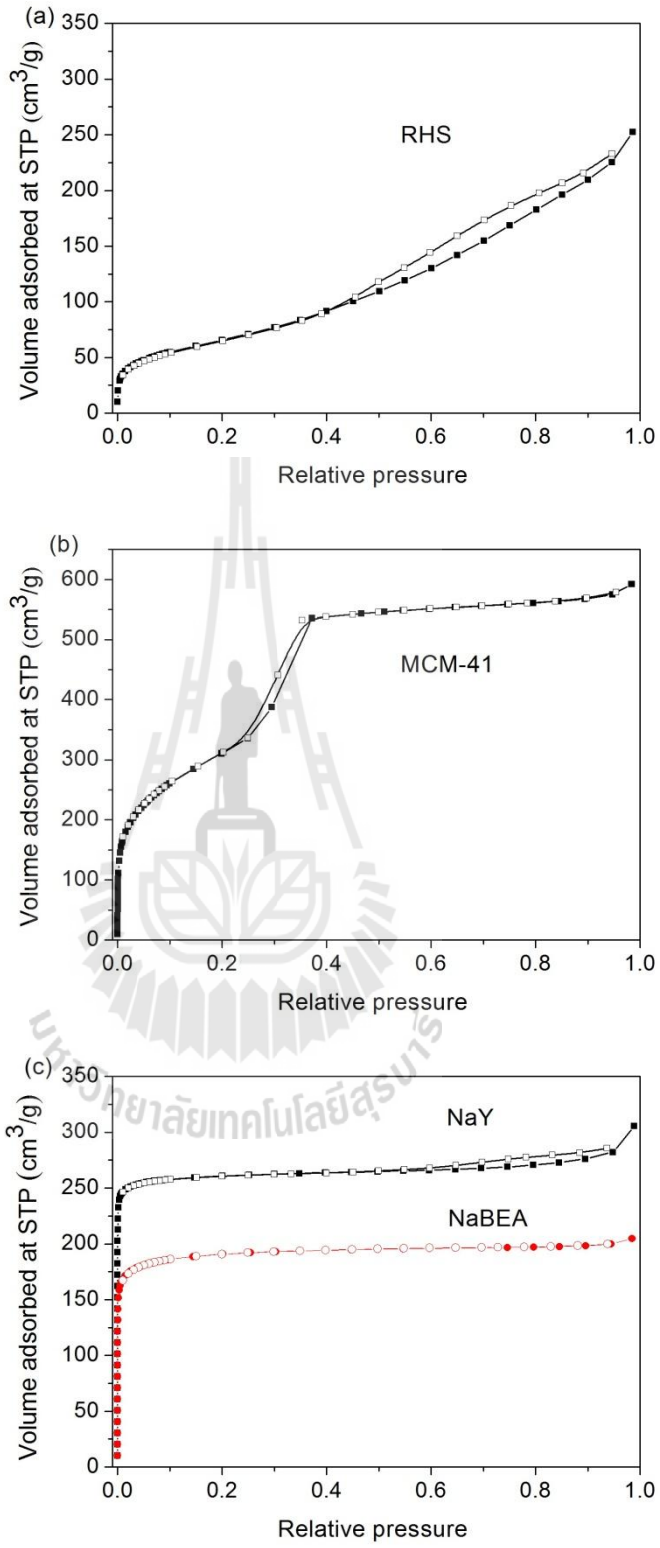

Figure 3.2 Nitrogen adsorption (filled)–desorption (empty) isotherm of RHS (a), MCM-41 (b), and zeolite NaY and NaBEA (c).

Properties of all adsorbents including Si/Al ratio, surface area and pore volume are shown in Table 3.1. The Si/Al ratio corresponded to differences of the Al concentration in the zeolite structure. The higher Si/Al ratio indicates the lower amount of Al and the lower amount of exchangeable cation in the adsorbents. In addition, these zeolites contained surface silanol groups which could form hydrogen bond (Hashimoto, 2003). The Si/Al ratio of RHS and MCM-41 were much higher than those in the zeolites because these materials consisted mainly of silica and a small amount of alumina in the silica source. As a result, these materials had lower cation-exchange capacity than the zeolites. Because MCM-41 had the highest surface area (Table 3.1), it was likely to have the highest amount of surface silanol groups which could act as adsorption sites. It was reported that MCM-41 which had higher surface area than silica gel and zeolite ZSM-5 also had higher amount of silanol groups (Braga et al., 2011).

Table 3.1 Properties of adsorbents.

Type of adsorbent	**Si/Al ratio from XRF**	**BET Surface area (m^2/g)**	**Average pore diameter (nm)**
RHS	174.9	220	6.7
MCM-41	143.0	1251	3.3
NaY	2.2	870	2.2
NaBEA	14.2	632	2.0

3.3.2 Adsorption of analytical reagent grade paraquat

Figure 3.3 shows adsorption of paraquat on all adsorbents from the concentrations from 80 mg/L to 720 mg/L. The capacity was in the order: NaY > NaBEA > MCM-41 > RHS. RH-MCM-41 had higher surface area and pore diameter than NaY and NaBEA but had lower adsorption capacity. The trend of adsorption capacity was similar to the trend of Al content (Table 3.1) suggesting that the adsorption depended on Si/Al ratio. The results from fitting with Langmuir and Freundlich isotherm are shown in Table 3.2. The adsorption on all samples fitted well with Langmuir isotherm with correlation coefficient around 0.99. The monolayer adsorption capacity (q_m) showed that NaY was the most effective adsorbent.

Because the molecular size of paraquat, 0.64×0.34×1.34 nm (Zhang et al., 2006) is smaller than the cavity sizes of NaY and NaBEA, it could be adsorbed in the zeolite cavities by ion exchange with cations (Zhang et al., 2006; Ibrahim and Haneen, 2009). Thus, the exchange capacity depends on Si/Al ratio. When an Al atom is present in the zeolite framework, a negative charge is generated and the balancing caion is required (Na^+ in this case). Because Si/Al ratio of NaY was lower than that of NaBEA, NaY has a higher exchange capacity. A further study on paraquat adsorption was only done on NaY.

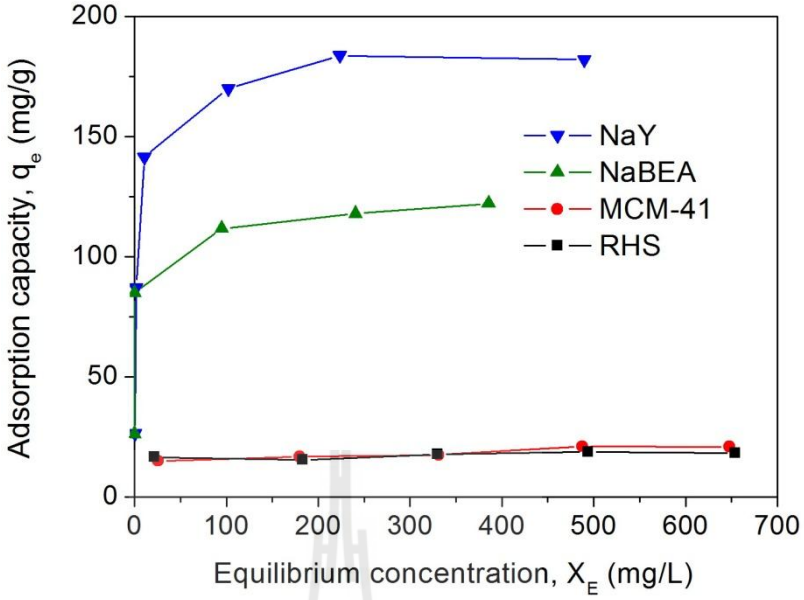

Figure 3.3 Adsorption of analytical reagent grade paraquat on NaY, NaBEA, MCM-41, and RHS. Each adsorption experiment was done in triplicate with 0.05 g of zeolite and 20 mL of various paraquat concentrations at room temperature for 1 h.

Table 3.2 Correlation coefficient of paraquat adsorption by Langmuir and Freundlich adsorption isotherm and adsorption capacity (q_m) of analytical reagent grade paraquat.

adsorbents	**R^2**		**Langmuir equation**	**q_m (mg/g-adsorbent)**
	Freundlich	**Langmuir**		
RHS	0.3587	0.9962	$q = 1.05X_E/(1+0.06X_E)$	18.9
MCM-41	0.8110	0.9859	$q = 0.56X_E/(1+0.03X_E)$	21.3
NaY	0.8343	0.9997	$q = 42.37X_E/(1+0.23X_E)$	185.2
NaBEA	0.5833	0.9992	$q = 44.29X_E/(1+0.36X_E)$	122.0

3.3.3 Adsorption Isotherm of paraquat on NaY

The adsorption of both analytical reagent grade and commercial grade paraquat with various initial concentrations was studied on NaY to see whether or not the blue dye in the commercial sample interferes the paraquat adsorption. As shown in Figure 3.4, both systems gave nearly identical adsorption isotherm suggesting that blue dye had no effect on the paraquat adsorption on NaY. The monolayer adsorption capacity calculated from Langmuir equation were 185.2 and 181.8 mg/g-adsorbent in analytical reagent grade and commercial grade paraquat solutions, respectively. Nur et al. (2005) reported that paraquat adsorbed on the hydrophilic internal pores of commercial NaY whereas the blue dye in paraquat and Cibacron Blue 3GA did not adsorb.

Comparison of adsorbent type, adsorption conditions and maximum capacity is shown in Table 2.1 of Chapter II. The ratio of adsorbent weight and solution volume from this work was comparable to that from literatures and our concentration range was the largest. These results revealed that NaY was among the best for paraquat adsorption. With high efficiency and simple preparation, NaY is an attractive adsorbent. A further investigation to understand the nature of adsorption and to improve its capacity is being carried out.

Gibbs free energy (ΔG) was evaluated to confirm the adsorption nature. The Langmuir constant K_A can be used for calculating the free energy change using the following equation:

$$\Delta G = -RT \ln K_A \qquad \ldots(3.5)$$

where R is the gas constant, T is the absolute temperature, and K_A is the

adsorption constant. The obtained ΔG was -27.4 kJ/mol; paraquat adsorption was favorable.

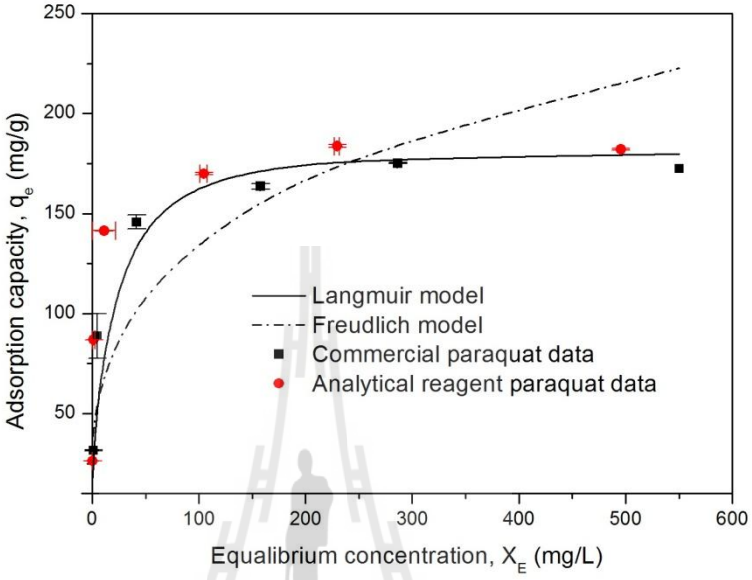

Figure 3.4 Isothermal adsorption of paraquat (analytical reagent grade and commercial grade) on NaY at room temperature. Each experiment was done in triplicate with 0.05 g of NaY and 20 mL of 80 to 1000 ppm paraquat solutions.

3.3.4 Paraquat adsorption kinetic of NaY

Kinetic experiment was done with 0.05 g of NaY and 20 mL of 650 ppm of commercial paraquat shown in Figure 3.5. The result showed equilibrium adsorption of 182 mg/g-adsorbent (70 % paraquat adsorption). The equilibrium was reached in 5 min. It was reported in the literature that it took about 5 min for a commercial NaY for the initial paraquat concentration 300 ppm and the equilibrium adsorption capacity was only 18.8 mg/g-adsorbent (Nur et al., 2005).

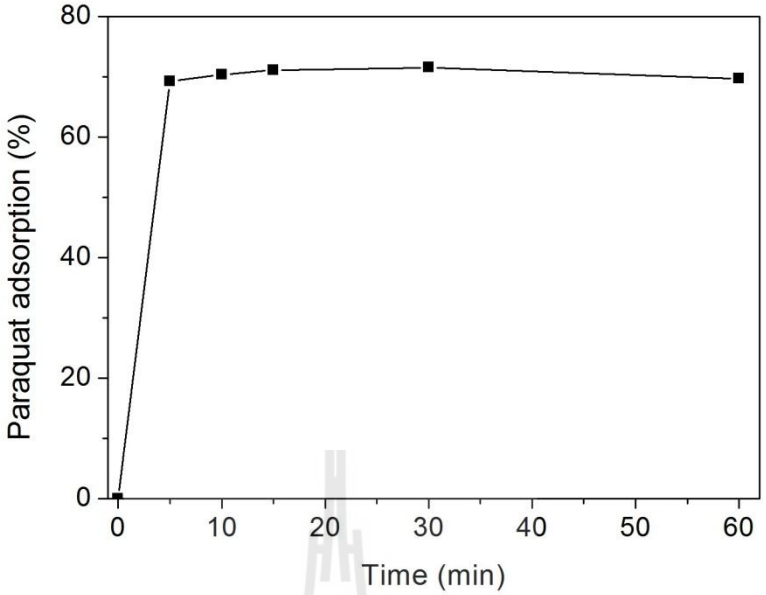

Figure 3.5 Adsorption of paraquat on NaY zeolite. Experimental was done with 0.05 g of NaY and 20 mL of 650 ppm of commercial paraquat.

3.3.5 Adsorption of blue dye

Figure 3.6a shows adsorption of blue dye on RHS, MCM-41, NaY and NaBEA. The adsorption was in the following order: MCM-41 > RHS > NaBEA > NaY. Because the adsorption was highest on MCM-41 which had the highest surface area among these adsorbents, it was likely that the adsorption occurred on silanol groups. From the paraquat adsorption experiment, NaY adsorbed both analytical reagent grade and commercial paraquat similarly. Thus, the adsorption of the blue dye on NaY did not interfere the paraquat adsorption. The results suggested that the adsorption of the blue dye was not through the ion exchange mechanism (Nur et al., 2005).

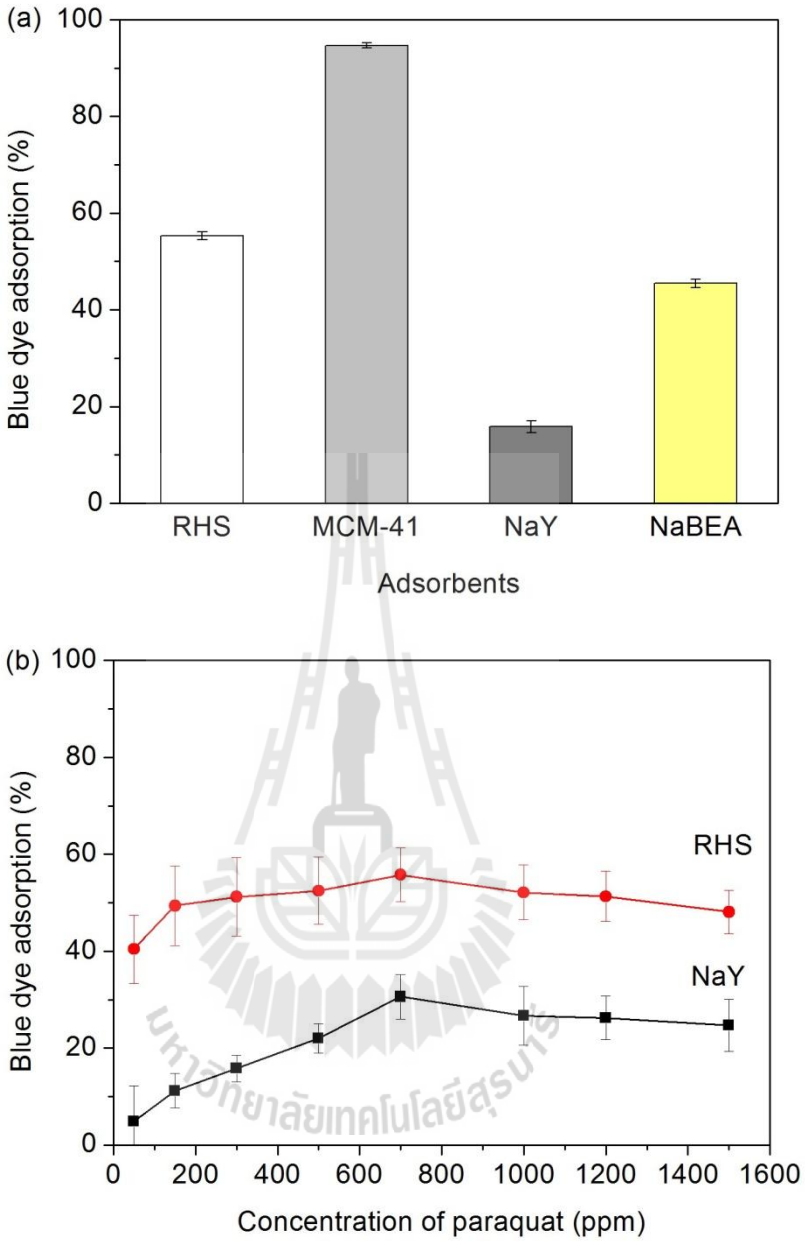

Figure 3.6 Adsorption of blue dye on NaY, NaBEA, MCM-41, and RHS (a). Experiment was done with 0.05 g of zeolite and 20 mL of 50 ppm commercial paraquat. Adsorption of blue dye on RHS and NaY (b). Each experiment was done in triplicate with 0.05 g of adsorbents and 20 mL of commercial grade paraquat.

Although MCM-41 was the best adsorbent for the blue dye, it was not cost effective because its synthesis requires an expensive template. In contrast, RHS could be produced easily with a low cost. Thus, a mixture of NaY and RHS is suggested for the removal of both paraquat and blue dye. The sum of blue dye removal efficiency from NaY and RHS was nearly the same as that from MCM-41. Finally, Figure 3.6b shows adsorption of blue bye in various concentration of commercial grade paraquat on RHS and NaY. As the paraquat concentration increased, the percent adsorptions of the blue dye on NaY were nearly constant but those on RHS showed a more decrease. It was possible that the adsorption sites were fully occupied. The mixture of RHS and NaY could still effectively remove the blue dye in all concentration range.

3.4 Conclusions

Paraquat adsorption was investigated on rice husk silica (RHS) and porous materials derived from RHS including MCM-41, NaY and NaBEA. These materials were different in pore structure, surface area and Si/Al ratio. RHS was amorphous silica with wide pore range; MCM-41 is a mesoporous silica; NaY and NaBEA are microporous aluminosilicates. The adsorption on all adsorbents fitted well with Langmuir model; the highest adsorption capacity of 185.2 mg/g was obtained on NaY; and the adsorption mechanism was cation exchange. In the study of commercial grade paraquat, blue dye did not interfere the paraquat adsorption. Further study on adsorption of blue dye in commercial grade paraquat showed that the MCM-41 was the best adsorbent but RHS was also preferable because it could be obtained more easily and economically. The blue dye likely adsorbed on silanol groups. The

recommended adsorbent for commercial paraquat was a mixture of NaY and RHS because both paraquat and blue dye could be removed effectively.

3.5 References

Braga, P. R. S., Costa, A. A., de Macedo, J. L., Ghesti, G. F., de Souza, M. P., Dias, J. A. and Dias, S. C. L. (2011). Liquid phase calorimetric-adsorption analysis of Si-MCM-41: Evidence of strong hydrogen-bonding sites. **Microporous and Mesoporous Materials**. 139: 74-80.

Brigante, M., and Schulz, P. C. (2011). Adsorption of paraquat on mesoporous silica modification with titania: Effects of pH, ionic strength and temperature. **Journal of Colloid and Interface Science**. 363: 355-361.

Guisnet, M., and Gilson, J. P. (2002). **Zeolites for cleaner technologies.** London: Imperial College Press.

Hashimoto, S. (2003). Zeolite photochemistry: Impact of zeolites on photochemistry and feedback from photochemistry to zeolite science. **Journal of Photochemistry and Photobiology C: Photochemistry Reviews**. 4: 19-49.

Ibrahim, K. M., and Jbara, H. A. (2009). Removal of paraquat from synthetic wastewater using phillipsite–faujasite tuff from Jordan. **Journal of Hazardous Materials**. 163: 82-86.

Iglesias, A., Lopez, R., Gondar, D., Antelo, J., Fiol, S., and Arce, F. (2010). Adsorption of paraquat on goethite and humic acid-coated goethite. **Journal of Hazardous Materials**. 183: 664-668.

Khemthong, P., Prayoonpokarach, S., and Wittayakun, J. (2007). Synthesis and characterization of zeolite LSX from rice husk. **Suranaree Journal of Science and Technology**. 14: 367-379.

Loiha, S., Prayoonpokarach, S., Songsiriritthigun, P., and Wittayakun, J. (2009). Synthesis of zeolite beta with pretreated rice husk silica and its transformation to ZSM-12. **Materials Chemistry and Physics**. 115: 637-640.

Pateiro-Moure, M. P., Estévez, M. A., and Gándara, J. S. (2010) Competitive and non-competitive adsorption/desorption of paraquat,diquat and difenzoquat in vineyard-devoted soils. **Journal of Hazardous Materials**. 178: 194-201.

Nur, H., Manan, A. F. N. A., Wei, L., Muhid, M. N. M., and Hamdan, H. (2005). Simultaneous adsorption of a mixture of paraquat and dye by NaY zeolite covered with alkylsilane. **Journal of Hazardous Materials**. B117: 35-40.

Rintramee, K., Föttinger, K., Rupprechter, G., and Wittayakun, J. (2012). Ethanol adsorption and oxidation on bimetallic catalysts containing platinum and base metal oxide supported on MCM-41. **Applied Catalysis B: Environmental**. 115: 225-235.

Roland, E., and Kleinschmit, P. (2003). Zeolites. **Ullmann's Encyclopedia of Industrial Chemistry**. Vol.39. Weinheim: Wiley-VCH.

Rouquerol, F., Rouquerol, J., and Sing, K. (1999). **Adsorption by Powders and Porous Solids**. London: Academic Press.

Seki, Y., and Yurdakoç, K. (2005). Paraquat adsorption onto clays and organoclays from aqueous solution. **Journal of Colloid and Interface Science**. 287: 1-5.

Suntres, Z. E. (2002). Role of antioxidants in paraquat toxicity. Toxicology. 180, 65-77.

Thailand Chem Track. (2001). Information on Hazardous Chemicals and Occupational Diseases. **Paraquat dichloride** [On-line] Available: http://www.chemtrack.org/ HazMap-Agent-Info.asp?ID=1125.

Tsai, W. T., Hsien, K. J., Chang, Y. M., and Lo, C. C. (2005). Removal of herbicide paraquat from an aqueous solution by adsorption onto spent and treated diatomaceous earth. **Bioresource Technology**. 96: 657-663.

Tsai, W. T., Lai, C. W., and Hsien, K. J. (2004). Adsorption kinetics of herbicide paraquat from aqueous solution onto activated bleaching earth. **Chemosphere**. 55: 829-837

Tsai, W., and Lai, C. (2006) Adsorption of herbicide paraquat by clay mineral regenerated from spent bleaching earth. **Journal of Hazardous Materials**. 134: 144-148.

United States Environmental Protection Agency. (1997). Paraquat dichloride, **R.E.D Facts Environmental Protection Agency, office of prevention pesticides, and toxic substances**. Washington DC.

Wittayakun, J., Khemthong, P., and Prayoonpokarach, S. (2008). Synthesis and characterization of zeolite NaY from rice husk silica. **Korean Journal of Chemical Engineering**. 25: 861-864.

Zhang, H., Kim, Y., and Dutta, P. K. (2006). Controlled release of paraquat from surface-modified zeolite Y. **Microporous and Mesoporous Materials**. 88: 312-318.

CHAPTER IV

PARAQUAT ADSORPTION ON ZEOLITE X IN SODIUM FORM AND ALUMINIUM MCM-41

Abstract

The aim of this chapter is to determine paraquat adsorption capacity of zeolite NaX and Al-MCM-41 (with Al content of 10, 15, 20 and 25 wt. %). All adsorbents were synthesized by hydrothermal method using rice husk silica. The NaX structure and mesoporous structure of Al-MCM-41 were confirmed by X-ray diffraction. Surface area of each adsorbent, determined by N_2 adsorption-desorption analysis was higher than 650 m^2/g. Al content and geometry was determined by X-ray fluorescence and ^{27}Al nuclear magnetic resonance, respectively. Morphology of Al-MCM-41 was studied by transmission electron microscopy and macropores and defects were observed. The paraquat adsorption on all adsorbent was conducted with the concentration ranged from 80 to 560 mg/L. All isotherms fitted well with Langmuir model. The adsorption capacity from NaX was 120.3 mg/g-adsorbent. From Al-MCM-41, the 10%Al-MCM-41 gave the lowest capacity of 51.6 mg/g-adsorbent and the other samples had adsorption capacity of 66 mg/g-adsorbent.

4.1 Introduction

Paraquat is used widely in Thailand including Nakhon Ratchasima province which has the largest area of cassava cultivation. However, paraquat is highly toxic which mention in Chapter III. There are several reports that paraquat was misused as a suicide agent which causes death when swallowed (National Institutes of Health, 2014). A convenient method which was used in previous work is adsorption.

Paraquat removal by adsorption on RHS and porous materials synthesized from RHS including zeolite NaY, NaBEA and MCM-41 was reported in previous work (Rongchapo, Sophiphun, Rintramee, Prayoonpokarach, and Wittayakun, 2013). The adsorption capacity increased with Al content in the following order: NaY > NaBEA > MCM-41 > RHS. The proposed mechanism was ion exchange. To further improve the adsorption capacity, a zeolite with higher Al content was investigated in this work. Zeolite NaX was selected because it has similar structure to NaY but with higher Al content. Moreover, improvement in paraquat adsorption on MCM-41 was investigated. Although MCM-41 had lower adsorption capacity than zeolites, it was the best adsorbent for blue dye in the commercial paraquat (Rongchapo et al., 2013). Thus, it is still worthwhile to improve its adsorption capacity for paraquat. This could be achieved by adding Al into the framework of MCM-41.

4.2 Experimental

4.2.1 Synthesis of NaX and Al-MCM-41

Zeolite NaX was synthesized by hydrothermal method using sodium silicate and alumina trihydrate solutions with a method modified from Robson (2001) and Khemthong et al. (2007). Sodium silicate solution was prepared by slowly adding 13.7 g of RHS into 50 mL of 5.5 M NaOH solution under magnetic stirring. Alumina source was prepared by adding 24.4 g of alumina trihydrate into 25 mL of 25 M NaOH solution under magnetic stirring at 100 °C until dissolved, cooled to 25 °C and mixed with 50 g of distilled water. The sodium silicate solution (55 g) and alumina trihydrate solution (25 g) were separately mixed with 153 mL of 1.4 M NaOH solution. Then, both solutions were quickly mixed together, stirred for 30 min, transferred into a polypropylene bottle, capped and sealed with paraffin film. Crystallization was carried out at 90 °C for 14 h; the sample was cooled down to room temperature and washed with distilled water and dried at 100 °C overnight.

Al-MCM-41 with various Al contents were synthesized using sodium silicate from RHS, hexadecyltrimethylammonium bromide (CTAB, ≥ 99 %w/w, Acros) and sodium aluminate with a method modified from literatures (Chen et al., 1997; Preethi et al., 2008). A template solution was prepared by dissolving 4 g of CTAB in 30 mL of distilled water. The Al-MCM-41 was synthesized by hydrothermal method using a gel containing 10, 15, 20 and 25 wt. % of Al. The gel was prepared by adding the CTAB solution to the sodium silicate solution under stirring 30 min followed by adding sodium aluminate solution, also under stirring until a complete mixing was achieved. The mixture pH was adjusted to 9 by 2 M H_2SO_4, transferred into a Teflon-lined stainless steel autoclave and crystallized at 110

°C for 72 h. After cooled down to room temperature, the solid was washed with distilled water, separated by centrifugation, dried at 100 °C overnight and calcined at 600 °C for 6 h.

4.2.2 Characterization of NaX and Al-MCM-41

The phases of NaX and Al-MCM-41 samples were confirmed by powder XRD using a Bruker D8 ADVANCE with Cu K_α radiation at 40 kV and 40 mA. Si, Al and Na content in the Al-MCM-41 was determined using energy dispersive X-ray fluorescence (EDXRF) spectrometer (Oxford ED2000). The N_2 adsorption-desorption isotherms were obtained from a Micromeritics ASAP 2010 at liquid N_2 temperature. The samples were degassed at 300^oC under vacuum for 8 h before the measurement. Surface area and micropore volume were calculated with BET and t-plot method, respectively. Morphology of Al-MCM-41was studied by was studied by TEM (Tecnai G20 LaB6, FEI-2012) with an accelerating voltage of 200 kV. The sample was suspended in absolute ethanol, dropped on carbon-coated copper grid and brought to dryness. Moreover, the Al-MCM-41 samples were analyzed by ^{27}Al MAS NMR using Bruker Avance III 500 MHz.

4.2.3 Adsorption activity

Adsorption experiment and calculation was conducted with a procedure described by Rongchapo et al. (2013). In a 125 mL PP bottle, 0.05 g of adsorbent was added into 20 mL of paraquat solution in the concentration range of 80 - 560 mg/L. The mixture was stirred for a given time at room temperature. After the adsorption period, the solution was separated by filtration using a 0.45 µm nylon syringe filter. The filtrate was analyzed for paraquat using UV-Vis spectrophotometer

(Varian Cary 1E) at λ_{max} of 257 nm, respectively. The Langmuir and Freundlich isotherms were used to explain paraquat adsorption on NaX and Al-MCM-41.

4.3 Results and discussion

4.3.1 Characteristic of NaX and Al-MCM-41

The XRD pattern of NaX and Al-MCM-41 are shown in Figure 4.1a and 4.1b, respectively. Characteristic XRD peaks of NaX were sharp and strong indicating that the obtained NaX had high crystallinity. The hkl of strong peaks are assigned by comparing with simulated powder XRD pattern of hydrated NaX (Treacy and Higgins, 2001). The XRD patterns of Al-MCM-41 (Figure 4.1b) were similar to those in the literatures (Chen et al., 1997; Preethi et al., 2008). The peaks of alumina were not observed indicating a good dispersion of Al. As the Al content increased, the peak intensities were lower. This could be from either the less uniform structure or secondary scattering from oxides of aluminum. Moreover, the main peak shifted slightly to higher degree with Al loading indicating the decreased pore and successive Al construction in structure. Similar observation was reported by Preethi et al. (2008) from Al-MCM-41 with Si/Al ratio of 25, 50, 75 and 100 and Chen et al. (1997) from Al-MCM-41 with Si/Al ratio of 10, 50, 100 and ∞. This result indicated the downside of Al addition to the formation of mesoporous structure.

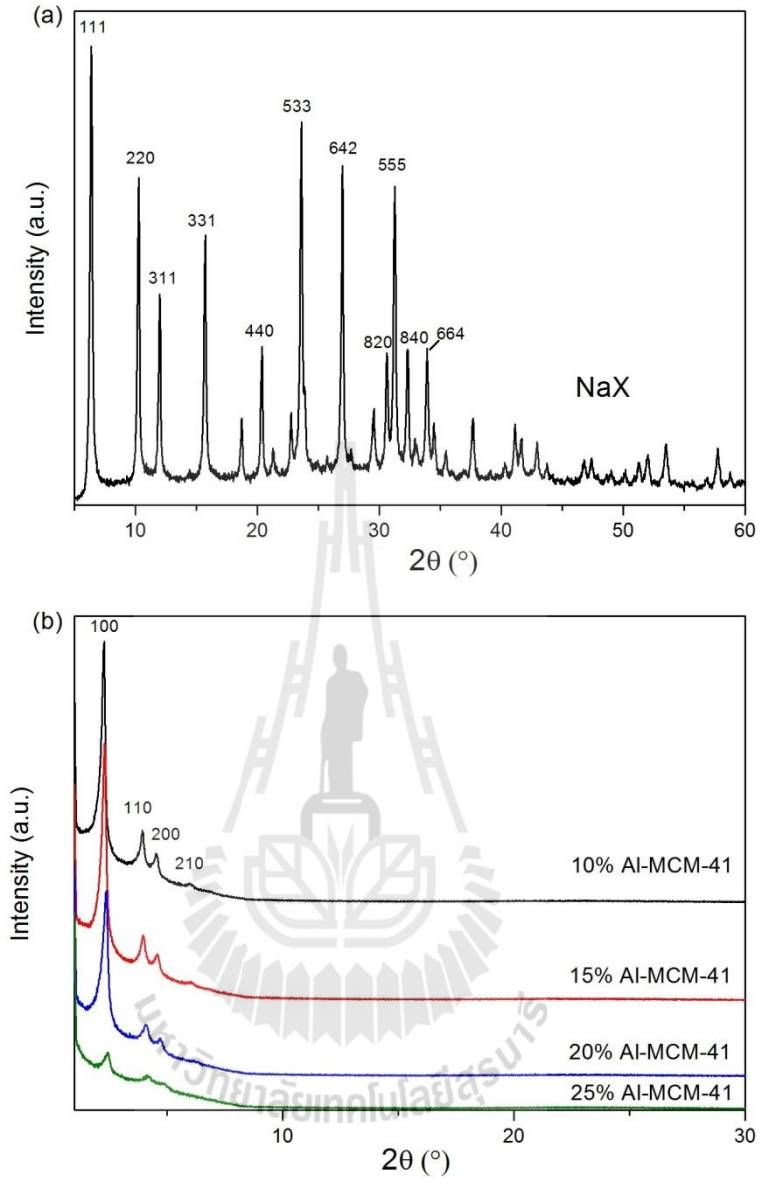

Figure 4.1 XRD pattern of NaX showing hkl of the strong peaks (a) and Al-MCM-41 with Al amount of 10, 15, 20 and 25 wt. % (b). The peaks in the pattern of Al-MCM-41 correspond to the plane 100, 110, 200 and 210.

N_2 adsorption-desorption isotherms of NaX and Al-MCM-41 is shown in Figure 4.2a and 4.2b, respectively. The isotherm of NaX was type I which is a characteristic of microporous material such as zeolite. The uptake volume increased rapidly at the beginning due to adsorption mainly in micropores and on external surface area. Then, the adsorption became nearly constant indicating complete monolayer coverage. The isotherm of all Al-MCM-41 samples (Figure 4.2b) was type IV. The rapid uptake at low relative pressure indicated monolayer coverage and the gradual increase afterward indicated multilayer adsorption. An increase at the relative pressure between 0.25 and 0.45 corresponded to condensation in mesopores (F. Rouquerol, J. Rouquerol, and Sing, 1999). A hysteresis loop at the relative pressure of 0.4 - 1.0 indicated the presence of macropore. This hysteresis loop was not observed in Al-free MCM-41 (Rongchapo et al., 2013). The adding Al to the synthesis gel could cause defect in the Al-MCM-41. The hysteresis loop in high pressure range was also reported in Al-MCM-41 synthesized from alkaline treated ZSM-5 (Zhang and Yan, 2013). In addition, the work by González, Pesquera, Perdigo´n, and Blanco (2009) showed similar adsorption isotherm from Al-MCM-41 with Si/Al ratio of 20, 30 and 50 but the hysteresis loop was not reported. They also reported that the wall thickness decreased when the Al content increased.

The BET surface areas of NaX and Al-MCM-41 samples are presented in Table 4.1. Their surface areas are in the same range as that of NaY which was 870 m^2/g (Rongchapo et al., 2013). The surface area of 25%Al-MCM-41 was the lowest suggesting the poorest order.

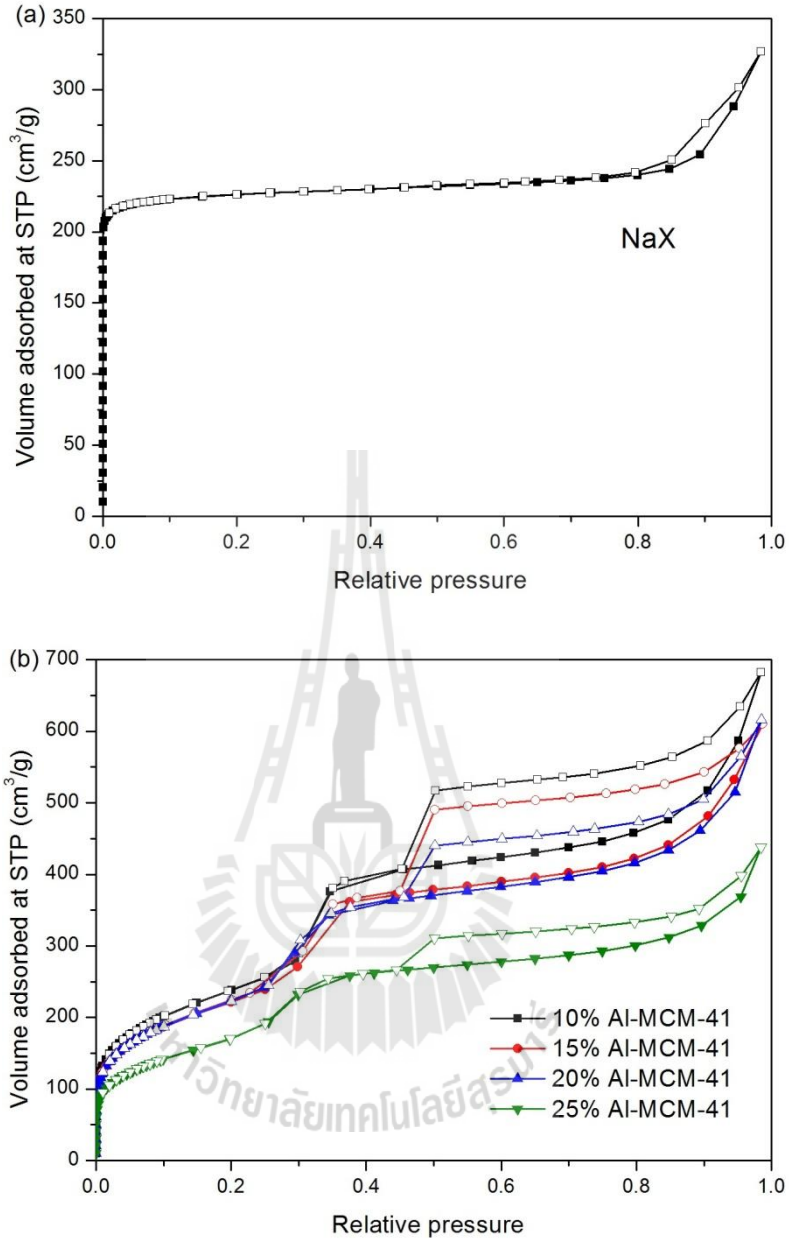

Figure 4.2 Nitrogen adsorption-desorption isotherm of NaX (a) and Al-MCM-41 with Al amount of 10, 15, 20 and 25 wt. % (b). The filled symbols are data from adsorption and the hollow symbols are data from desorption.

The Si/Al and Na/Al ratio of the gel and solid product from element analysis by EDXRF are shown in Table 4.1. The Si/Al values in the solid products are higher than those in the gel indicating that partial amount of Al incorporated to the structure. The Na/Al values from the gel were higher than in the solid. After the synthesis, the solid product was washed thoroughly with water. When an Al atom is in tetrahedral structure, a negative charge is generated and a balancing cation is needed. Thus, the Na/Al ratio is one. In our cases, the Na/Al ratio of one was obtained only from 20%Al-MCM-41. In the other samples, Na cation probably bonded to the surface by replacing proton in the silanol groups.

Table 4.1 Data of element content and surface area of all Al-MCM-41.

Sample	Gel Si/Al ratio	Si/Al ratio from XRF	Gel Na/Al ratio	Na/Al ratio from XRF	BET Surface area (m^2/g)
10%Al-MCM41	7.78	10.92	8.84	2.78	847
15%Al-MCM41	5.18	8.77	6.47	1.65	805
20%Al-MCM41	3.88	7.48	5.02	1.09	832
25%Al-MCM41	3.11	5.90	4.15	0.53	654
NaX	1.24	1.27	15.6	1.37	735

Figure 4.3 displays ^{27}Al MAS NMR spectra of the Al-MCM-41. The main peak was observed around 55 mg/L corresponding to tetrahedral coordinated aluminum (Chen et al., 1997; González et al., 2009). The intensity increased with Al content consistent with the XRF results.

TEM images of Al-MCM-41 are shown in Figure 4.4. Ordered hexagonal mesostructure, defects and macropores were observed from all samples, confirming that loading with Al lower the sample uniformity.

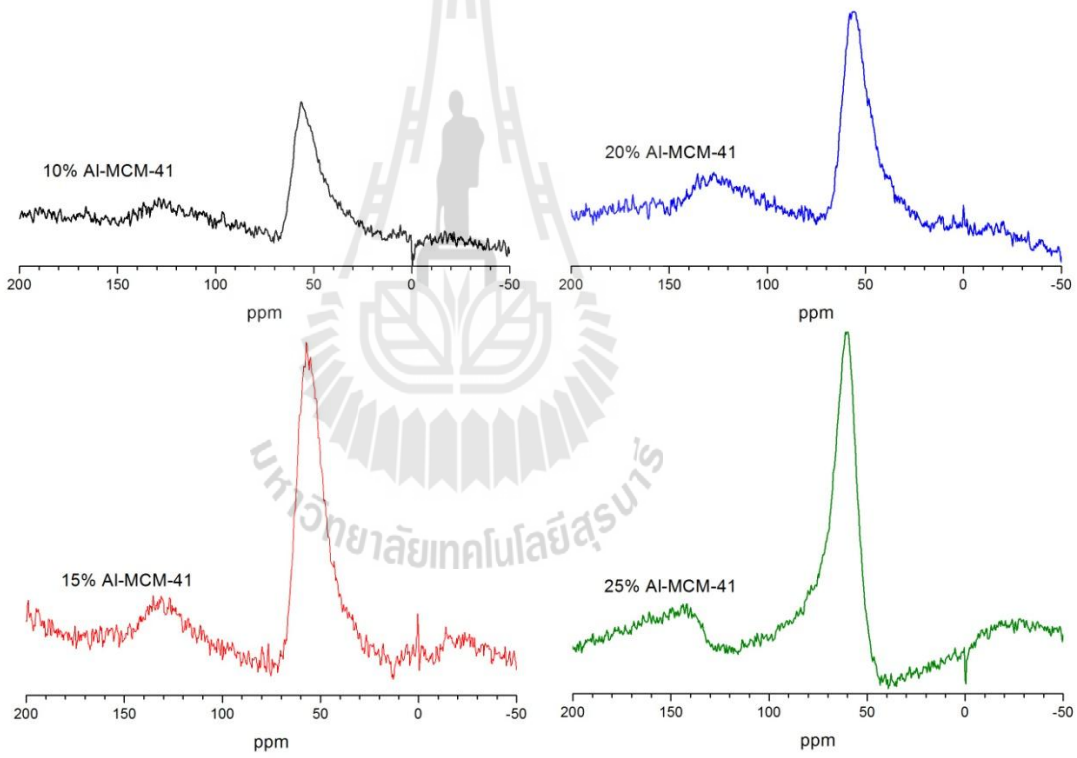

Figure 4.3 ^{27}Al MAS NMR spectrum of the Al-MCM-41 with Al amount of 10, 15, 20 and 25 wt. %.

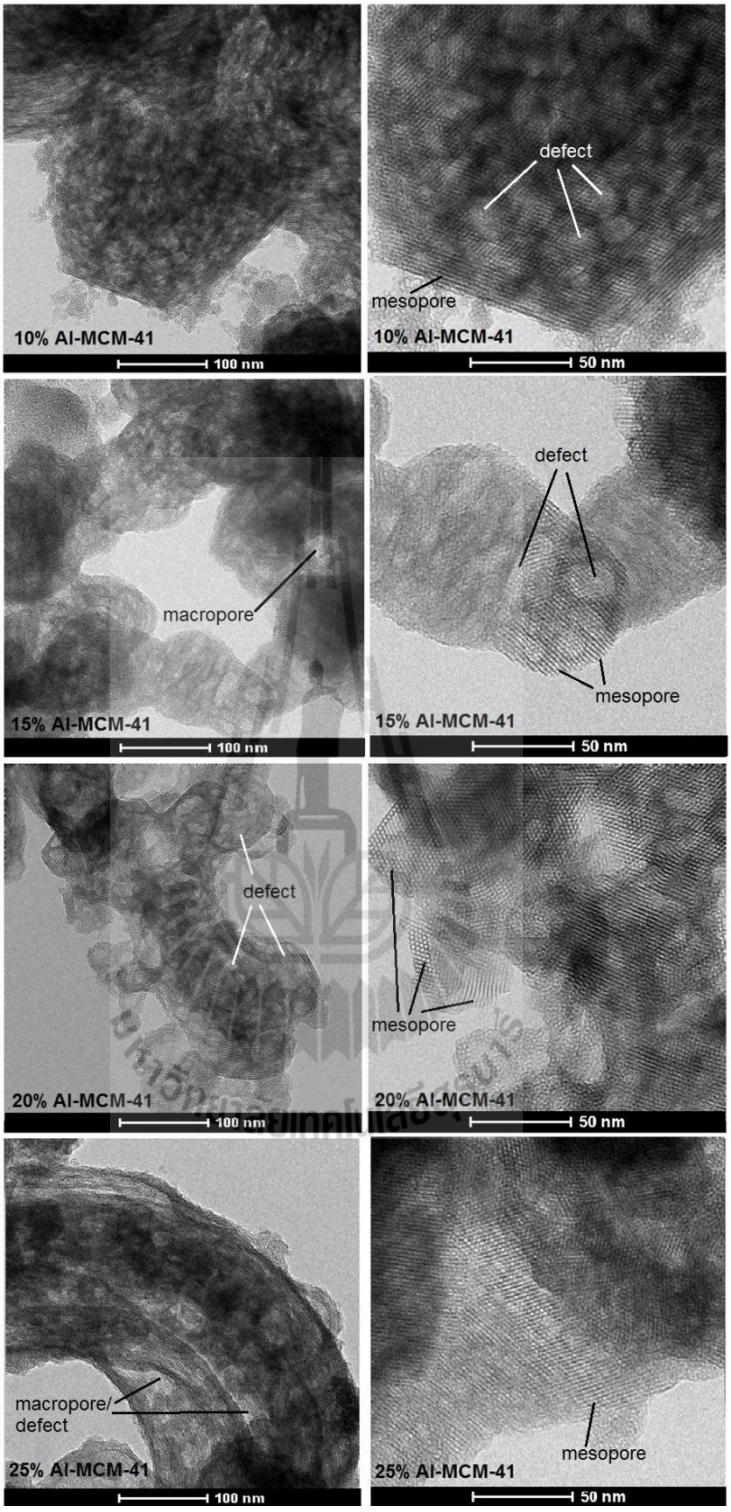

Figure 4.4 TEM images of Al-MCM-41 with Al amount of 10, 15, 20 and 25 wt. %.

4.3.2 Paraquat adsorption on NaX and Al-MCM-41

Paraquat adsorption isotherm on NaX and Al-MCM-41 are shown in Figure 4.5. The adsorption on NaX was higher than all Al-MCM-41 in all concentration. NaX had higher Al content and thus, a higher ion exchange capacity than Al-MCM-41. For Al-MCM-41, the adsorption capacities from all Al-MCM-41 were higher than that from MCM-41 (Rongchapo et al., 2013). When Al is incorporated in the framework of MCM-41, a charge balancing cation is required and the cation can be exchange with paraquat. 10%Al-MCM-41 had the lowest adsorption capacity due to the lowest Al content. The adsorption capacity of 15%Al-MCM-41 and 20%Al-MCM-41 were similar because their surface area and Al content were simialr. Although 25%Al-MCM-41 had the highest Al content, its surface area was the lowest. Thus, it gave similar adsorption capacity to other Al-MCM-41.

When the data from each sample was fitted with Langmuir and Freundlich isotherms, Langmuir model gave R^2 coefficient more than 0.99 (Table 4.2). The maximum capacities calculated from Langmuir equation are included in table 4.2. Compared to our previous work (Rongchapo et al., 2013), the adsorption capacities from NaX and Al-MCM-41 were still lower than that from NaY. Although NaX has the same structure to NaY and has higher Al content, the surface area of NaX was lower than that of NaY. The lower surface area implied the lower number of cavity which contains the adsorption sites. For Al-MCM-41, the addition of Al into the framework of MCM-41 increased the adsorption sites but the Al content was still much lower than that in NaX. However, higher Al content was not suitable because it could lead to more defect and lower surface area as seen in 25%Al-MCM-41. Another strategy to improve the adsorption of MCM-41 was reported by Brigante and

Avera (2014) by the use of mixed surfactant to produce MCM-41 with uniform particle size.

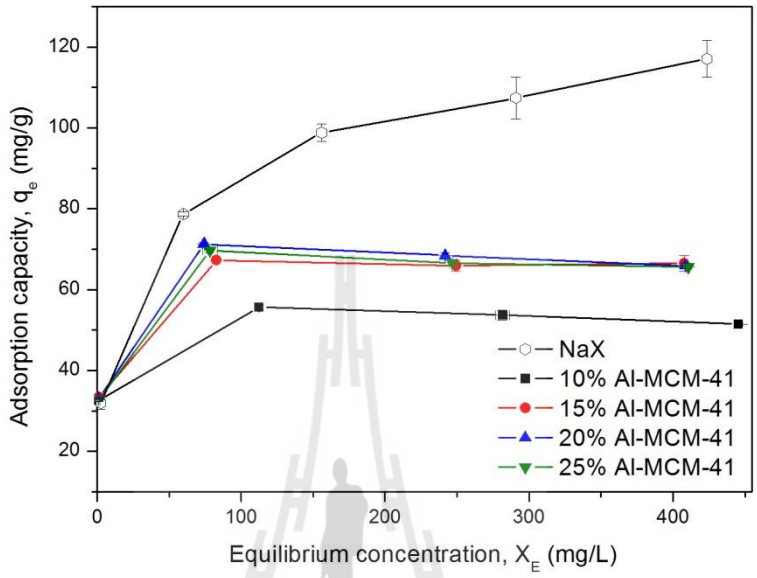

Figure 4.5 Isothermal adsorption of paraquat (analytical reagent grade) on NaX and Al-MCM-41 at room temperature. Each experiment was done in triplicate with 0.05 g of NaY and 20 mL of 80 - 560 ppm paraquat solutions. All isotherms fit well with Langmuir model.

Moreover, NaX was used for the adsorption of both chemical grade and commercial paraquat, with various initial concentrations. The difference is that the commercial contained blue dye which may interfere the paraquat adsorption. Figure 4.6 shows the adsorption of both paraquat samples on NaX. The monolayer adsorption capacity calculated from Langmuir equation of chemical grade paraquat solution was 120.3 mg/g-adsorbent and commercial grade paraquat solution was

113.7 mg/g. From the similar adsorption capacity, molecules of blue dye unlikely affected the paraquat adsorption on NaX.

Table 4.2 Correlation coefficient (R^2) from Freundlich and Langmuir model, and maximum adsorption capacity of paraquat adsorption from Langmuir model.

adsorbents	**Freundlich**	**Langmuir**		**Reference**
	R^2	**R^2**	**Maximum capacity (mg/g-adsorbent)**	
NaY	0.8343	0.9997	185.2	Rongchapo et al., 2013
NaX	0.9912	0.9940	120.3	This work
MCM-41	0.8110	0.9859	21.3	Rongchapo et al., 2013
10%Al-MCM41	0.8853	0.9986	51.6	This work
15%Al-MCM41	0.9220	0.9982	66.4	This work
20%Al-MCM41	0.8753	0.9991	66.1	This work
25%Al-MCM41	0.8923	0.9997	65.6	This work
MCM-41 (from mixed templates)	N/A	1.00	77.4	Brigante and Avena, 2014

N/A : Not available

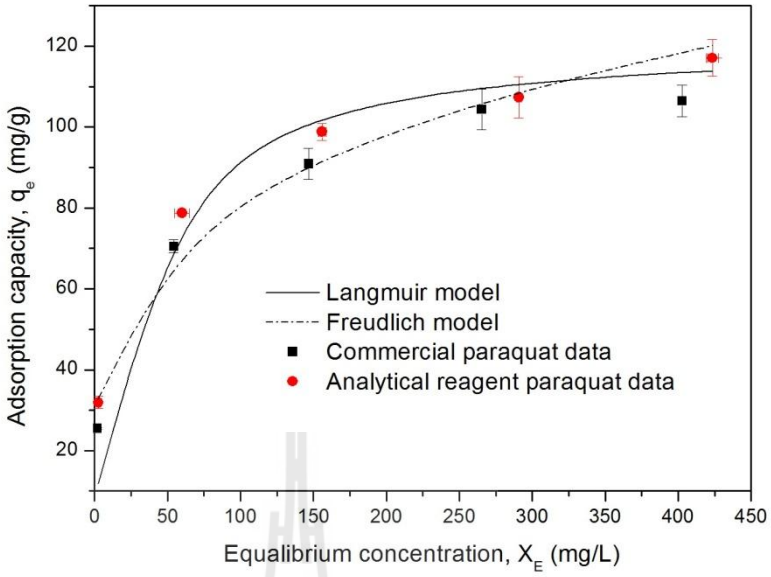

Figure 4.6 Isothermal adsorption of analytical reagent paraquat and commercial paraquat onto NaX at room temperature. Experimental were done with 0.05 g of NaX and 20 mL of various initial concentration at room temperature for 1 h.

4.4 Conclusions

Zeolite NaX was synthesized by hydrothermal method using rice husk silica. Its structure was confirmed by XRD. The surface area determined from N_2 adsorption-desorption was 735 m^2/g and the Si/Al ration determined by XRF was 1.27. The paraquat adsorption capacity from NaX was 120.3 mg/g-adsorbent.

Al-MCM-41 with various Si/Al ratios was synthesized by hydrothermal method by adding Al source to the synthesis gel. The mesoporous structure was confirmed by XRD, N_2 adsorption-desorption and TEM. The Si/Al ratio was determined by XRF. The tetrahedral coordination of Al was confirmed by ^{27}Al MAS NMR. Moreover, macropores and defect was observed in TEM images. The paraquat adsorption

capacity from all Al-MCM-41 was lower than zeolite NaX. The paraquat adsorption isotherm on NaX and Al-MCM-41 fitted well with Langmuir model.

4.5 References

Brigante, M., and Avera, M. (2014). Synthesis, characterization and application of hexagonal mesoporous silica for pesticide removal from aqueous solution. **Microporous and Mesoporous Materials**. 191: 1-9.

Chen, X., Huang, L., Ding, G., and Li, Q. (1997). Characterization and catalytic performance of mesoporous molecular sieves Al-MCM-41 materials. **Catalysis Letters**. 44: 123-128.

González, F., Pesquera, C., Perdigo´n, A., and Blanco, C. (2009). Synthesis, characterization and catalytic performance of Al-MCM-41 mesoporous materials. **Applied Surface Science**. 255: 7825-7830.

Khemthong, P., Prayoonpokarach, S., and Wittayakun, J. (2007). Synthesis and characterization of zeolite LSX from rice husk. **Suranaree Journal of Science and Technology**. 14: 367-379.

National Institutes of Health. (2014). **MedlinePlus.** [On-line] Available: http://www.nlm.nih.gov/medlineplus/ency/article/001085.htm.

Preethi, M. E. L., Revathi, S., Sivakumar, T., Manikandan, D., Divakar, D., Rupa, A. V., and Palanichami, M. (2008). Phenol Hydroxylation Using Fe/Al-MCM-41 Catalysts. **Catalysis Letters**. 120: 56-64.

Robson, H. (ed) (2001). **Verified Syntheses of Zeolitic Materials 2nd Revised Edition**. [On-line] Available: http://www.iza-online.org/synthesis.

Rongchapo, W., Sophiphun, O., Rintramee, K., Prayoonpokarach, S., and Wittayakun, J. (2013). Paraquat adsorption on porous materials synthesized from rice husk silica, **Water Science and Technology**. 68: 863-869.

Rouquerol, F., Rouquerol, J., and Sing, K. (1999). **Adsorption by Powders and Porous Solids**. London: Academic Press.

Treacy, M. M. J., and Higgins, J. B. (eds) (2001). **Collection of Simulated XRD Powder Patterns for Zeolites 4th Revised Edition**. London: Elsevier Store.

Zhang, Z., and Yan Z. (2013). Highly hydrothermally stable Al-MCM-41 with accessible void defects, **Journal of Porous Materials**. 20: 309-317.

CHAPTER V

COMPREHENSION OF PARAQUAT ADSORPTION ON FAUJASITE ZEOLITE Y AND X IN SODIUM FORM

Abstract

This chapter reports nature of paraquat adsorption on zeolite NaY which had the highest paraquat adsorption capacity and NaX which had a higher Al content than NaY. The bare and paraquat containing zeolites (PQY and PQX) were characterized by XRD, N_2 adsorption-desorption analysis, FTIR and MAS NMR. The paraquat adsorption did not change the zeolite structure. Paraquat adsorbed in micropores, resulting in a decrease of the zeolite surface area. The presence of paraquat was confirmed by FTIR. Moreover, results from ^{23}Na MAS NMR indicated that interaction of Na^+ cation in NaX was stronger than that in NaY making it less exchangable with paraquat.

5.1 Introduction

One of the most used pesticides in Nakhon Ratchasima is a herbicide paraquat. It is a toxic compound (Suntres, 2002; USEPA, 1997) with a high solubility and not degradable by light. It easily contaminates and accumulates in surface water (Pateiro-Moure et al., 2010). Paraquat can be removed by adsorption on various porous materials (Brigante and Schulz, 2011; Ibrahim and Haneen, 2009; Rongchapo et al.,

2013; Rongchapo, Deekamwong, Loiha, Prayoonpokarach, and Wittayakun, 2015; Nur et al., 2005).

In Chapter III, paraquat adsorption was studied on porous adsorbents synthesized from rice husk silica (RHS) including RHS, mesoporous silica MCM-41, Zeolite NaY and NaBEA. The adsorption capacities were in the following order: NaY > NaBEA > MCM-41 > RHS and seemed to depend on the Al content in the adsorbents. The maximum adsorption capacity was obtained from NaY with the value 185.2 mg/g-adsorbent. The adsorption of paraquat occurred through cation exchange (Rongchapo et al., 2013). In Chapter IV, an attempt to increase the adsorption capacity was done on adsorbents with a higher Al content including Al-MCM-41 and zeolite NaX. Since NaX had a higher Al content than NaY, it was expected to adsorb paraquat with higher than NaY. However, the maximum adsorption capacity of NaX was around 120 mg/g-adsorbent), much lower than that of NaY (Rongchapo et al., 2015). Base on the adsorption capacity and density of supercages in faujasite structure, the number of paraquat cation in supercage of NaY and NaX were 2 and 1, respectively. Thus, the nature of paraquat adsorption on NaY and NaX was further studied.

Zeolite Y and X have a three-dimensional structure with 0.74 nm diameter window openings connecting 1.3 nm diameter supercages (Guisnet and Gilson, 2002). Zhang et al. (2006) reported that paraquat which has a dimension of 1.34 x 0.64 x 0.34 nm can be readily ion-exchanged into the zeolite Y. A similar behavior was expected from zeolite X. The Si/Al ratios of NaY are 1.5-3.0 in zeolite Y and those of NaX are 1.5 > x > 1.0 (Guisnet and Gilson, 2002). Although NaX has higher exchange capacity (lower Si/Al ratio) than NaY, it had a lower paraquat adsorption

capacity (Rongchapo et al., 2013; Rongchapo et al., 2015). Thus, it was an objective of this work to compare characteristic of bare zeolites (NaY and NaX) and those containing paraquat (PQY and PQX) to understand the nature of adsorption.

5.2 Experimental

5.2.1 Chemical and materials

Paraquat, commercial grade (27.6 %w/v, Masda) was used in the adsorption. NaY and NaX were used as adsorbents were synthesized as described in Chapter III and IV. Zeolites containing paraquat (PQY and PQX) were prepared by adding 1.0 g of adsorbent into 1000 ppm of paraquat solution and stirred at room temperature for 60 min. The adsorbent was separated, washed with 5 L of distilled water and dried at 90 ^{o}C, 24 h.

5.2.2 Characterization

Phase and structure of zeolite were confirmed by powder X-ray diffraction (XRD) using a Bruker D8 ADVANCE with Cu K_{α} radiation at 40 kV and 40 mA. The N_2 adsorption-desorption analysis was done at relative pressure from 0.01 to 0.99 on a Micromeritics ASAP 2010 analyzer. The samples were degassed at 300 ^{o}C for bare adsorbents and 150 ^{o}C for paraquat containing adsorbents, both under vacuum for 8 h before the measurement. The surface area was calculated from BET method. External surface area and micropore area were calculated with t-plot method. A product with the highest degree of transformation was characterized further by Fourier transform infrared, (FTIR) using a Bruker Tensor 27 FTIR with ATR mode. IR spectra were in the range of 4,000 cm^{-1} to 300 cm^{-1} with a resolution of 2 cm^{-1}.

Moreover, the NaY and NaX samples were analyzed by ^{23}Na and ^{27}Al MAS NMR using Bruker Avance III 500 MHz.

5.3 Results and discussion

5.3.1 XRD patterns

XRD patterns of NaY, NaX, PQY and PQX are shown in Figure 5.1. Main peaks of PQY and PQX were similar to those of the bare zeolites (Rongchapo et al., 2013; Rongchapo et al., 2015). XRD results indicated that paraquat adsorption did not change the zeolite structure.

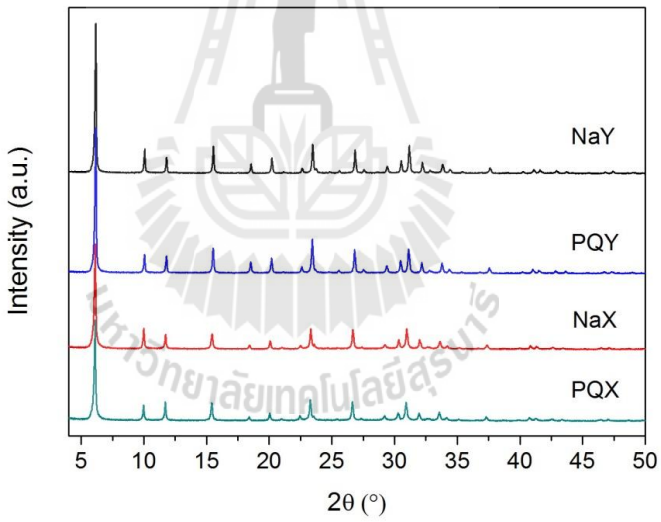

Figure 5.1 XRD patterns of bare zeolites (NaY and NaX) and paraquat adsorbed on adsorbent zeolites (PQY and PQX).

5.3.2 N_2 adsorption-desorption isotherms

N_2 adsorption-desorption isotherms of all samples are shown in Figure 5.2. As reported in Chapter III and IV, the isotherms of bare NaY and NaX were type

I, a characteristic of microporous material (Rongchapo et al., 2013; Rongchapo et al., 2015). After paraquat adsorption, the isotherms of PQY and PQX were still type I but the volume adsorbed amount decreased. This result indicated that paraquat adsorbed mainly in micropores.

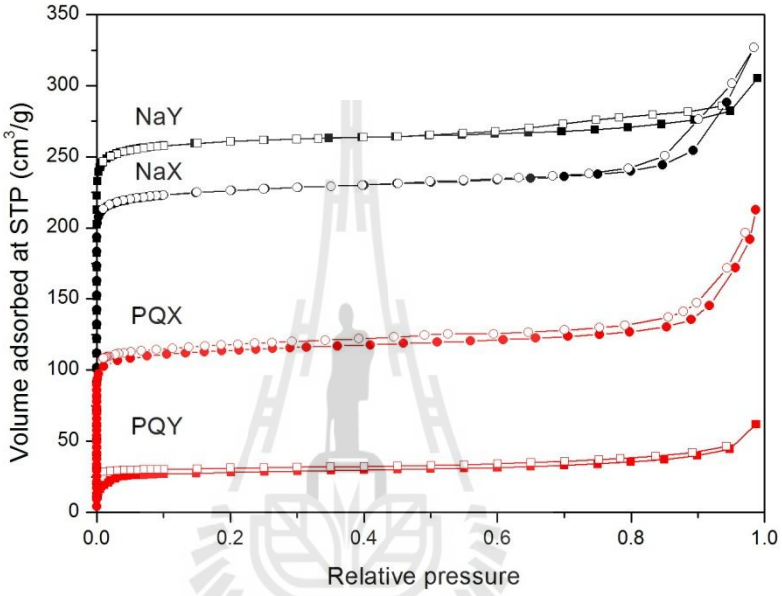

Figure 5.2 Nitrogen adsorption (filled)–desorption (empty) isotherm of bare zeolites (NaY and NaX) and paraquat adsorbed on adsorbent zeolites (PQY and PQX).

Surface areas of the samples are shown in Table 5.1. The surface are of PQY was much lower than that of NaY. The surface area of PQX decreased about a half of that of NaX. The main decrease was from micropore area indicating that it was the adsorption site for paraquat. PQY had a lower surface area than POX, consistent with their paraquat adsorption capacities which were 185 and 120 mg-paraquat per g-adsorbent, respectively.

Table 5.1 The surface area of NaY and NaX with and without paraquat (PQ) obtained from N_2 adsorption-desorption isotherm.

Samples	Surface area [a] (m^2/g)	External surface area [b] (m^2/g)	Micropore surface area [b] (m^2/g)
NaY	870	66	804
PQY	92	24	68
NaX	735	71	664
PQX	381	39	342

[a] BET method

[b] t-plot method

5.3.3 FTIR spectra

Figure 5.3 shows FTIR spectra of the bare NaY and NaX, and paraquat containing ones PQY and PQX. Peaks of functional groups in paraquat were observed in the spectra of PQY and PQX. The peaks positions including 2990, 1639 and 1504 cm^{-1} were assigned to the C-H bond, C=N or C-N bond and C=C bond in aromatic rings, respectively (Hsu and Pan, 2007; Dinis-Oliverira et al., 2008).

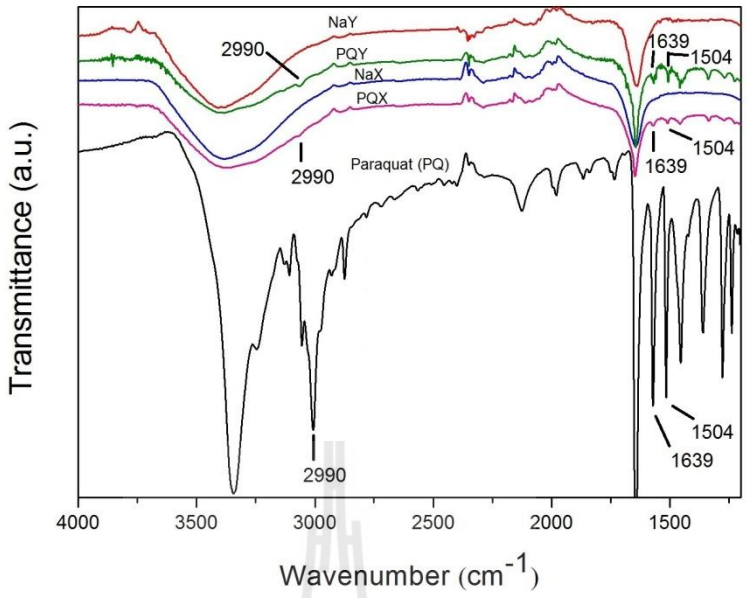

Figure 5.3 FTIR spectra of bare zeolites (NaY and NaX) and paraquat containing zeolites (PQY and PQX).

5.3.4 ^{27}Al MAS NMR

Figure 5.4 displays ^{27}Al MAS NMR spectra of NaY and NaX. The main peak from both samples was observed around 60 ppm corresponding to tetrahedral coordinated aluminum in zeolite (Kondo et al., 2010; Liu and Pinnavaia, 2002). The intensity increased with Al content which was consistent with the XRF results. The result showed that Al site which was active site in the zeolite was not different in NaY and NaX.

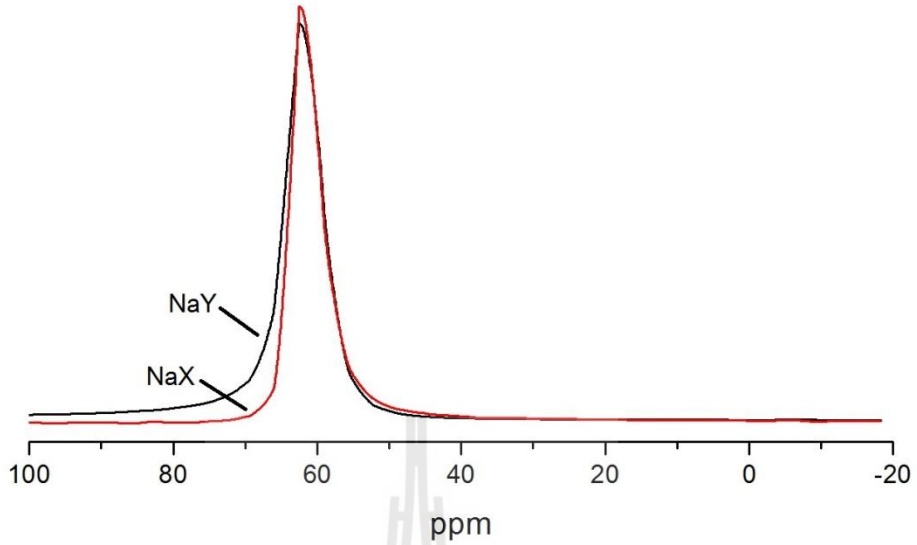

Figure 5.4 ^{27}Al MAS NMR spectrum of bare zeolites (NaY and NaX).

5.3.5 ^{23}Na MAS NMR

Figure 5.5 displays ^{23}Na MAS NMR spectra of NaY and NaX using NaCl as a standard of Na^+. The main peak of NaY was at -8.32 ppm whereas that from NaX was -7.07 ppm. The lower chemical shift was obtained at the higher Si/Al ratio of materials because of the longer distance between Na^+ cation and O atom in the framework (Lee and Stebbins, 2003). Therefore, Na^+ cation in NaY had a weaker interaction with the zeolite framework and could be exchanged more easily than that in NaX.

Feuerstein, Hunger, Engelhardt, and Amoureux (1996) studied characteristic of Na^+ cation in dehydrated NaX and NaY with various Si/Al ratio by ^{23}Na MAS NMR. The results of ^{23}Na MAS NMR show peak of Na^+ cation for site I, I′ and II (Na^+ cations are located near of the six-ring window in the hexagonal prism, β-cage and in the supercage, respectively) in NaY. In contrast, Na^+ cation locations in

NaX were near the idealized site III at the four rings in the supercage. The Na^+ cation at site II and III in supercage could exchange with paraquat (Zhang et al., 2006). However, the interaction of Na^+ cation at site III in NaX was stronger than Na^+ cation at site II in NaX, making it difficult for the exchange. Consequently, NaX had a lower paraquat adsorption capacity than NaY.

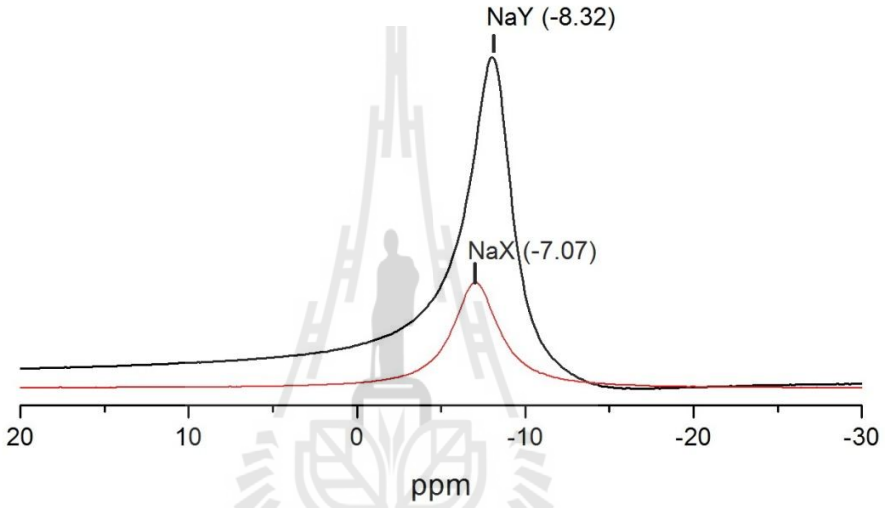

Figure 5.5 ^{23}Na MAS NMR spectrum of bare zeolites (NaY and NaX).

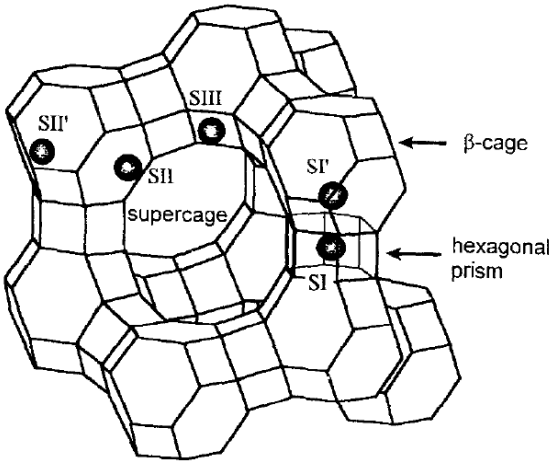

Figure 5.6 Cation positions in faujasite zeolite (Feuerstein et al., 1996).

5.4 Conclusions

Characteristic of bare zeolites (NaY and NaX) and paraquat containing zeolites (PQY and PQX) were studied. XRD pattern of PQY and PQX did not change from those of the bare ones. The N_2 adsorption-desorption isotherm was still in type I but the surface area decreased significantly. The surface areas of PQY and PQX were consistent with the paraquat adsorption capacity. Almost all the micropore area of NaY was occupied by paraquat whereas half of that was occupied in the case of NaX. The presence of paraquat after adsorption was confirmed by FTIR. Paraquat adsorption did not change the structure of NaY and NaX. Moreover, ^{23}Na MAS NMR indicated that interaction of Na^+ cation in NaX was stronger than in NaY, making it less favorable for ion exchange with paraquat.

5.5 References

Brigante, M., and Schulz, P. C. (2011). Adsorption of paraquat on mesoporous silica modification with titania: Effects of pH, ionic strength and temperature. **Journal of Colloid and Interface Science**. 363: 355-361.

Dinis-Oliveira, R. J., Pinho, P. G., Ferreira, A. C. S., Silva, A. M. S., Carlos Afonso, C., Bastos, M. L., Remião, F., Duarte, J. A., and Carvalho, F. (2008). Reactivity of paraquat with sodium salicylate: Formation of stable complexes. **Toxicology**. 249: 130-139.

Feuerstein, M., Hunger, M., Engelhardt, G., and Amoureux, J. P. (1996). Characterisation of sodium cations in dehydrated zeolite NaX by ^{23}Na MAS NMR spectroscopy. **Solid State Nuclear Magnetic Resonance**. 7: 95- 103.

Guisnet, M., and Gilson, J. P. (2002). **Zeolites for cleaner technologies**. London: Imperial College Press.

Hsu, S., and Pan, T. (2007). Adsorption of paraquat using methacrylic acid-modified rice husk. **Bioresource Technology**. 98: 3617-3621.

Ibrahim, K. M., and Jbara, H. A. (2009). Removal of paraquat from synthetic wastewater using phillipsite–faujasite tuff from Jordan. **Journal of Hazardous Materials**. 163: 82-86.

Kondo, J. N., Nishitani, R., Yoda, E., Yokoi, T., Tatsumi, T., and Domen, K. (2010). A comparative IR characterization of acidic sites on HY zeolite by pyridine and CO probes with silica–alumina and γ-alumina references. **Physical Chemistry Chemical Physics**. 12: 11576-11586.

Lee, S. K., and Stebbins, J. F. (2003). The distribution of sodium ions in aluminosilicate glasses: A high-field Na-23 MAS and 3Q MAS NMR study. **Geochimica et Cosmochimica Acta**. 67: 1699-1709.

Liu, Y., and Pinnavaia, T. J. (2002). Aluminosilicate mesostructures with improved acidity and hydrothermal stability. **Journal of Materials Chemistry**. 12: 3179-3190.

Nur, H., Manan, A. F. N. A., Wei, L., Muhid, M. N. M., and Hamdan, H. (2005). Simultaneous adsorption of a mixture of paraquat and dye by NaY zeolite covered with alkylsilane. **Journal of Hazardous Materials**. B117: 35-40.

Pateiro-Moure, M. P., Estévez, M. A., and Gándara, J. S. (2010) Competitive and non-competitive adsorption/desorption of paraquat,diquat and difenzoquat in vineyard-devoted soils. **Journal of Hazardous Materials**. 178: 194-201.

Rongchapo, W., Deekamwong, K., Loiha, S., Prayoonpokarach, S., and Wittayakun, J. (2015). Paraquat adsorption on NaX and Al-MCM-41. **Water Science and Technology**. 71: 1347-1353.

Rongchapo, W., Sophiphun, O., Rintramee, K., Prayoonpokarach, S., Wittayakun, J. (2013). Paraquat adsorption on porous materials synthesized from rice husk silica. **Water Science and Technology**. 68: 863-869.

Suntres, Z. E. (2002). Role of antioxidants in paraquat toxicity. Toxicology. 180, 65-77.

United States Environmental Protection Agency. (1997). Paraquat dichloride, **R.E.D Facts Environmental Protection Agency, office of prevention pesticides, and toxic substances**. Washington DC.

Zhang, H., Kim, Y., and Dutta, P. K. (2006). Controlled release of paraquat from surface-modified zeolite Y. **Microporous and Mesoporous Materials**. 88: 312-318.

CHAPTER VI

PHOTOCATALYTIC DEGRADATION OF PARAQUAT BY USING TITANIUM DIOXIDE ON RICE HUSK SILICA AND ZEOLITE Y IN SODIUM FORM

Abstract

Photocatalysts were prepared by using TiO_2 at 10 and 30 wt. % grafted on rice husk silica (RHS) and zeolite NaY. The photocatalysts were characterized by X-ray diffraction and N_2 adsorption-desorption analysis. TiO_2 in anatase phase was well dispersed on the external surface area of the supports. Paraquat adsorption on the catalysts (determined before the photocatalytic testing) mainly occurred on the supports. The adsorption on TiO_2/NaY was much higher than that on TiO_2/RHS. In photocatalytic testing, both 10 and 30% TiO_2/NaY catalysts were not active probably due to high adsorption of paraquat on the supports. In contrast, both TiO_2/RHS catalysts were active and the best photocatalyst was 30% TiO_2/RHS. The supported catalyst showed a higher activity than the bare TiO_2 indicating the enhancement from the dispersion of RHS. Moreover, the photocatalytic degradation of paraquat on 30% TiO_2/RHS was similar to the commercial TiO_2 (P25) with the same TiO_2 content.

6.1 Introduction

Paraquat has been extensively used as a herbicide. It has a high solubility in water and does not photodegrade in aqueous solution (USEPA, 1994) resulting in its accumulation in water. It is highly toxic and could be removed by adsorption on porous materials (Rongchapo et al., 2013). Although adsorption is an easy process to remove paraquat, the toxicity of paraquat is not reduced. Thus, degradation of paraquat is necessary. Paraquat can be degraded by photocatalysis of titanium dioxide (TiO_2) (Florêncio et al., 2004; Moctazuma et al., 1999). Paraquat could be reduced by excited electrons (e-) and further degraded to other products (Florêncio et al., 2004). TiO_2 is a semiconductor with a band gap energy of 3.2 eV. Since it can be activated by light such as ultraviolet and sunlight, TiO_2 is widely used as a photocatalyst (Sobczyński and Dobosz, 2001). However, TiO_2 has a small particle size, low surface area and high tendency to agglomerate in a suspension, and low adsorption ability for the pollutants (Keneko and Okura, 2002).

Incorporation of an adsorbent with a high surface material such as SiO_2 into TiO_2 could enhance the photocatalytic activity (Vohra and Tanaka, 2003). Previously, the paraquat removal by adsorption on rice husk silica (RHS) and porous materials synthesized from RHS including zeolite NaY, NaBEA and MCM-41 was reported (Rongchapo et al., 2013). RHS and NaY which has the lowest and highest paraquat adsorption capacity, respectively, were used as a supports in this work. Artkla et al. (2009) reported that TiO_2 at 10 wt. % grafted on RH-MCM-41 from tetrabutylorthotitanate (TBOT) had anatase phase which was more active for photocatalytic degradation of methyl orange than Ti-RH-MCM-41 prepared by adding tetrabutyl orthotitanate (TBOT) in a synthetic gel of RH-MCM-41. TiO2 was

obtained only from grafting method and the framework Ti was produced from hydrothermal method. In this work, TiO_2 was prepared with the same precursor, TBOT with grafting method to produce only the active anatase. The TiO_2 precursor which was prepared 10 wt. % (Artkla et al., 2009) and 30 wt. % was incorporated with RHS and NaY to increase paraquat interaction on the surface and improve dispersion of TiO_2, both cases, to promote photocatalysis of paraquat.

6.2 Experimental

6.2.1 Chemicals and materials

Chemicals for the preparation of the RHS and zeolite NaY synthesis were hydrochloric acid (37% HCl, Carlo-Erba), sodium aluminate (~55 – 56% of $NaAlO_2$, Riedel-de Haën), sodium hydroxide (97% NaOH, Carlo-Erba), and rice husk. RHS and NaY were used as a support of photocatalyst which had been prepared follow the procedure described in Chapter III. TBOT (99% $C_{16}H_{36}O_4Ti$, Acros), nitric acid (65% HNO_3, Carlo-Erba) and NaOH were used in TiO_2 synthesis and TiO_2 on support preparations. A commercial TiO_2 powder (P25, Degussa), known as the best photocatalyst, was used as a bench mark for comparison. Paraquat, commercial grade (27.6 %w/v, Masda), was used in the photocatalytic activity.

6.2.2 Preparation of photocatalyst

The preparation of TiO_2 sol was prepared by an acid catalyzed sol-gel formation method modified from the literature (Artkla et al., 2009). Firstly, an appropriate amount of TBOT to produce 10 and 30 wt. %Titania was added gradually to an aqueous solution of 1 M HNO_3 acid (40 mL) under continuous stirring for 1.5-2

h to produce a transparent sol. Subsequently, the mixture was diluted with deionized water and the pH was adjusted to 3 with 1 M NaOH to give a turbid colloid. The required amount of RHS and NaY to produce TiO_2/RHS and TiO_2/NaY was added to the turbid colloid suspension. The resulting mixed suspension was agitated by a magnetic stirrer for another 2 h at room temperature, separated by centrifugation and washed several times with deionized water until the pH of the filtrate was about 6. The resulting TiO_2/RHS and TiO_2/NaY were dried overnight in an oven and calcined in a muffle furnace at 300 °C for 1 h.

6.2.3 Characterization of photocatalysts

Phase and structure were confirmed by powder X-ray diffraction (XRD) using Bruker axs diffractometer D5005 with Cu K_α radiation. The N_2 adsorption-desorption analysis was done on a Micromeritics ASAP 2010 analyzer. The samples were degassed at 300 °C under vacuum for 8 h before the measurement. Surface area was obtained from BET method. Amount of TiO_2 on RHS and NaY was determined using an energy dispersive X-ray fluorescence (EDXRF) spectrometer (Oxford ED2000).

6.2.4 Paraquat adsorption of all catalysts

Paraquat adsorption was done in a 1-L beaker. The system comprised of 0.1 g/L of catalyst concentration and 250 mL of 15 ppm paraquat solution. The mixture was stirred at room temperature to monitor at 5, 10, 15, 30, 45, 60, 90 and 120 min. The adsorbent was separated by a 0.45 μm nylon syringe filter. The paraquat concentration was determined by Ultraviolet-Visible spectrophotometer (Varian Cary 1E) at λ_{max} of 257 nm (Nur et al., 2005; Iglesias et al., 2010).

6.2.5 Photocatalytic testing

The photocatalytic testing was divided into three parts including photolysis of paraquat, optimum catalyst concentration and photocatalytic degradation of paraquat. All experiments were carried out in a one-litre beaker containing 250 mL of 15 ppm paraquat solution and radiated with four 18-W fluorescent black light lamps (Toshiba, with the wavelength range 300-400 nm). In photolysis, paraquat concentration was monitored after illumination without catalyst at 5, 10, 15, 30, 45, 60, 90 and 120 min. From the optimum catalyst concentration, the dispersed solutions were varied at three concentrations: 0.3, 0.1 and 0.05 g/L by using P25 as a standard photocatalyst. The photocatalysis was carried out by stirring 250 mL of 15 ppm paraquat solution with the optimum concentration of catalyst at room temperature. Samples were taken at various times and the catalyst was separated by a syringe filter. The paraquat concentration in the filtrate was determined by a UV-Vis spectrophotometer at λ_{max} of 257 nm.

6.3 Results and discussion

6.3.1 Characterization of photocatalysts

XRD patterns of all prepared catalysts are shown in Figure 6.1. The patterns of both P25 and prepared TiO_2 (Figure 6.1a) show characteristic peaks of TiO_2. Anatase (A) phase, active phase, was observed at 25.32, 37.85, 48.09, and 53.93 degree. Moreover, a strong peak of rutile (R) phase was observed at 27.48 degree (Brigante and Schulz, 2011). P25 has a mixed phase of anatase and rutile (Raj and Viswanathan, 2009). The prepared TiO_2 from sol-gel method showed only the anatase phase. Figure 6.1b shows the XRD patterns of RHS and TiO_2/RHS. RHS shows a

broad peak around 22 degree which is a characteristic of amorphous silica (Rongchapo et al., 2013). The pattern of RHS after grafting with TiO_2 was different. The intensity of the broad peak around 22 degree decreased in the pattern of 10%TiO_2/RHS and peak around 25 degree (anatase phase) was observed from 30%TiO_2/RHS. The XRD patterns of NaY and TiO_2/NaY (Figure 6.1c) also confirmed the structure of NaY after TiO_2 grafting. Peaks of TiO_2 were not observed from 10% and 30%TiO_2/NaY indicating a good dispersion of TiO_2.

N_2 adsorption-desorption isotherms of all prepared catalysts are shown in Figure 6.2. Figure 6.2a shows the isotherm of P25 which was type II, a characteristic of non-porous materials (Raj and Viswanathan, 2009). The isotherm of the prepared TiO_2 was type IV (Zhang et al., 2015), a characteristic of mesoporous materials with a type H2 hysteresis loop which is a characteristic of interconnected pores (Rouquerol et al., 1999). The isotherm of RHS and TiO_2/RHS (Figure 6.2b) indicated that it had broad pore range with both micropores and mesopores. Figure 6.2c shows the isotherm of NaY and TiO_2/NaY. Both isotherms were type I, which is a characteristic of microporous materials (Rongchapo et al., 2013). A type H2 hysteresis loop was observed in the isotherm of 30%TiO_2/NaY indicating pores interconnectivity.

Properties of all prepared catalysts including amount of TiO_2, surface area, external surface area and pore volume are shown in Table 6.1. The mass percentage of TiO_2 confirmed the different content as expected from the preparation. On NaY support, surface area, external surface area and pore volume decreased with the TiO_2 amount indicating that TiO_2 located on both external surface and pore area. On RHS support, the surface area decreased with the TiO_2 amount but the external

surface area increased and the pore volumes were not significantly different. The results indicated that TiO_2 located on the external surface of RHS.

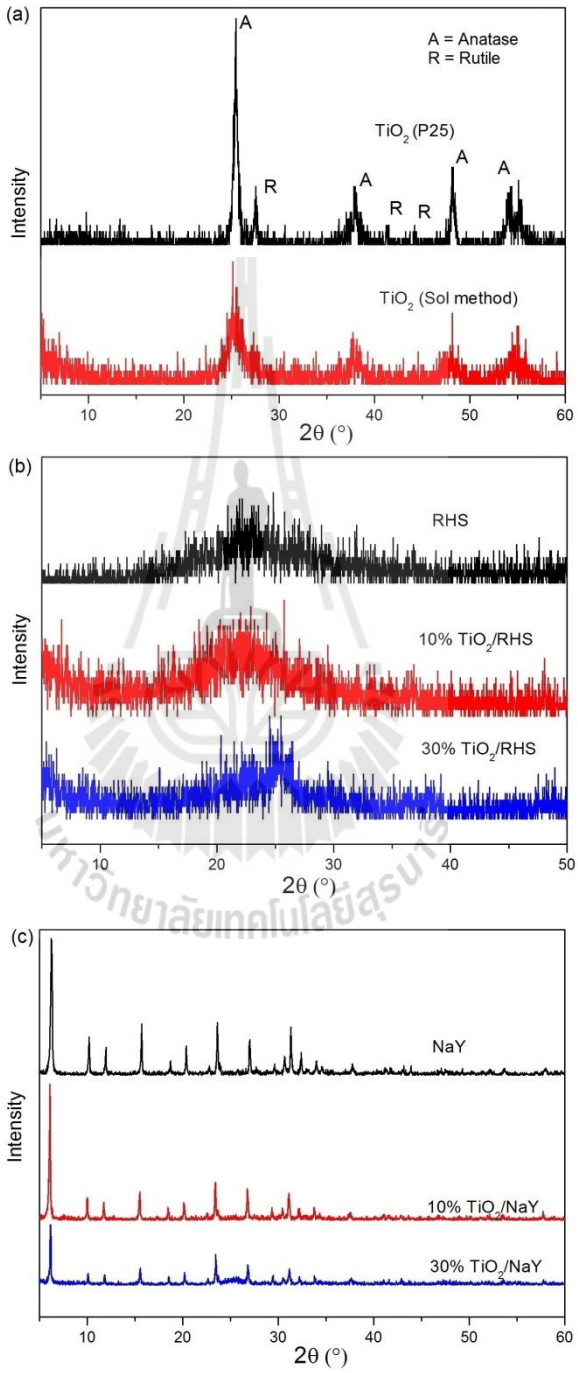

Figure 6.1 XRD patterns of TiO_2 (a), RHS and TiO_2/RHS (b), and NaY and TiO_2/NaY (c).

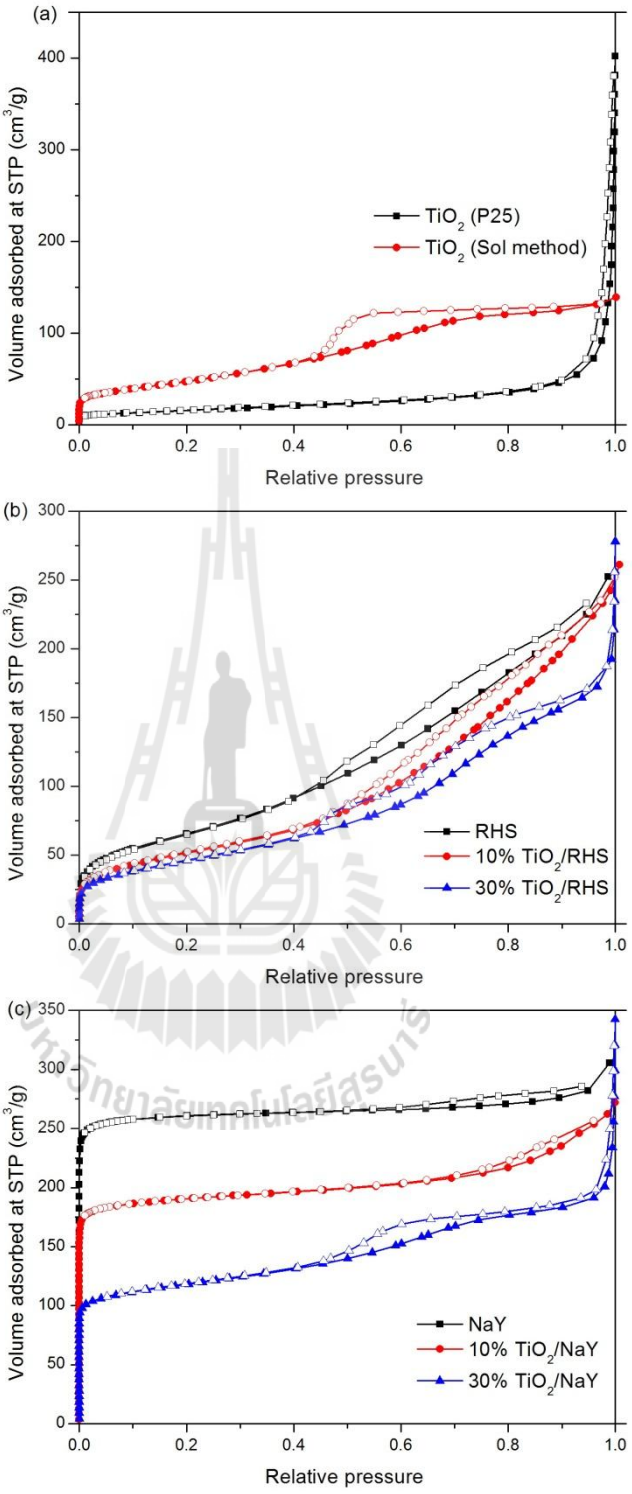

Figure 6.2 Nitrogen adsorption (filled)–desorption (empty) isotherm of TiO_2 (a), RHS and TiO_2/RHS (b), and NaY and TiO_2/NaY (c).

Table 6.1 Properties of supporting material and photocatalysts.

Sample	TiO_2 (%mass) from EDXRF	Surface area [a] (m^2/g)	External surface area [b] (m^2/g)	Pore volume [b] (cm^3/g)
TiO_2 (P25)	100.0	55.3	56.6	0
TiO_2 (Sol-gel method)	100.0	175.5	21.3	0.17
RHS	-	220 [c]	57.6	0.19
10%TiO_2/RHS	9.9	183.5	101.0	0.17
30%TiO_2/RHS	25.9	165.0	60.5	0.16
NaY	-	870 [c]	66	0.37
10%TiO_2/NaY	10.0	673.6	83.3	0.26
30%TiO_2/NaY	33.0	529.1	40.3	0.25

[a] BET method

[b] t-plot method

[c] Rongchapo et al., 2013

6.3.2 Photolysis of paraquat

Figure 6.3 shows paraquat concentration after irradiation with UV light at various times. The concentration was essentially unchanged confirming that paraquat could not be degraded by UV light without the catalyst.

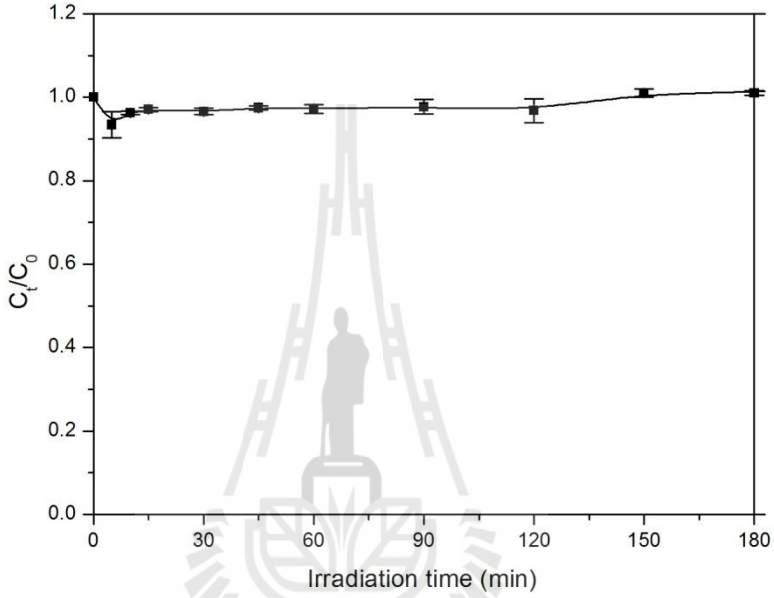

Figure 6.3 Photolysis (degradation with only light) of paraquat under UV light.

6.3.3 Concentration of catalyst

Figure 6.4 shows photocatalytic degradation of paraquat by P25 with various catalyst amounts. The degradation with the catalyst concentration 0.05 g per liter of paraquat (0.05g/L) was slow. The degradations from the concentration 0.1 g/L and 0.3 g/L was similar with a complete degradation in 150 min. Because the less amount of catalyst would cause the less light obstruction, the concentration 0.1 g/L was considered to be more suitable and used in further experiments.

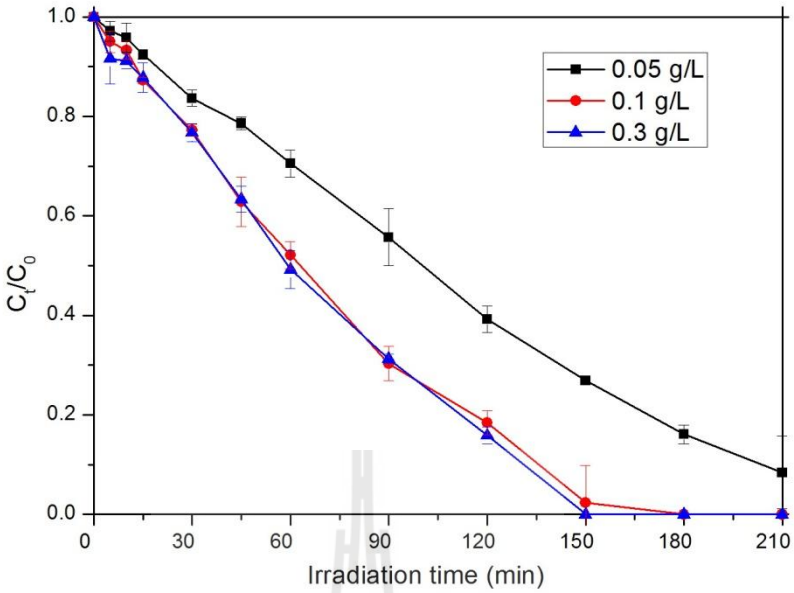

Figure 6.4 Photacatalytic degradation of paraquat by P25.

6.3.4 Activity of photocatalysts with paraquat

Figure 6.5 shows paraquat adsorption on all photocatalysts at various times using 15 ppm paraquat concentration. P25 had the lowest adsorption because it had the lowest surface area. The prepared TiO_2 had the higher adsorption than P25 because it had the higher surface area. The low adsorption on TiO_2 indicated that it was not the main adsorption site for paraquat. The adsorption on all catalysts became nearly constant with time indicating a monolayer adsorption. The NaY-supported catalysts had the higher adsorption than the RHS-supported catalysts. Moreover, the less TiO_2 content gave the higher adsorption ability. The results indicated that adsorption depended on the supporting materials. The adsorption of each sample reached the equilibrium in approximately 60 min. Thus, this time was applied for the dark condition before the irradiation. Moreover, the concentration after adsorption of each catalyst was used as an initial concentration for photocatalytic degradation.

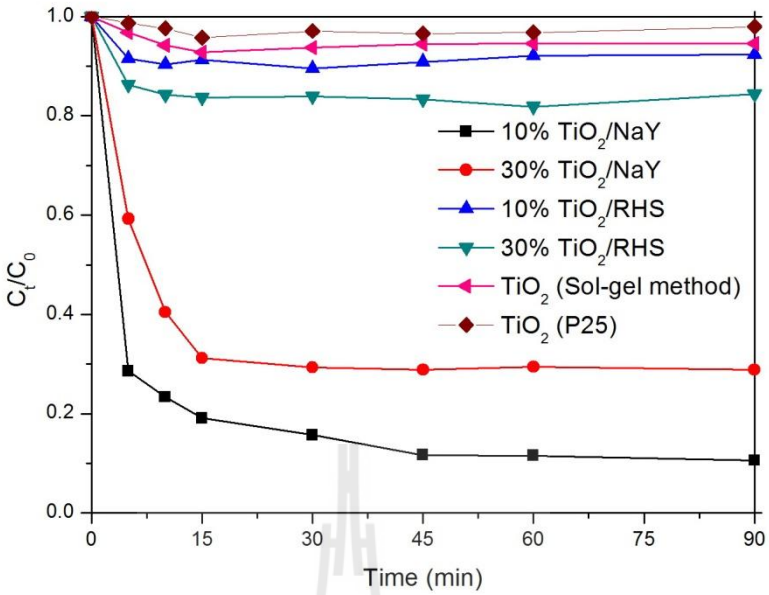

Figure 6.5 Adsorption of paraquat by all catalysts.

Prior to the photocatalytic testing of TiO_2/NaY and TiO_2/RHS, the activity was determined on NaY and RHS for comparison. The degradation was not observed indicating that the bare supports had no contribution to the photocatalysis. Bhattacharyya et al. (2004) reported a similar behavior that zeolite and siliceous materials were not significantly active to remove methyl orange by photodegradation.

Figure 6.6 shows photocatalytic activity of all prepared catalysts. The degradation was not observed from TiO_2/NaY probably due to the high adsorption ability. Paraquat might just act as a transporter for the excited electrons without degradation. The result indicated that NaY which had the high adsorption ability was not a suitable support for the photocatalysts. A slight increase of the paraquat with time indicated that some paraquat was released back to the solution.

On RHS, the 10% TiO_2/RHS did not show the photocatalytic activity probably due to a low TiO_2 loading. The decrease of paraquat concentration was

observed from the test over 30% TiO_2/RHS. Thus, it was the best photocatalyst in this study. In addition, 30% TiO_2/RHS showed a higher activity than the prepared TiO_2. This result indicated the photodegradation activity of TiO_2 could be enhanced by supporting on a material with low adsorption ability.

Finally, comparisons between 30% TiO_2/RHS and TiO_2 from sol-gel synthesis with the standard P25 at the same TiO_2 content are shown in Figure 6.7. The ability of 30% TiO_2/RHS to degrade paraquat was comparable to P25. Both of them showed a complete paraquat removal within 180 min.

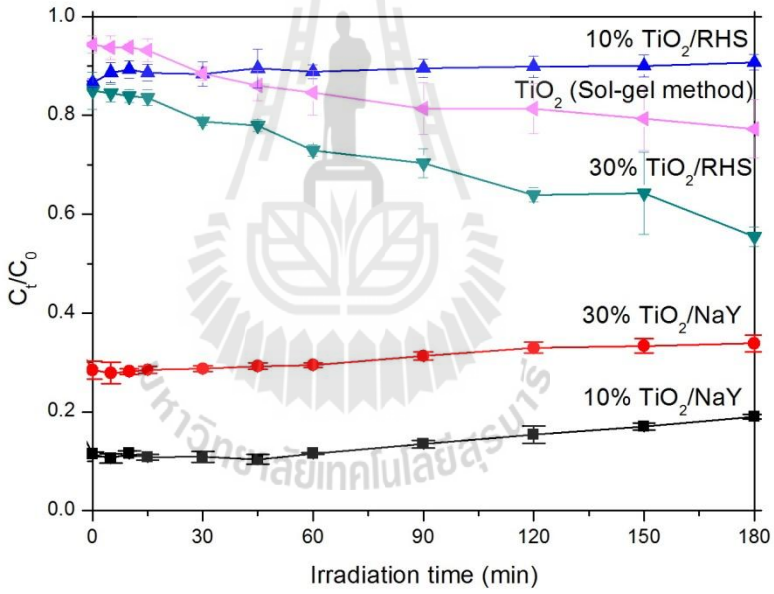

Figure 6.6 Photocatalytic activities of prepared catalysts.

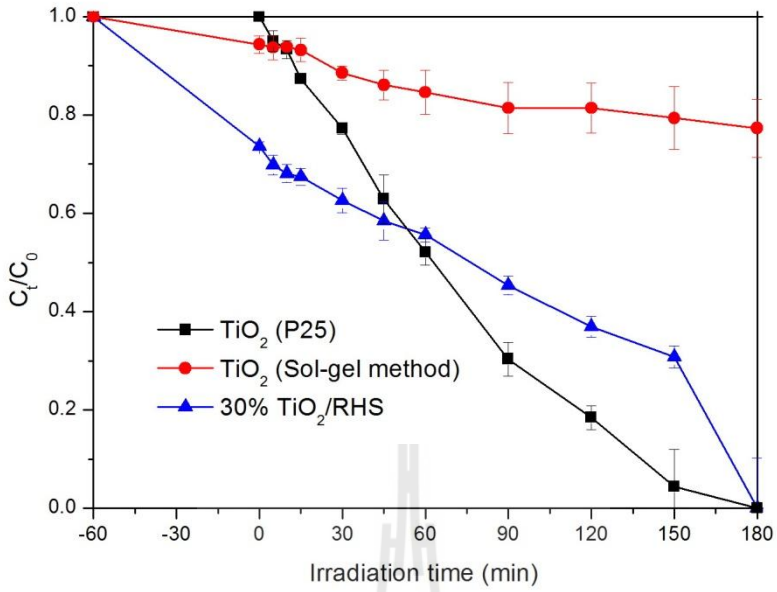

.

Figure 6.7 Comparison of photocatalytic activity at the same TiO_2 content.

6.4 Conclusions

Photocatalysts were prepared by grafting TiO_2 on RHS and NaY. The amount of TiO_2 was 10 and 30 wt.%; the phase of TiO_2 was anatase. The TiO_2/RHS and TiO_2/NaY catalysts had lower surface areas and pore volumes than the parent supports; the more decrease was obtained from the higher TiO_2 loading. Before the photocatalytic testing, paraquat adsorption on the samples were determined. The adsorption on TiO_2/NaY was higher than TiO_2/RHS. The adsorption on TiO_2/NaY decreased with the higher TiO_2 loading. In contrast, the adsorption on TiO_2/RHS increased with the TiO_2 loading. In the photocatalytic testing, TiO_2/NaY catalysts were not active probably due to the high paraquat adsorption. For TiO_2/RHS catalysts, the degradation ability was observed on 30% TiO_2/RHS with the better performance than the un-supported TiO_2. Base on the same TiO_2 content, the photocatalytic

degradation of paraquat on 30% TiO_2/RHS was comparable to the commercial P25, completed in 180 min.

6.5 References

Artkla, S., Wantala, K., Srinameb, B., Grisdanurak, N., Klysubun, W., and Wittayakun, J. (2009). Characteristics and photocatalytic degradation of methyl orange on Ti-RH-MCM-41 and TiO_2/RH-MCM-41. **Korean Journal of Chemical Engineering**. 26: 1556-1562.

Bhattacharyya, A., Kawi, S., and Ray, M. B. (2004). Photocatalytic degradation of orange II by TiO_2 catalysts supported on adsorbents. **Catalysis Today**. 98: 431-439.

Brigante, M., and Schulz, P. C. (2011). Adsorption of paraquat on mesoporous silica modification with titania: Effects of pH, ionic strength and temperature. **Journal of Colloid and Interface Science**. 363: 355-361.

Florêncio, M. H., Pires, E., Castro, A. L., Nunes, M. R., Borges, C., and Costa, F. M. (2004). Photodegradation of diquat and paraquat in aqueous solutions by titanium dioxide: evolution of degradation reactions and characterization of intermediates. **Chemosphere**. 55: 345-355.

Iglesias, A., Lopez, R., Gondar, D., Antelo, J., Fiol, S., and Arce, F. (2010). Adsorption of paraquat on goethite and humic acid-coated goethite. **Journal of Hazardous Materials**. 183: 664-668.

Kaneko, M., and Okura, I. (2002). **Photocatalysis : Science and Technology**. New York: Springer.

Moctezuma, E., Leyva, E., Monreal, E., Villegas, N., and Infante, D. (1999). Photocatalytic degradation of the herbicide “paraquat”. **Chemophere**. 39: 511-517.

Nur, H., Manan, A. F. N. A., Wei, L., Muhid, M. N. M., and Hamdan, H. (2005). Simultaneous adsorption of a mixture of paraquat and dye by NaY zeolite covered with alkylsilane. **Journal of Hazardous Materials**. B117: 35-40.

Raj, K. J. A., and Viswanathan, B. (2009) Effect of surface area, pore volume and particle size of P25 titania on the phase transformation of anatase to rutile. **Indian Journal of Chemistry**. 48A: 1378-1382.

Rongchapo, W., Sophiphun, O., Rintramee, K., Prayoonpokarach, S., and Wittayakun, J. (2013). Paraquat adsorption on porous materials synthesized from rice husk silica. **Water Science and Technology**. 68: 863-869.

Rouquerol, F., Rouquerol, J., and Sing, K. (1999). **Adsorption by Powders and Porous Solids**. London: Academic Press.

Sobczyński, A., and Dobosz, A. (2001). Water purification by photocatalysis on semiconductors. **Polish Journal of Environmental Studies**. 10: 195-205.

United States Environmental Protection Agency. (1994). Imidacloprid Pesticide Fact Sheet, **U.S. Environmental Protection Agency**. Washington DC.

Vohra, M.S., and Tanaka, K. (2003). Photocatalytic degradation of aqueous pollutants using silica-modified TiO_2. **Water Research**. 37: 3992-3996.

Zhang, F., Sun, D., Yu, C., Yin, Y., Dai, H., and Shao, G. (2015). A sol-gel route to synthesize SiO_2/TiO_2 well-ordered nanocrystalline mesoporous photocatalysts through ionic liquid control. **New Journal of Chemistry**. 39: 3065-3070.

CHAPTER VII

ADSORPTION AND PHOTOCATALYTIC DEGRADATION OF IMIDACLOPRID

Abstract

Imidacloprid is an insecticide used widely in cassava cultivation in Nakhon Ratchasima, Thailand. It can be transferred from soil to groundwater and has a long life time. The removal of imidacloprid was studied by adsorption on Al-MCM-41 with Al content of 10, 15 and 25 wt. % synthesized by hydrothermal method using rice husk silica (RHS). The adsorption was not the appropriate removal method because imidacloprid from the adsorbent was transferred back to the solution after 30 min. The removal was also investigated by photocatalysis using TiO_2/NaY and TiO_2/RHS with the TiO_2 content of 30 wt. % prepared by grafting method. In the photocatalytic testing, 0.3 g/L of catalyst concentration and four 18-W fluorescent black light lamps were used. Imidacloprid was not adsorbed by the catalysts and it was degraded by light without photocatalysts. The removal was improved in the presence of the catalysts. TiO_2/NaY and TiO_2/RHS showed a similar activity for imidacloprid photodegradation with the removal about 30% after 240 min. However, the removal from both catalysts was much lower than that from P25 which was nearly complete.

7.1 Introduction

One of the most common insecticides is imidacloprid which is widely used in Nakhon Ratchasima in cassava cultivation. Although data of toxicity is not available, it may cause minimal redness to eyes and affect animal organs (USEPA, 1994). Tišler, Jemec, Mozetic, and Trebše (2009) showed toxicity of imidacloprid in aquatic organisms. Imidacloprid can be adsorbed in soil and transferred to groundwater (Flores-Céspedes et al., 2006). Moreover, imidaclroprid in a solution could be degraded at high pH. It can be degraded slowly in water when exposed to light; which use a long to degrade because of its half-life was 355 days (USEPA, 1994). Therefore, the removal of imidacloprid is interesting for further investigation.

One of the most common removal methods is adsorption which is efficient, simple, fast, and not expensive. Iimidacloprid can be adsorbed in soil which has major component of clay about 59.73% (Flores-Céspedes et al., 2006). Since the clay composed of Si, O, and Al, other adsorbents that contain Si and Al may be applicable to imidacloprid adsorption. Another common method is photocatalytic degradation by TiO_2 (Kitsiou et al., 2009; Malato et al., 2002). However, the well-known limitations of TiO_2 are small particle size and low surface area (Kaneko and Okura, 2002). TiO_2 supported on adsorbent is an alternative catalyst in this field.

The aim of the work in this chapter is to study the adsorption and photocatalytic degradation of imidacloprid. The adsorbents synthesized from rice husk silica (RHS) including NaY, RHS and Al-MCM-41 and the photocatalysts were TiO_2/NaY and TiO_2/RHS prepared by grafting method as reported in Chapter VI.

7.2 Experimental

7.2.1 Materials

Rice husk silica (RHS), NaY and Al-MCM-41 with 10, 15 and 25 wt. % of Al content were used as adsorbents. Chemicals for the preparation of the RHS and zeolite were synthesized by methods follow the procedure described in Chepter III and IV (Rongchapo et al., 2013; Rongchapo et al., 2015). 30 wt. %TiO_2/NaY and TiO_2/RHS were prepared by an acid catalyzed sol-gel grafting method follow the procedure described in Chapter VI. P25 (Degussa) was used as a photocatalyst for comparison. Imidacloprid, commercial grade (70 %w/w, Bayer) was used in the adsorption and photocatalytic activity.

7.2.2 Adsorption

Adsorption experiment was conducted on all adsorbent in a 125 mL polypropylene bottle. The system comprised of 0.05 g of NaY and RHS with high imidacloprid concentration (380 ppm) of 20 mL by stirring at room temperature for 60 min. At adsorption period, the adsorbent and imidacloprid solution were separated by using a 0.45 µm nylon syringe filter. The paraquat solutions were analyzed by UV-Vis spectrophotometer (Varian Cary 1E) at λ_{max} of 270 nm. The imidacloprid concentration was determined according to calibration curve of standard solutions. An adsorption kinetic experiment of imidacloprid by Al-MCM-41 was carried out by stirring 20 mL of 80 ppm imidacloprid solution at room temperature. The solution was contacted for 5, 10, 15, 30 and 60 min with 0.05 g of Al-MCM-41.

7.2.3 Photocatalytic degradation

Details of photocatalytic degradation included photolysis, finding optimum catalyst concentration and determination of the photocatalytic activity. All experiments were done in a 1-L beaker containing 250 mL of 15 ppm paraquat solution and radiated with four 18-W fluorescent black light lamps (Toshiba, with the wavelength range 300-400 nm). In photolysis, paraquat concentration was monitored after illumination without catalyst at 5, 10, 15, 30, 45, 60, 90 min and every 30 min until 480 min. The catalyst concentration was varied at 0.5, 0.3 and 0.1 g/L by using P25 as a standard photocatalyst. Photocatalytic activity was carried out by stirring 250 mL of 15 ppm imidacloprid solutions with photocatalyst in optimum concentration at room temperature. Samples were taken less than 10% of all at various times and were filtrated by syringe filter.

7.3 Results and discussion

7.3.1 Adsorption

NaY and RHS were tested for adsorption. These adsorbents are different in properties. NaY adsorbs a hydrophilic pollutant whereas RHS adsorbs a hydrophobic pollutant (Rongchapo et al., 2013). Imidacloprid adsorption of NaY and RHS are shown in Table 7.1. Imidacloprid was adsorbed by NaY and RHS less than 5% at around 380 mg/L initial concentration in 60 min. The low adsorption on NaY was from the properly of imidacloprid, a neutral compound. The adsorption on RHS was adsorbed also low. This result might be contributed from the low surface area of RHS compared to NaY.

Table 7.1 Imidacloprid adsorption on NaY and RHS.

Sample	Initial concentration (mg/L)	Equilibrium concentration (mg/L)	% Adsorption	Adsorption capacity (mg/g)
NaY	384.00	374.73	2.41	3.40
RHS	384.00	367.80	4.22	6.39

Moreover, Al-MCM-41 at various Al content was studied. Because MCM-41 is also a siliceous material, the same as RHS but with a higher surface area. Al was added into the structure of MCM-41 to improve adsorption property which called Al-MCM-41 (Rongchapo et al., 2015). Figure 7.1 shows imidacloprid adsorption on 10, 20 and 25%Al-MCM-41 at various times. The amount of imidacloprid decreased on 25 %Al-MCM-41 at 30 min, although imidacloprid transfer to the solution before and after 30 min. The adsorption of imidacloprid did not reach equilibrium in 60 min and was not stable. It was possible that imidacloprid can stay on surface of Al-MCM-41 and migrated back in to the solution. Therefore, NaY and RHS which adsorbed imidacloprid at 60 min had low adsorption with the same reason. These results assured that the adsorption method was not suitable for imidaclroprid removal. imidacloprid was adsorbed in soil and then transferred back to water (Nemeth-Konda et al., 2002; Flores-Céspedes et al., 2006).

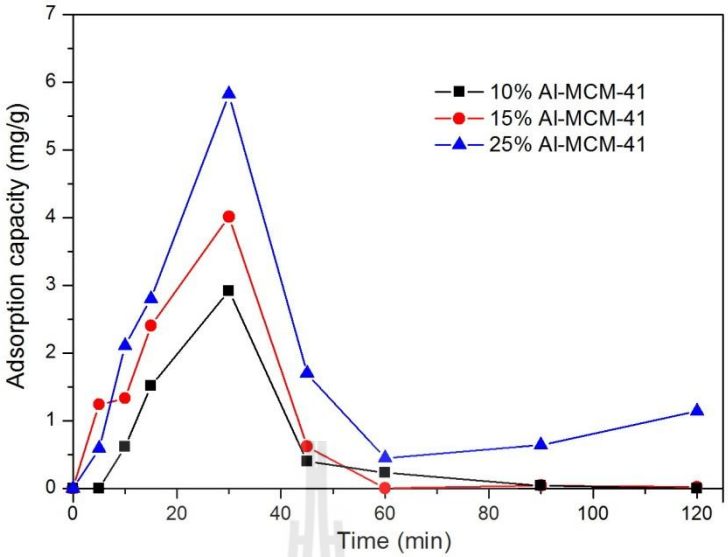

Figure 7.1 Adsorption of paraquat and imidacloprid on Al-MCM-41 in various times.

7.3.2 Photolysis and photocatalysis of imidaclopid

Result of photocatalytic degradation included photolysis, optimum catalyst concentration and photocatalytic activity. Irradiation of imidacloprid concentration at 15 ppm with UV light at various times is shown in Figure 7.2. Imidacloprid concentration decreased with time indicating that it was degraded by UV light. (USEPA, 1994). However, the degradation was slow. Therefore, the photocatalysis could be an alternative method.

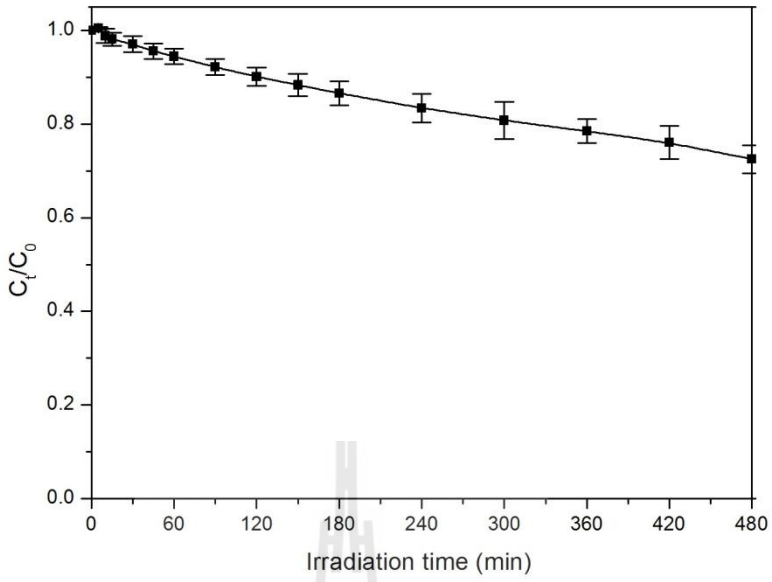

Figure 7.2 Photolysis (degradation without photocatalyst) of imidacloprid under UV light.

The optimum catalyst concentration was determined. The result is shown in Figure 7.3 that the concentration 0.3 g of P25/L of imidacloprid was suitable because the complete removal was achieved in 210 min. However, high catalysts concentration was not practical because the turbid mixture obstructed the light. Therefore, 0.3 g/L of catalyst concentration was used in the further study.

Activity of 30%TiO_2/NaY and 30%TiO_2/RHS catalysts before (adsorption) and after irradiation (photocatalytic degradation) are shown in Figure 7.4. Both catalysts slightly adsorbed imidacloprid, probably only on the support. Photocatalytic activity of 30%TiO_2/NaY and 30%TiO_2/RHS were around 30% in 240 min whereas a complete degradation was obtained from P25. The type of support had no influence on the catalytic activity. Despite the low activity, photocatalytic degradation was better than adsorption.

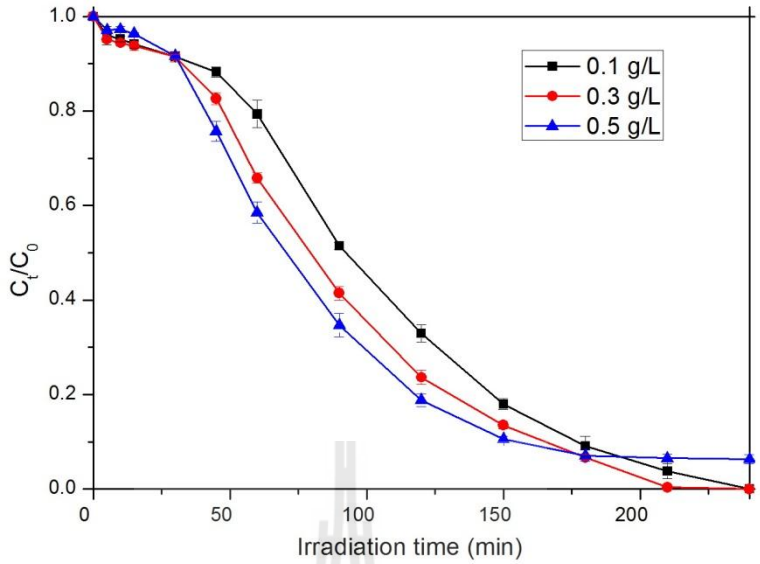

Figure 7.3 Photacatalytic degradation of imidacloprid by P25 with various catalyst concentrations.

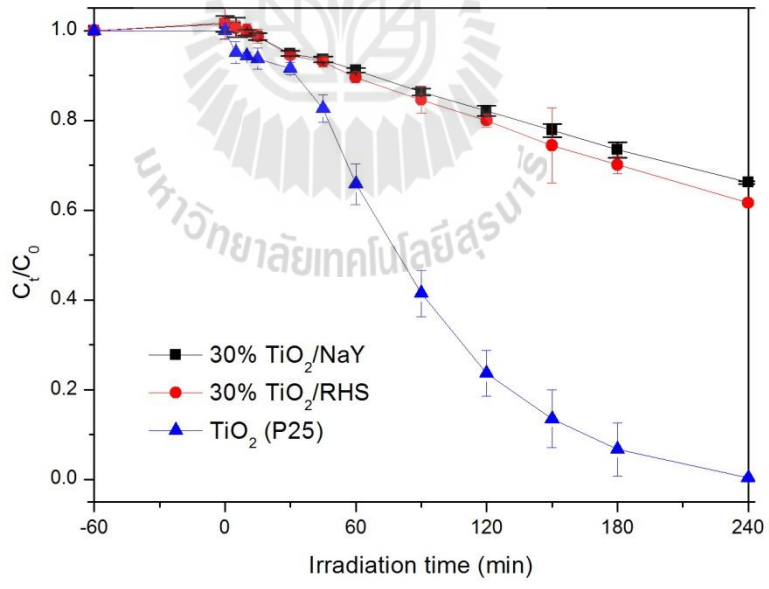

Figure 7.4 Photacatalytic degradation of imidacloprid with 30%TiO_2/RHS and 30%TiO_2/NaY compared with P25.

7.4 Conclusions

Removal of imidacloprid from aqueous solution was studied by adsorption and photocatalytic degradation. In the adsorption, RHS, NaY and Al-MCM-41 syntehsized by hydrothermal method with 10, 15 and 25 wt. % content were as an adsorbent. The adsorption of imidacloprid did not reach equilibrium and was not stable probably due to imidacloprid can transfer into two phases of solid and solution. Thus, the adsorption method was not suitable for imidaclroprid removal. In the photocatalytic degradation, 30%TiO_2/NaY and 30%TiO_2/RHS were used as photocatalysts which compared with P25. Imidacloprid was degraded by photolysis. In photocatalysis, the concentration of catalyst at 0.3 g/L was used. TiO_2/NaY and TiO_2/RHS showed a similar activity giving around 30% degradation. Both catalysts were less active than P25. Although photocatalytic degradation was slow to remove imidacloprid, it was better than adsorption and photolysis.

7.5 References

Flores-Céspedes, F., Fernández-Pérez, M., Villafranca-Sánchez, M., and González-Pradas, E. (2006). Cosorption study of organic pollutants and dissolved organic matter in a soil. **Environmental Pollution**. 142: 499-456.

Kaneko, M., and Okura, I. (2002). **Photocatalysis : Science and Technology**. New York: Springer.

Kitsiou, V., Filippidis, N., Mantzavinos, D., and Poulios, I. (2009). Heterogeneous and homogeneous photocatalytic degradation of the insecticide imidacloprid in aqueous solutions. **Applied Catalysis B: Environmental**. 86: 27-35.

Nemeth-Konda, L., Fuleky, Gy.,Morovjan, Gy., and Csokan, P. (2002). Sorption behaviour of acetochlor, atrazine, carbendazim, diazinon, imidacloprid and isoproturon on Hungarian agricultural soil. **Chemosphere**. 48: 545-552.

Malato, S., Blanco, J., Cáceres, J., Alba, A. R. F., Agüera, A., and Rodriguez, A. (2002). Photocatalytic treatment of water-soluble pesticides by photo-Fenton and TiO_2 using solar energy. **Catalysis Today**. 76: 209-220.

Rongchapo, W., Deekamwong, K., Loiha, S., Prayoonpokarach, S., and Wittayakun, J. (2015). Paraquat adsorption on NaX and Al-MCM-41. **Water Science and Technology**. 71: 1347-1353.

Rongchapo, W., Sophiphun, O., Rintramee, K., Prayoonpokarach, S., and Wittayakun, J. (2013). Paraquat adsorption on porous materials synthesized from rice husk silica. **Water Science and Technology**. 68: 863-869.

Tišler, T., Jemec, A., Mozetic, B., and Trebše, P. (2009). Hazard identification of imidacloprid to aquatic environment. **Chemosphere**. 76: 907-914.

United States Environmental Protection Agency. (1994). Imidacloprid Pesticide Fact Sheet, **U.S. Environmental Protection Agency**. Washington DC.

CHAPTER VIII

ACTIVITY OF TITANIUM DIOXIDE HYBRIDIZED WITH REDUCED GRAPHENE OXIDE FOR PHOTOCATALYTIC DEGRADATION OF ORGANIC POLLUTANTS: EFFECT OF ION TYPE

Abstract

Reduced graphene oxide (rGO) is a two-dimensional carbonaceous material with graphene-like structure with an excellent electron transport ability which makes it a low-cost alternative to noble metal. Cooperation of rGO with TiO_2 can improve photocatalytic activity because it can prevent a recombination between a substrate radical with an excited electron. The objective of this work was to investigate activity of rGO/P25 hybrid material for photocatalytic degradation of organic pollutants. The study was conducted in a cylindrical Pyrex reactor which was radiated with a 300-W Xe arc lamp. Light was passed through a 10 cm IR water filter and a cutoff filter. In the study, rGO/P25 with rGO content of 1 wt. % was tested for three groups of organic pollutants including anionic (2,4-dichlorophenoxyacetic acid and acid orange 7), cationic (methylene blue and rhodamine B) and neutral pollutants (4-chlorophenol). The rGO/P25 did not show higher photooxidation than P25. The study at pH 3 and pH 6 for all organic pollutants indicated that the oxidation process

hydroxyl radical. Thus, the charge of the pollutions had no influence on the activity of rGO on P25.

8.1 Introduction

The commercial TiO_2 P25 containing both anatase and rutile forms with the ratio to 3–4:1 is widely known as the best photocatalyst. However, there are same drawbacks of P25 including a fast agglomeration and low adsorption ability due to a small particle size (~26 nm) and low surface area (~56 m^2/g) (Ohno, Sarukawa, Tokieda, and Matsumura, 2001; Raj and Viswanathan, 2009). Such drawbacks result in a rapid recombination of excited electron and positive hole pair. To solve the problem, P25 can be dispersed on a support material.

Graphene has received a considerable attention in recent years confirmed by an increase in number of publications in photocatalytic application from 1% in 2008 to 28.4% in 2014 (Scopus). Xiang, Yu, and Jaroniec (2012) reviewed properties and works on graphene-based photocatalysts. The review included preparation and application in photocatalytic degradation of pollutants, hydrogen generation and disinfection. Graphene enhances the photocatalytic activity by increasing the catalyst adsorptivity and ability to transfer photogenerated electron which decreases the recombination between the excited electron and the positive hole pair (Fan, Lai, Zhang, and Wang, 2011; Zhang, Lv, Y. Li, Wang, and J. Li, 2010; Zhou, Zhu, Yang, Jiang, and Li, 2011). Graphene has useful properties including large specific surface area (~2,600 m^2/g), high thermal conductivity (~ 5000 W/m. K) and excellent charge carriers at room temperature (200000 $cm^2/V.s$) (Peplow, 2013; Raccichini, Varzi, Passerini, and Scrosati, 2015).

Graphene is well known in two types: graphene oxide (GO) and reduced graphene oxide (rGO or RGO). Figure 8.1 shows processes occurring during preparation of GO and rGO. The suspension of graphene in an aqueous solution was prepared from oxidation and exfoliation of graphite presented in the GO form. The GO is employed in photocatalysis to improve the activity of photocatalyst. However, the GO surface is rich of oxygen-containing groups such as carboxylic and hydroxyl functional groups. Reduction of GO to remove the surface functional groups could convert it to rGO which produced π-conjugation structure (Bosch-Navarro, Carlos, Martí-Gastaldo, Sánchez-Royo, and Gómez Gómez, 2012; Raccichini et al., 2015). The rGO improves the activity of photocatalytic materials by charge separation and electron transport.

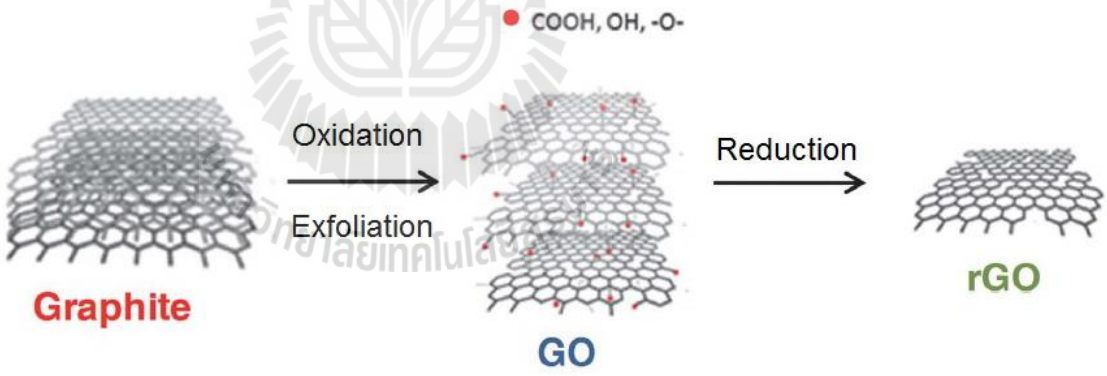

Figure 8.1 Process of GO and rGO preparation (Bosch-Navarro et al., 2012).

One of the research interests in Professor Wonyong Choi's group in POSTECH, South Korea is to combine GO or rGO with the photocatalysts. Moon et al. (2014) reported that of rGO improved the photocatalytic activity of P25 on oxidation of arsenite (As(III) to As(V)). Their results confirmed that the activity of

rGO/P25 was better than P25 and Pt/P25. rGO loading of 0.6-1.0 wt. % on P25 gave similar activity. In another work, the photocatalytic activity of eight commercial TiO_2 samples including P25 was studied on degradation of 19 substrates. P25 is the best photocatalyst for many organic pollutants such as 4-chlorophenol and rhodamine B (Ryu and Choi 2008). In the study to improve the activity of P25 on the degradation of organic pollutants, the substrates were separated into groups of ion (Ryu and Choi 2008).

The objective of this work was to investigate photocatalytic degradation of three ion groups of organic pollutants by using P25 and rGO/P25 containing 1 wt. % rGO. The pollutants included anionic (2,4-dichlorophenoxyacetic acid and acid orange 7), cationic (methylene blue and rhodamine B) and a neutral one (4-chlorophenol). The structures of these pollutants are shown in Figure 8.2. Seck et al. (2012) reported the photocatalytic degradation of 2,4-dichlorophenoxyacetic acid by using P25. The 2,4-dichlorophenoxyacetic acid is extensively used in agricultural to control weeds in cereal crops but it is considered to be potentially dangerous to both animals and humans. 4-chlorophenol is used as an intermediate in organic synthesis of dyes and drugs. Moreover, the hazardous substances could be the organic intermediates produced during the degradation (Hoffmann, Martin, Choi, and Bahnemann, 1995). Finally, Acid orange 7, methylene blue and rhodamine B were represented in colored dye effluent. Wastewater from dyeing process is a main environmental pollution. There are many works to study the removal of these dyes from water (Houas et al., 2001; Konstantinou and Albanis 2004; Lodha, Jain, and Punjabi, 2011). All organic pollutants in this work were degraded by photooxidation.

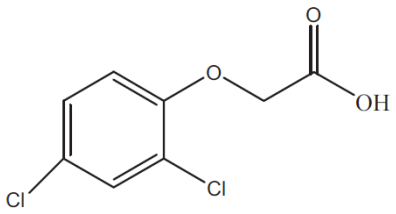

2,4-dichlorophenoxyacetic acid

(Seck et al., 2012)

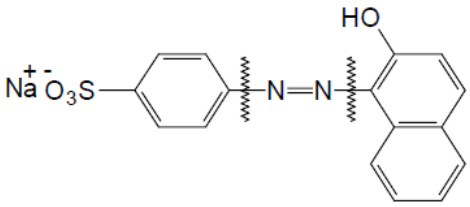

Acid orange 7

(Konstantinou and Albanis 2004)

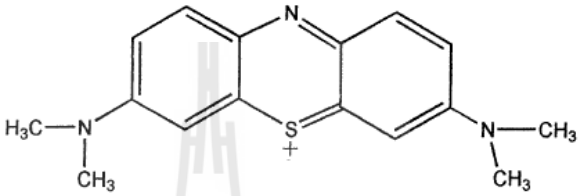

Methylene blue (Houas et al., 2001)

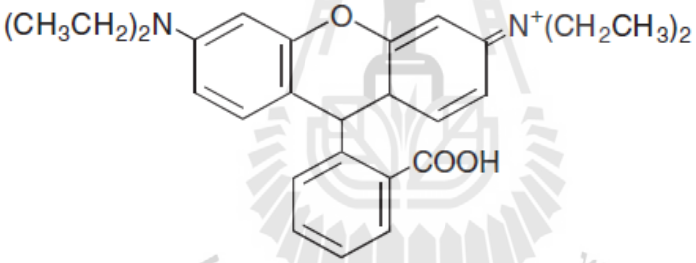

Rhodamine B

(Lodha et al., 2011)

4-chlorophenol

(Hoffmann et al., 1995)

Figure 8.2 Structures of five organic pollutants.

8.2 Experimental

8.2.1 Materials and condition for reaction

Five substrate compounds for the activity testing are 2,4-dichlorophenoxyacetic acid (Sigma), acid orange 7 (Aldrich), methylene blue (Aldrich), rhodamine B (Aldrich) and 4-chlorophenol (Sigma)**.** Reduced graphene

oxide (rGO) was prepared by Gun-hee Moon at POSTECH, South Korea. Graphene oxide (GO) (natural graphite completely oxidized by modified Hummers method and exfoliated into single-layer) was prepared by reduction (Moon, D. Kim, H. Kim, Bokare, and Choi, 2014). TiO_2 used in this work was the commercial TiO_2 (P25, Degussa). The rGO/P25 was also prepared by Moon with a method described in the literature.

All reactions were studied at pH 3 and 6. The pH of the suspension was adjusted with $HClO_4$ or NaOH solution. For adsorption study the suspension was stirred in darkness for 30 min. A 300-W Xe arc lamp was used as a light source, 10-cm IR water filter and a cutoff filter ($\lambda > 320$ nm) were used to light cutoff and focused onto a cylindrical Pyrex reactor (60 mL) with a quartz window. The reactor was openned to ambient air to prevent the depletion of dissolved dioxygen and stirred magnetically during irradiation. Sample aliquots were withdrawn from the reactor intermittently during the illumination and filtered through a 0.45 μm PTFE syringe filter to the remove photocatalyst particles.

8.2.2 Photocatalytic degradation of ion groups

In this part, rGO/P25 with rGO content of 1 wt. % was investigated on three groups of organic pollutants including anionic, cationic and neutral pollutants. Concentration of photocatalysts was 0.1 g/L. The catalysts were dispersed in distilled water by ultra-sonication before a stock solution of organic pollutant was added. An initial concentration of the 30 mL pollutants was fixed at 500 μM for 2,4-dichlorophenoxyacetic and 100 μM for all dyes and 4-chlorophenol. The suspension

initial pH was 3 for the degradation of 4-chlorophenol and both 3 and 6 for the degradation of 2,4-dichlorophenoxyacetic acid and dyes.

The degradation of 2,4-dichlorophenoxyacetic acid and 4-chlorophenol were monitored using a high performance liquid chromatograph (HPLC: Agilent 1100 series) equipped with a diode array detector and a Zorbax 300SB C18 column (4.6 mm ×150 mm). The eluent consisted of a binary mixture of 0.4% acetic acid solution and acetonitrile for the analysis of 2,4-dichlorophenoxyacetic acid (7:3 by volume) and 0.1% phosphoric acid solution and acetonitrile for the analysis of 4-chlorophenol (8:2 by volume). The color bleaching of acid orange 7, rhodamine B, and methylene blue was monitored by measuring the absorbance with a UV-Vis spectrophotometer (Shimadzu UV-2401PC) at λ_{max} of 485, 554, and 663 nm, respectively.

8.3 Results and discussion

8.3.1 Adsorption and degradation of anions

Adsorption and degradation of 2,4-dichlorophenoxyacetic acid and acid orange 7 of pH 3 and pH 6 are shown in Figure 8.3 and 8.4. The adsorption of both compounds on P25 and rGO/P25 was low at both pHs. The adsorption of P25 and rGO/P25 was not different due to low rGO loading. The pH 3 was studied because it was the studied pH for P25 in the previous work (Ryu and Choi 2008). At pH 3, photocatalytic degradation of 2,4-dichlorophenoxyacetic acid on P25 was slightly better than rGO/P25. The degradation on both catalysts was complete in 105 min. Thus, the combination between rGO and P25 did not improve the photocatalytic

activity. At pH 6, the degradation of 2,4-dichlorophenoxyacetic acid on both catalysts was slower than that at pH 3. P25 was also slightly better than rGO/P25. The result indicated that pH had no effect to improve the activity of rGO on P25. From the literature (Borji, Nasseri, Mahvi, Nabizadeh, and Javadi, 2014) the trend of pH depended on acid-base equilibrium on the catalyst surface and species in the solution which leads to a lack of positive charges on the surface and increase negative charges in the solution at high pH. The degradation of 2,4-dichlorophenoxyacetic acid at high pH was better than that at low pH (Seck et al., 2012). However, both catalysts with pH 3 showed a high activity in this work. For acid orange 7, the degradation of on both catalysts was complete in 120 min at pH 3 which was better than the degradation at pH 6. Trend of the activity of both catalyst for the degradation of acid orange 7 was similar as the degradation of 2,4-dichlorophenoxyacetic acid. In anions group, the degradation was high at pH 3 because of ionization state of the catalyst surface in positive charge (Houas et al., 2001). However, rGO did not improve the activity of P25 in the degradation of anions.

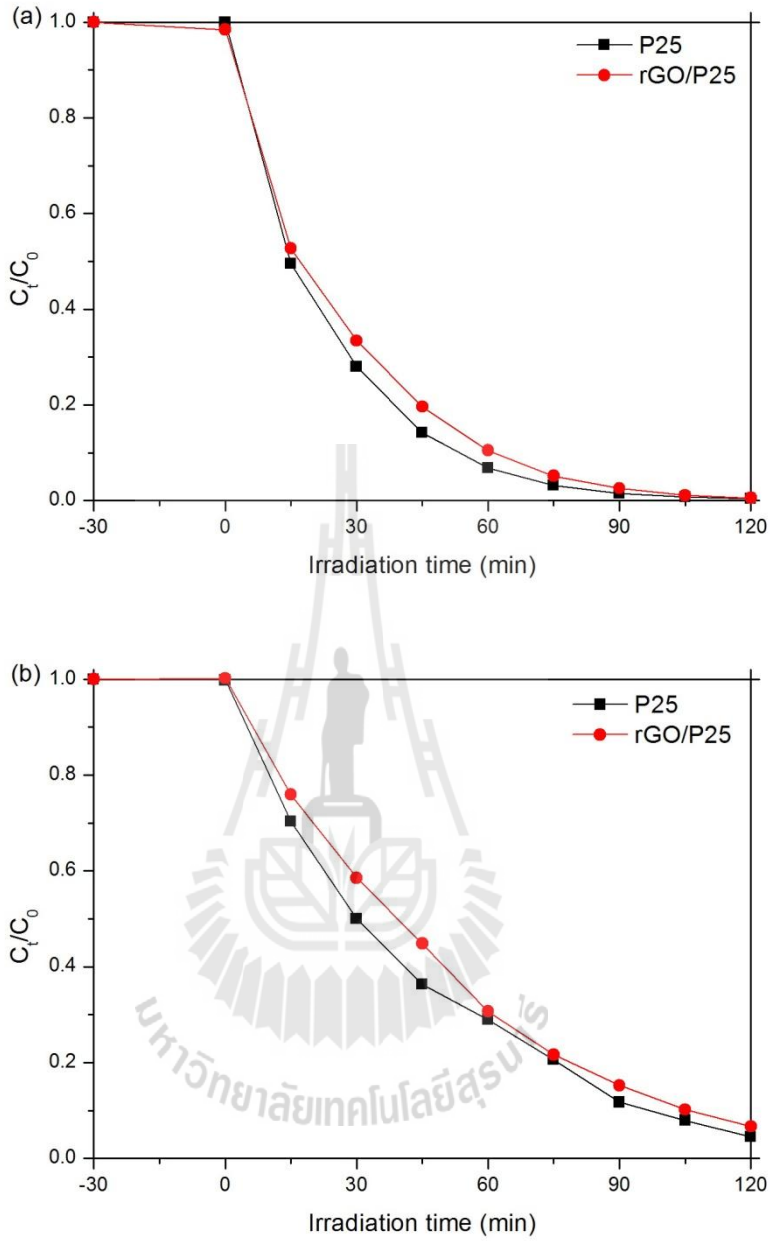

Figure 8.3 Photocatalytic degradation of 2,4-dichlorophenoxyacetic acid (anion) at pH 3 (a) and 6 (b).

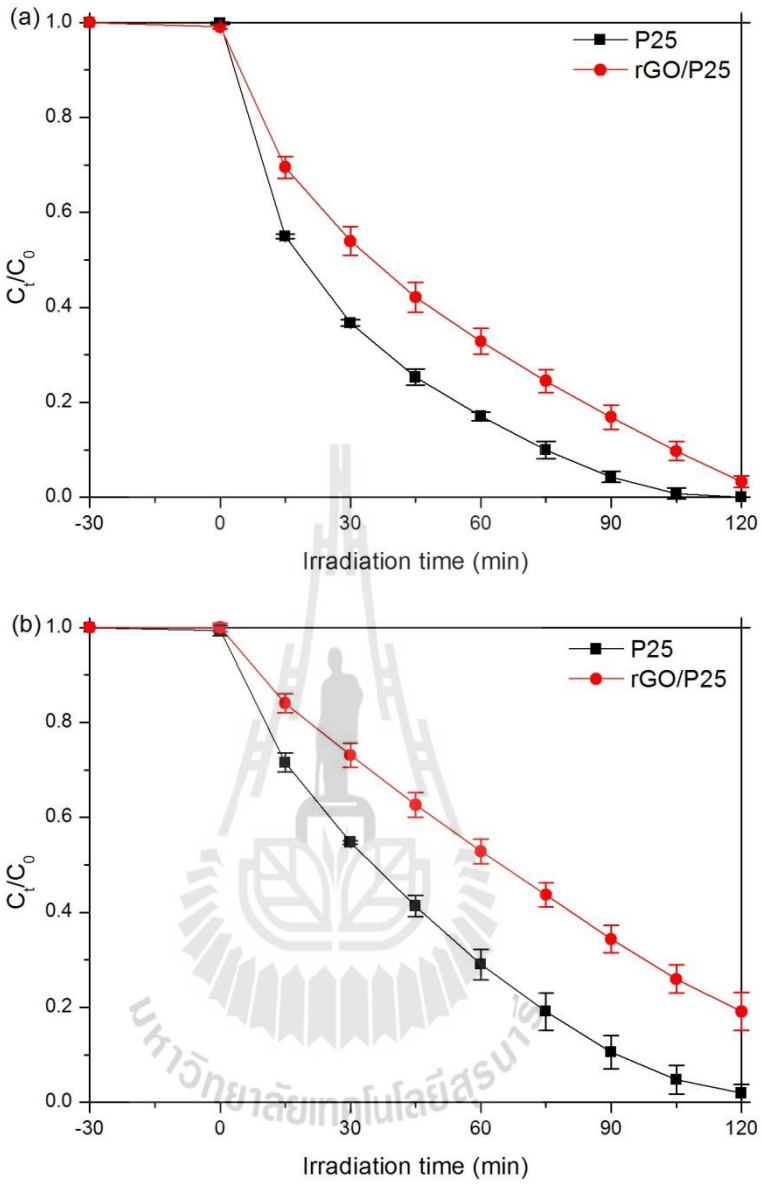

Figure 8.4 Photocatalytic degradation of acid orange 7 (anion) at pH 3 (a) and 6 (b).

8.3.2 Adsorption and degradation of cations

Adsorption and degradation of methylene blue and rhodamine B with pH 3 and pH 6 are shown in Figure 8.5 and 8.6. The adsorption of methylene blue on rGO/P25 was slightly higher than P25 at pH 3 because positive charge of P25 surface (Houas et al., 2001) could not interact with cationic methylene blue. Although rGO/P25 had higher adsorption than P25, the photocatalytic degradation was the opposite. This result indicated that rGO could not improve the activity of P25. At pH 6, the adsorption of P25 was slightly higher than rGO/P25 because the catalyst surface had a negative charge (Houas et al., 2001). Thus, the degradation on P25 was better than rGO/P25.

The adsorption of rhodamine B on P25 and rGO/P25 was not different at both pHs. At pH 3, photocatalytic degradation on P25 was slightly better than rGO/P25. The degradation on both catalysts was not complete in 120 min. Thus, the combination between rGO and P25 did not improve the photocatalytic activity. The results of the cation degradation indicated that rGO could not enhance the activity of P25.

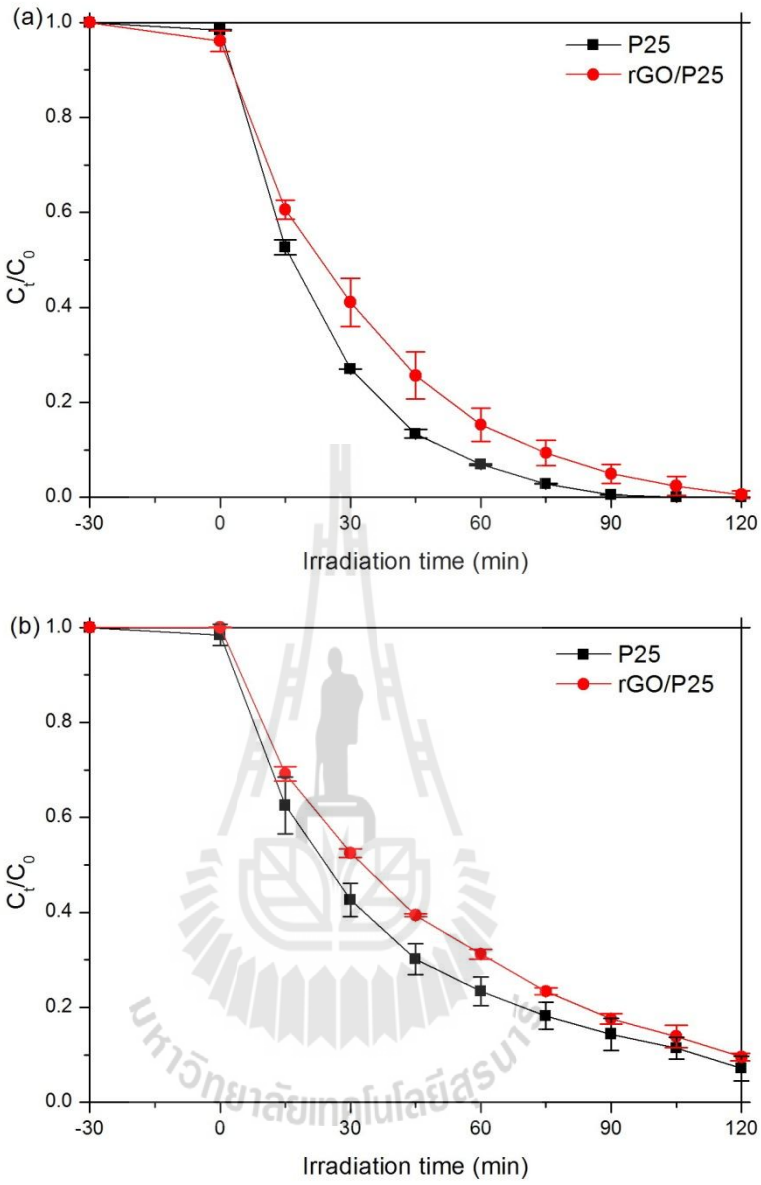

Figure 8.5 Photocatalytic degradation of methylene blue (cation) at pH 3 (a) and 6 (b).

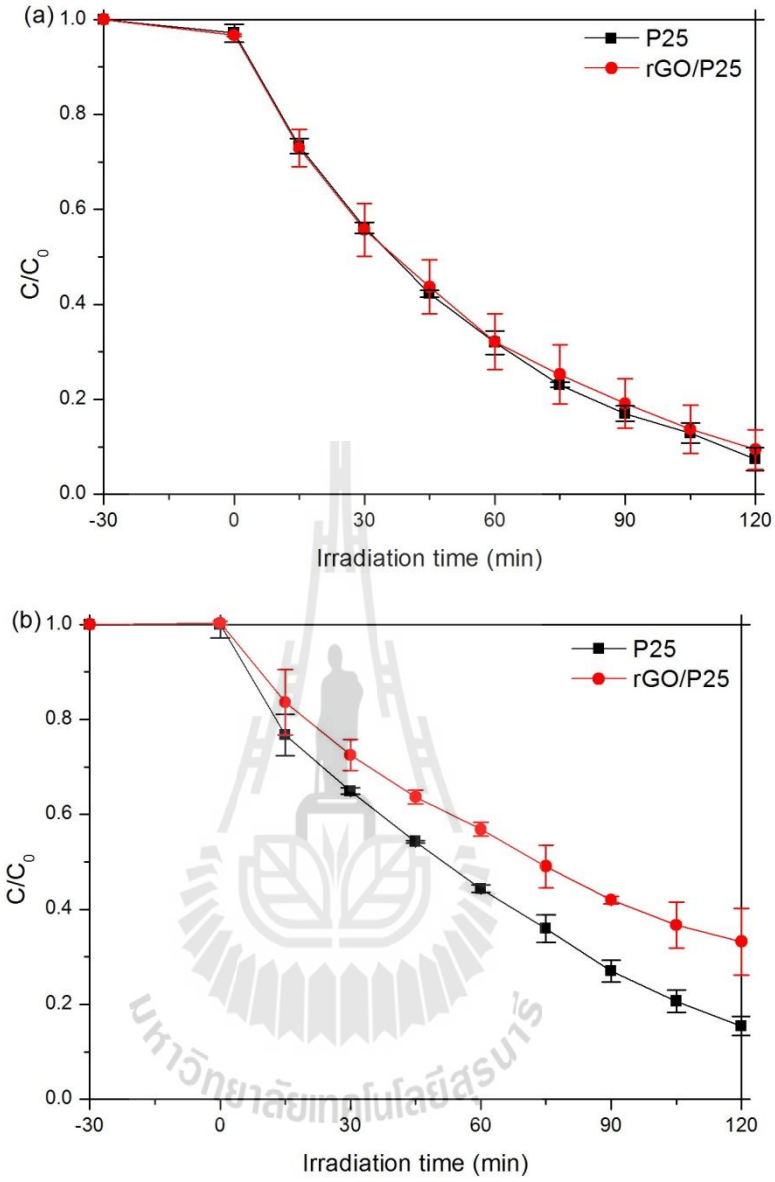

Figure 8.6 Photocatalytic degradation of rhodamine B (cation) at pH 3 (a) and 6 (b).

8.3.3 Adsorption and degradation of neutral compound

The adsorption and photocatalytic degradation of 4-chlorophenol on P25 and rGO/P25 were not different at pH 3 shown in Figure 8.7. The results indicated that rGO/P25 catalyst was not superior to P25.

The activity rGO/P25 at 1 wt. % rGO was not better than P25 for the degradation of all organic pollutants. The organic pollutants were degraded by using photooxidation (Hoffmann et al., 1995; Houas et al., 2001; Konstantinou and Albanis 2004; Lodha et al., 2011; Seck et al., 2012) which were the same process of As(III) to As(V) (Moon et al., 2014). However, oxidation process of photocatalytic degradation could occur in two pathways. The first was a direct pathway by using the h^+ in valence band of photocatalyst (Kaneko and Okura, 2002). Another pathway was oxidation of pollutant such as dye compound via successive attacks by OH• radicals in which the radicals were produced for oxidation of water (Konstantinou and Albanis 2004). Moon et al. (2014) reported that the activity of rGO/P25 in photocatalytic oxidation of arsenite was better than P25 which the process on oxidation of arsenite could occur via both oxidation pathways. In contrast, all pollutants in this work were oxidized by using main pathway of OH• radicals. Effect of OH• radicals in the reaction might relate with the activity of rGO.

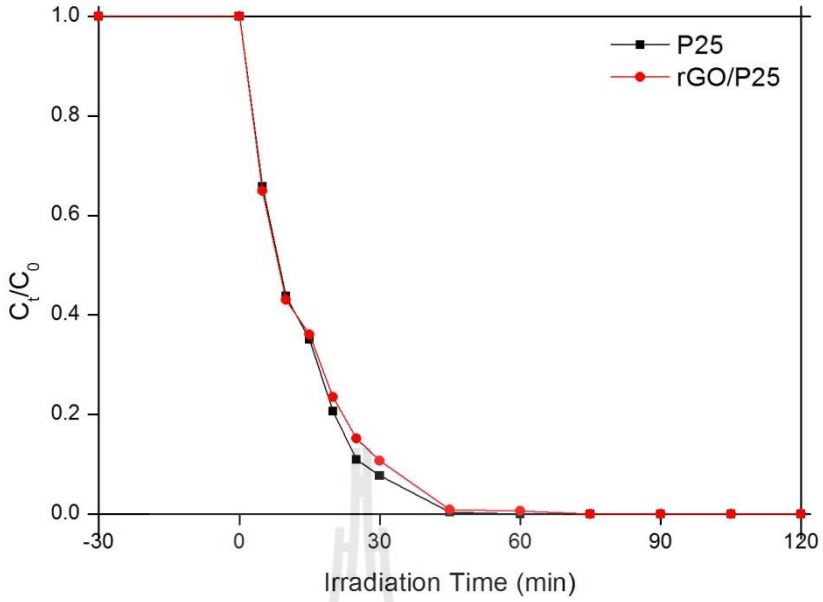

Figure 8.7 Photocatalytic degradation of 4-chlorophenol (neutral compound) at pH 3.

8.4 Conclusions

A hybrid material containing 1 wt. % of rGO and P25 was investigated on the photocatalytic degradation via oxidation including anionic, cationic and neutral pollutants. Adsorption and photocatalytic degradation of all pollutants were tested in pH 3 and pH 6. The adsorption of all compounds on P25 and rGO/P25 was low at both pHs. The photocatalytic degradation of all compounds on P25 and rGO/P25 at pH 3 was higher than at pH 6. However, P25 exhibited a higher performance than rGO/P25 for the photocatalytic degradation of organic pollutants in three ion groups. Thus, the charge of the pollutions had no influence on the activity of rGO on P25.

8.5 References

Borji, S. H., Nasseri, S., Mahvi, A. H., Nabizadeh, R., and Javadi, A. H. (2014). Investigation of photocatalytic degradation of phenol by Fe(III)-doped TiO_2 and TiO_2 nanoparticles. **Journal of Environmental Health Science and Engineering**. 12: 101-110.

Bosch-Navarro, C., Carlos, E., Martí-Gastaldo, C., Sánchez-Royo, J. F., and Gómez Gómez, M. (2012). Influence of the pH on the synthesis of reduced graphene oxide under hydrothermal conditions. **Nanoscale**. 4: 3977-3982.

Fan, W., Lai, Q., Zhang, Q., and Wang, Y. (2011). Nanocomposites of TiO_2 and reduced graphene oxide as efficient photocatalysts for hydrogen evolution. **Journal of Physical Chemistry C**. 115: 10694-10701.

Hoffmann, M. R., Martin, S. T., Choi, W., and Bahnemann, D. W. (1995). Environmental applications of semiconductor photocatalysis**. Chemical Reviews**. 95(1): 69-96.

Houas, A., Lachheb, H., Ksibi, M., Elaloui, E., Guillard, C., and Herrmann, J. (2001). Photocatalytic degradation pathway of methylene blue in water. **Applied Catalysis B: Environmental**. 31: 145-157.

Kaneko, M., and Okura, I. (2002). **Photocatalysis : Science and Technology**. New York: Springer.

Konstantinou, I. K., and Albanis, T. A. (2004). TiO_2-assisted photocatalytic degradation of azo dyes in aqueous solution: kinetic and mechanistic investigations: A review **Applied Catalysis B: Environmental**. 49: 1-14.

Lodha, S., Jain, A., and Punjabi, P. B. (2011). A novel route for waste water treatment: Photocatalytic degradation of rhodamine B. **Arabian Journal of Chemistry**. 4: 383-387.

Moon, G., Kim, D., Kim, H., Bokare, A. D., and Choi, W. (2014). Platinum-like behavior of reduced graphene oxide as a cocatalyst on TiO_2 for the efficient photocatalytic oxidation of arsenite. **Environmental Science and Technology Letters**. 1: 185-190.

Ohno, T., Sarukawa, K., Tokieda, K., and Matsumura, M. (2001). Morphology of a TiO_2 Photocatalyst (Degussa, P-25) Consisting of anatase and rutile crystalline phases. **Journal of Catalysis**. 203: 82-86

Peplow, M. (2013). Graphene's dazzling properties promise a technological revolution, but Europe may have to spend a billion euros to overcome some fundamental problems. **Nature**. 503: 327–329.

Raccichini, R., Varzi, A., Passerini, S., and Scrosati, B. (2015). The role of graphene for electrochemical energy storage. **Nature Materials**. 14: 271-279.

Raj, K. J. A., and Viswanathan, B. (2009). Effect of surface area, pore volume and particle size of P25 titania on the phase transformation of anatase to rutile. **Indian Journal of Chemistry**. 48A: 1378-1382.

Ryu, J., and Choi, W. (2008). Substrate-specific photocatalytic activities of TiO_2 and multiactivity test for water treatment application. **Environmental Science and Technology**. 42: 294-300.

Seck, E. I., Doña-Rodríguez, J. M., Fernández-Rodríguez, C., González-Díaz, O. M., Araña, J., and Pérez-Peña, J. (2012). Photocatalytic removal of 2,4-dichlorophenoxyacetic acid by using sol-gel synthesized nanocrystalline and

commercial TiO_2: operational parameters optimization and toxicity studies. **Applied Catalysis B: Environmental**. 125: 28-34.

Xiang, Q., Yu, J., and Jaroniec, M. (2012). Graphene-based semiconductor photocatalysts. **Chemical Society Reviews**. 41: 782-796.

Zhang, H., Lv, X., Li, Y., Wang, Y., and Li, J. (2010). P25-graphene composite as a high performance photocatalyst. **ACS Nano**. 4(1): 380-386.

Zhou, K., Zhu, Y., Yang, X., Jiang, X., and Li, C. (2011). Preparation of graphene-TiO_2 composites with enhanced photocatalytic activity. **New Journal of Chemistry**. 35: 353-359.

CHAPTER IX

INVESTIGATION OF TITANIUM DIOXIDE HYBRIDIZED WITH REDUCED GRAPHENE OXIDE FOR REDUCTION AND OXIDATION

Abstract

Hybridization of rGO with P25 can improve photocatalytic activity because it can prevent recombination of photogenerated electron-hole for P25. The objective of this part was to study activity of rGO/P25 at the rGO content (1, 2, 4, 6, 8 and 10 wt. %) for the degradation of CCl_4 and H_2 production via reduction and the degradation of methylene blue via oxidation. All rGO/P25 catalysts exhibited a better performance than P25 for the reduction process. The catalyst with 2 wt. % was the best for CCl_4 degradation and that with 1 wt. % was the best for H_2 production. The enhancement for the reductive processes in photocatalysis was ascribed to the ability of rGO as a good electron transfer mediator. In the degradation of methylene blue at high concentration, all rGO/P25 catalysts were not superior to P25. Low concentration of methylene blue, the degradation of rGO/P25 gave the higher activity than P25. Hydroxyl radical (OH•), a product form positive hole, was the main oxidizer of methylene blue degradation and rGO. The rGO may hinder the activity of TiO_2 for oxidation because it could react with the produced OH•. Thus, P25 was the

best one at high methylene blue concentration because of competition of OH• using between rGO and methylene blue degradation.

9.1 Introduction

Recently, the study on combination of graphene and TiO_2 for photocatalysis has attracted a lot of attention because graphene can enhance efficiency of TiO_2. Several papers reported the efficiency of graphene/TiO_2 for photocatalytic degradation of pollutants such as aromatic compounds and dyes. Moreover, hydrogen production was enhanced by graphene on TiO_2 (Lui et al., 2012; Xiang, Yu, and Jaroniec, 2011; Zhang, Tang, Fu, and Xu, 2010; Zhou et al., 2011). The major reaction steps in this photocatalytic degradation mechanism under UV-light irradiation are summarized by the following equation (9.1-9.5).

$$TiO_2 + h\nu \rightarrow TiO_2 (e^- + h^+) \quad (9.1)$$

$$TiO_2 (e^-) + \text{Graphene} \rightarrow TiO_2 + \text{Graphene} (e^-) \quad (9.2)$$

$$\text{Graphene} (e^-) + O_2 \rightarrow \text{Graphene} + O_2^- \quad (9.3)$$

$$TiO_2 (h^+) + OH^- \rightarrow TiO_2 + OH\bullet \quad (9.4)$$

$$OH\bullet + \text{Pollutants} \rightarrow \text{Degradation products} \quad (9.5)$$

In general, a photocatalyst is excited by the light that results in the formation of excited electrons (e^-) in conduction band (CB) and positive holes (h^+) pair in valence band (VB) of the photocatalyst. The e^- acts as a reducer for reduction process. Graphene receives the e^- from TiO_2 which present in equation 9.1 and might transfer to reduction process of pollutants. The h^+ acts as an oxidizer for oxidation process. Several photocatalytic reductions have been studied, for example, degradation of

carbon tetrachloride (CCl_4) (Hoffmann et al., 1995) and hydrogen (H_2) production (Zhang and Cui, 2012) as shown in equation 9.6 and 9.7.

$$CCl_4 + e^- \rightarrow \bullet CCl_3 \quad (9.6)$$

$$2H^+ + 2e^- \rightarrow H_2 \quad (9.7)$$

The photocatalytic degradation of organic pollutants via oxidation was mentioned in Chapter VIII. One a pollutant adsorbed by rGO/P25 was methylene blue which was used as a representative sample which could be degraded by oxidation with OH• radicals. Kim, Choi, and Park (2010) reported the degradation of methylene blue by oxidation with OH• radicals which give Azure B (AB), Azure A (AA), Azure C (AC), and Thionine (Th) as intermediates shown in Figure 9.1. Oxidation process over photocatalyst can occur in a direct pathway by using the h^+ in VB and another pathway by using OH• radicals produced from oxidation of water with h^+. Oxidation of methylene blue occurred via successive attacks by OH• radicals. Moreover, all the pollutants in the chapter VIII, the degradation were studied via oxidation; the degradation by rGO/P25 with 1wt. % of rGO was less than P25. The rGO did not improve the activity of P25. This chapter involves a further study on the role of rGO to improve the efficiency of P25 in oxidation.

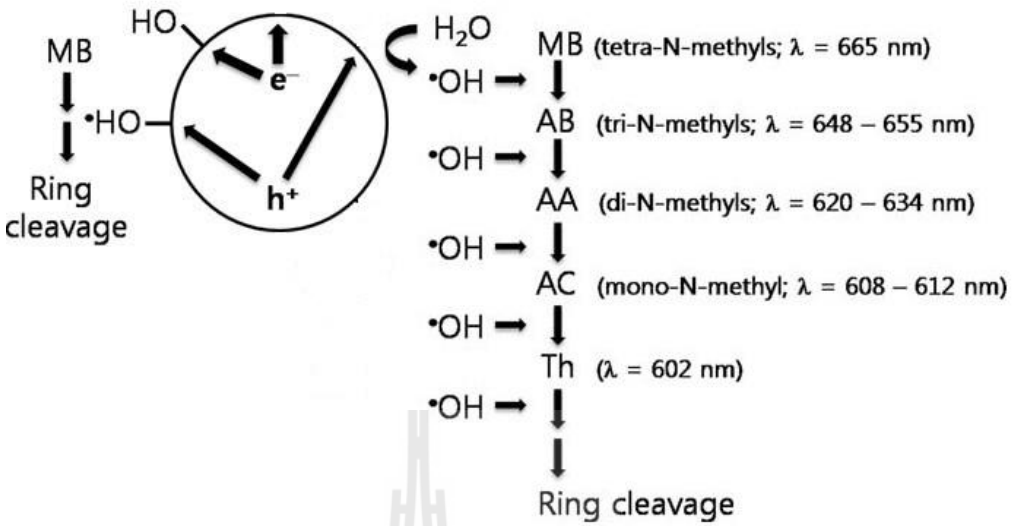

Figure 9.1 Photocatalytic degradation pathway of methylene blue in UV-irradiation (modified from Kim et al., 2010).

The rGO/P25 composites were studied for photocatalytic degradation of methylene blue. The testing condition and results are shown in Table 9.1. The rGO can enhance the degradation activity of P25 for methylene blue (Zhang, Lv, Y. Li, Wang, and J. Li, 2010; Zhang, Tang, Fu, and Xu, 2010). However, the results from the previous chapter showed that rGO did not improve the activity of P25 at the initial methylene blue concentration of 100 μM which was higher than that in other works (Zhang, Lv, Y. Li, Wang, and J. Li, 2010; Zhang, Tang, Fu, and Xu, 2010). The results indicated that rGO might hinder the activity of P25 because the produced OH• could react with rGO. Thus, a process to prepare rGO was considered. It is well known that rGO can be produced by the reduction of GO. Thus, the rGO surface is lack of oxygen-containing functional groups which might compete with the methylene blue degradation to use OH• . Radich, Krenselewski, Zhu, and Kamat (2014) studied

stability of rGO for photocatalysis and. They proposed that rGO on TiO_2 was oxidized and destroyed by OH• as shown in Figure 9.2. The objective of the work in this part was to investigate activity of rGO/P25 at 1, 2, 4, 6, 8 and 10 wt. % rGO content for the degradation of CCl_4 and H_2 production via reduction. The degradation of methylene blue via oxidation was tested by using rGO/P25 at 1, 4, and 10 wt. % rGO content with condition similar to the previous chapter to compare the efficiency with other works at low concentration of methylene blue.

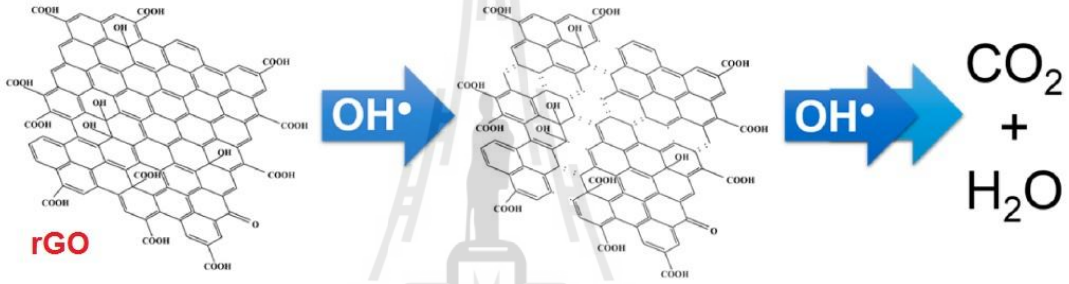

Figure 9.2 Oxidative fragmentation and mineralization of RGO during irradiation of TiO_2-rGO suspension (Radich et al., 2014).

9.2 Experimental

9.2.1 Materials and condition for reaction

Carbon tetrachloride (J. T. Baker), methanol (MeOH, J. T. Baker) and methylene blue (Aldrich) were used. Photocatalysts in this part were rGO/P25 with rGO amount of 1, 2, 4, 6, 8 and 10 wt. %. The rGO/P25 preparation, reactor and study condition were mentioned in the chapter VIII. The reactor was closed with a rubber septum for H_2 production and CCl_4 (volatile substrate) and stirred magnetically during irradiation or open to the ambient air for methylene blue degradation.

9.2.2 Photocatalytic reduction

In this part, 1, 2, 4, 6, 8 and 10 wt. % rGO/P25 were investigated for the degradation of CCl_4 and H_2 production via reduction. High concentration of CCl_4, 5 mM at 30 mL and catalyst powder was dispersed by ultra-sonication in distilled water at the catalyst concentration of 0.1 g/L. Methanol was fixed at 0.1 M in 30 mL of the reactor to serve as a hole scavenger for CCl_4 degradation. Quantification of Cl^- ion, product of CCl_4 degradation was performed by using an ion chromatograph (IC, Dionex DX-120) equipped with a Dionex IonPac AS 14 (4 mm x 250 mm) column and conductivity detector. The eluent solution was 3.5 mM Na_2CO_3/1 mM $NaHCO_3$.

In a photocatalytic hydrogen production experiment, 15 mg of the photocatalyst was dispersed by magnetic stirring in a 30 mL of 10% methanol/water aqueous solution. Before illumination, high-purity Ar gas was bubbled for 30 min to ensure the removal of residual oxygen. The resulting gas was detected periodically using a gas chromatograph (Hewlett Packard 6890 GC System) equipped with a thermal conductivity detector at intervals of 1 h with Ar as the carrier gas.

9.2.3 Photocatalytic oxidation

rGO/P25 with 1, 4, and 10 wt. % of rGO were tested for the degradation of methylene blue via oxidation. Catalyst powder was dispersed by ultra-sonication in distilled water at the catalyst concentration of 0.1 g/L. The concentration of methylene blue was fixed 100 μM at 30 mL of solution via the addition of methylene blue stock solution. The dye bleaching was monitored by measuring the absorbance with a UV-visible spectrophotometer (Shimadzu UV-2401PC) at λ = 663. For low concentration of methylene blue, the degradation of rGO/P25 also was tested

at the same condition without methylene blue and catalyst concentration used 50 μM methylene blue and 0.5 g/L catalyst concentration.

9.3 Results and discussion

9.3.1 Photocatalytic reduction

Concentrations of Cl^- from photocatalytic degradation of CCl_4 over P25 and rGO/P25 at pH 3 and pH 6 are presented in Figure 9.3. All rGO/P25 catalysts exhibited a better performance than P25 for the degradation of CCl_4. The best catalyst was 2 % rGO/P25 at pH 3 and pH 6. However, the activity of 2 % rGO/P25 at pH 6 (Cl^- production around 800 μM) was better than pH 3 (Cl^- production around 680 μM).

Figure 9.4 shows H_2 production at pH 3. All of rGO/P25 gave more amount of H_2 than P25 and 1%rGO/P25 was the best photocatalyst under this study condition. From the study of activity of rGO/P25 for photocatalytic reduction, the activity of P25 was enhanced by rGO. From literature on the utilization of rGO/P25 for H_2 production, rGO/P25 had a smaller band gap than P25 and the band gap decreased with the content of rGO (Fan et al., 2011). Moreover, rGO with P25 decreased in the solid state interface layer resistance and the charge transfer resistance on the surface of P25. Such behavior was the result from typical electrochemical impedance spectra with Nyquist plots which showed a shorter semicircle in the plot of rGO/P25 than P25. Thus, transporting properties rGO in the hybridized rGO/P25 could prevent the charge recombination (Zhang, Lv, Y. Li, Wang, and J. Li, 2010). Mechanism of rGO/P25 for H_2 production was proposed by Fan et al. (2011) and Xiang et al. (2011). The charge transfer and separation in the rGO/P25 system

occurred through two-dimensional p-conjugation structure of rGO sheets. rGO was an excellent electron acceptor and assisted the transfer of excited electrons which subsequently enhanced the photocatalytic reduction.

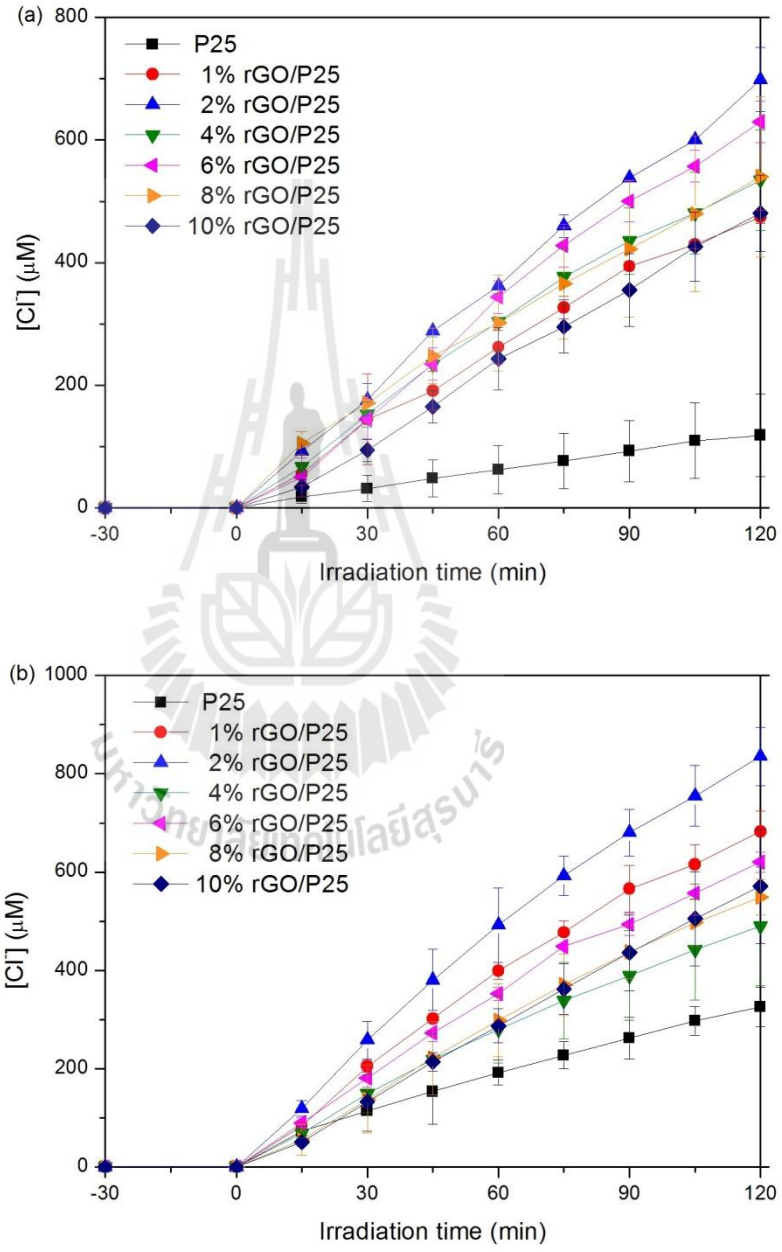

Figure 9.3 Photocatalytic degradation of CCl_4 was followed with Cl^- production at pH 3 (a) and 6 (b).

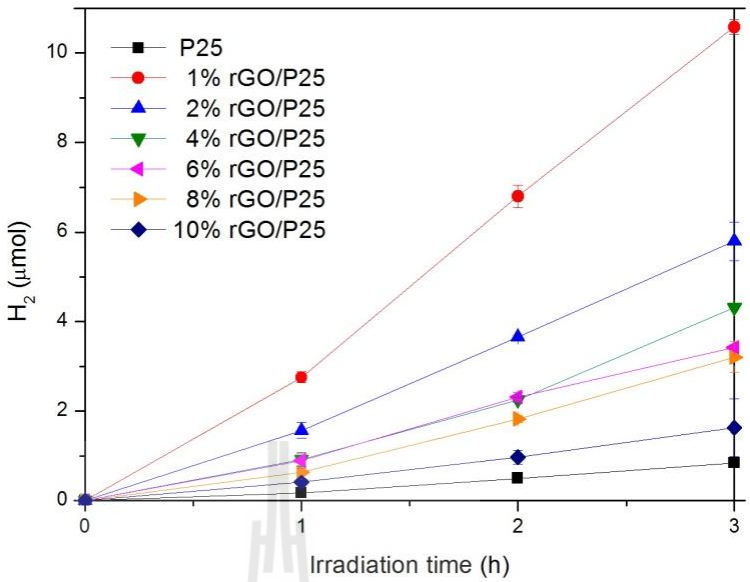

Figure 9.4 Photocatalytic production of H_2 at pH 3.

9.3.2 Photocatalytic oxidation

Photocatalytic oxidation was studied with the degradation of methylene blue. Results of methylene blue degradation by using P25 and rGO/P25 with 1, 4 and 10 wt. % of rGO were presented in Figure 9.5. The tests were done with 100 μM methylene blue and 0.1 g/L of catalyst concentration and 50 μM methylene blue and 0.3 g/L of catalyst concentration. In the dark condition, methylene blue was adsorbed by rGO/P25. The 10 %rGO/P25 showed a higher adsorption than other catalysts. At high methylene blue concentration and low catalyst amount, rGO adsorbed methylene blue but the photocatalytic activity of P25 was better than all photocatalysts. This result indicated that pollutant adsorption was not the major process to improve the activity of P25.

Table 9.1 The photocatalytic degradation of methylene blue at low concentration by bare P25 and rGO/P25 in various conditions.

Photocatalysts	conditions	Degradation efficiency / time	References
P25	$[methylene\ blue]_0$ = 27 μM,	25% , 60 min	Zhang, Lv, Y. Li,
1.0 wt. % rGO/P25	[Catalyst] = 0.1 g/L	85% , 60 min	Wang, and J. Li,
	Volume of solution = 40 mL		2010
	Light source: UV light		
P25	$[methylene\ blue]_0$ = 31.2 μM	60% , 50 min	Zhang, Tang, Fu,
0.2 wt. % rGO/P25	[Catalyst]= 0.125 g/L	70% , 50 min	and Xu, 2010
5.0 wt. % rGO/P25	Volume of solution = 160 mL	90% , 50 min	
10.0 wt. % rGO/P25	Light source: UV light	85% , 50 min	
30.0 wt. % rGO/P25		58% , 50 min	
P25	$[methylene\ blue]_0$ = 50 μM	72% , 15 min	This work
1.0 wt. % rGO/P25	[Catalyst]= 0.3 g/L	79% , 15 min	
4.0 wt. % rGO/P25	Volume of solution = 40 mL	89% , 15 min	
10.0 wt. % rGO/P25	Light source: UV-Vis light	92% , 15 min	

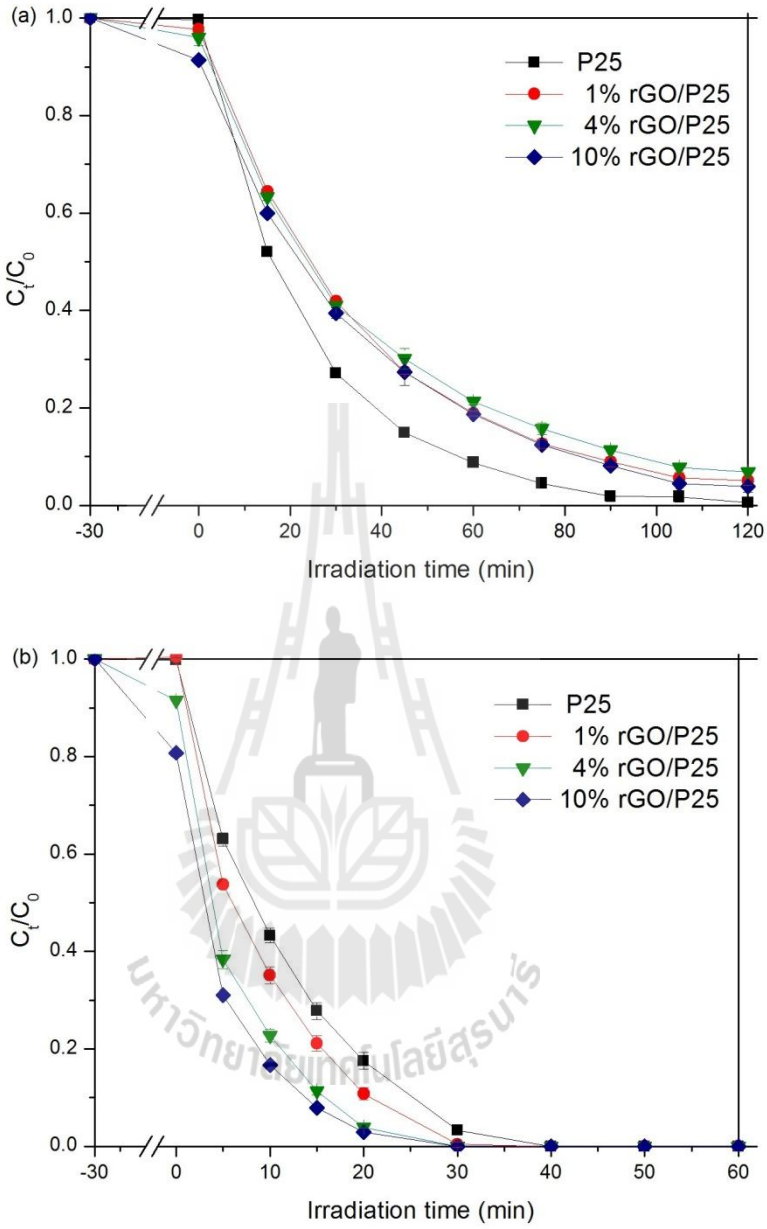

Figure 9.5 Photocatalytic degradation of methylene blue with 100 μM methylene blue and 0.1 g/L of catalyst concentration (a) and 50 μM methylene blue and 0.3 g/L of catalyst concentration (b).

At low concentration of methylene blue and high catalyst amount (low rGO content), the adsorption of methylene blue was not observed on 1 % rGO/P25 but still gave a better activity than P25. These results indicated that rGO could enhance the photocatalytic degradation of methylene blue because rGO adsorbed methylene blue and transferred photogenerated electron which decreased the recombination. Considering the preparation and property of rGO which was mentioned in the introduction part, rGO could be produced by the reduction of GO. Consequently, rGO surface lacked of oxygen-containing functional group which might compete methylene blue degradation to use OH•. Radich et al. (2014) studied stability of rGO for photocatalysis. They reported that rGO was oxidized by OH• . Behavior of rGO and OH• in photocatalysis was also studied. They irradiated TiO_2 and rGO which were dispersed in an aqueous solution. The result showed that TiO_2 and RGO aqueous suspension was essentially colorless as OH• radicals generated via UV excitation of TiO_2 oxidize rGO.

9.4 Conclusions

The activity of rGO/P25 at the rGO content of 1, 2, 4, 6, 8 and 10 wt. % was studied by using the photocatalytic reduction and oxidation. For the reduction, the degradation of CCl_4 and H_2 production were studied. All rGO/P25 catalysts exhibited higher performance than P25 for the reduction process. The catalyst with 2 %rGO/P25 was the best for CCl_4 degradation and that with 1 %rGO/P25 was the best for H_2 production. For the oxidation, the degradation of methylene blue was studied at high and low concentration. All rGO/P25 catalysts were not superior to P25 in the

degradation of methylene blue at high concentration. However, rGO/P25 had a better activity than P25 at low concentration of methylene blue.

The enhancement for the reductive processes in photocatalysis is ascribed to the ability of rGO as a good electron transfer mediator, whereas in the oxidation process rGO might hinder the activity of TiO_2 for organic pollutants which were degraded with the produced OH•. Since rGO could react with OH•, at high concentration of methylene blue, a competition of OH• using between rGO and methylene blue degradation was suggested.

9.5 References

Fan, W., Lai, Q., Zhang, Q., and Wang, Y. (2011). Nanocomposites of TiO_2 and reduced graphene oxide as efficient photocatalysts for hydrogen evolution. **Journal of Physical Chemistry C**. 115: 10694-10701.

Hoffmann, M. R., Martin, S. T., Choi, W., and Bahnemann, D. W. (1995). Environmental applications of semiconductor photocatalysis**. Chemical Reviews**. 95(1): 69-96.

Kim, J., Choi, W., and Park, H. (2010). Effects of TiO_2 surface fluorination on photocatalytic degradation of methylene blue and humic acid. **Research on Chemical Intermediates**. 36: 127-140

Liu, B., Huang, Y., Wen, Y., Du, L., Zeng, W., Shi, Y., Zhang, F., Zhu, G., Xua X., and Wang, Y. (2012). Highly dispersive {001} facets-exposed nanocrystalline TiO_2 on high quality graphene as a high performance photocatalyst. **Journal of Materials Chemistry**. 22: 7484-7491.

Radich, J. G., Krenselewski, A. L., Zhu, J., and Kamat, P. V. (2014). Is Graphene a stable platform for photocatalysis? mineralization of reduced graphene oxide with UV-irradiated TiO_2 nanoparticles. **Chemistry of Materials**. 26: 4662-4668.

Xiang, Q., Yu, J., and Jaroniec, M. (2011). Enhanced photocatalytic H_2-production activity of graphene-modified titania nanosheets. **Nanoscale**. 3: 3670-3768.

Zhang, X., and Cui, X. (2012). Graphene/semiconductor nanocomposites: preparation and application for photocatalytic hydrogen evolution. **Nanocomposites-New Trends and Developments**. 10: 239-257.

Zhang, H., Lv, X., Li, Y., Wang, Y., and Li, J. (2010). P25-graphene composite as a high performance photocatalyst. **ACS Nano**. 4(1): 380-386.

Zhang, Y., Tang, Z., Fu, X., and Xu, Y. (2010). TiO_2-Graphene nanocomposites for gas-phase photocatalytic degradation of volatile aromatic Pollutant: is TiO_2-graphene truly different from other TiO_2-carbon composite materials? **ACS Nano**. 4(12): 7303-7314

Zhou, K., Zhu, Y., Yang, X., Jiang, X., and Li, C. (2011). Preparation of graphene–TiO_2 composites with enhanced photocatalytic activity. **New Journal of Chemistry**. 35: 353-359.

CHAPTER X

CONCLUSIONS

Paraquat and imidachloprid are pesticides that can be dissolved and accumulated in water. In this thesis, removal of paraquat and imidacloprid by adsorption and photocatalytic degradation were investigated. Moreover, photocatalytic degradations of other organic pollutants which have similar property to paraquat or imidacloprid were studied.

Paraquat adsorption was investigated on rice husk silica (RHS) and porous materials derived from RHS including MCM-41, NaY and NaBEA. These materials were different in pore structure, surface area and Si/Al ratio. The adsorption on all adsorbents fitted well with Langmuir model; the highest adsorption capacity of 185.2 mg/g was obtained on NaY; and the adsorption mechanism was cation exchange. In the study of commercial grade paraquat, blue dye in a commercial grade paraquat did not interfere the adsorption. The blue dye was adsorbed on MCM-41 likely on silanol groups.

To increase the paraquat adsorption capacity, adsorbents with higher Al contents were studied including NaX which had a higher Al content than NaY and Al-MCM-41. Al-MCM-41 with various Si/Al ratios was synthesized by hydrothermal method by adding Al source to the synthesis gel. As expected, the paraquat adsorption

on Al-MCM-41 was higher than MCM-41. NaX was synthesized by hydrothermal method using rice husk silica. The surface area determined from N_2 adsorption-desorption was 735 m^2/g and the Si/Al ration determined by XRF was 1.27. The paraquat adsorption capacity from NaX was 120.3 mg/g-adsorbent which was lower than NaY.

Characteristic of bare zeolites (NaY and NaX) and paraquat containing zeolites (PQY and PQX) were studied. XRD pattern of PQY and PQX did not change from those of the bare ones. The N_2 adsorption-desorption isotherm was still in type I but the surface area decreased significantly. The surface areas of PQY and PQX were consistent with the paraquat adsorption capacity. Paraquat occupied almost all the micropore area of NaY whereas half of micropore area was occupied in the case of NaX. The presence of paraquat after adsorption was confirmed by FTIR. Paraquat adsorption did not change the structure of NaY and NaX. Moreover, ^{23}Na MAS NMR indicated that interaction of Na^+ cation in NaX was stronger than in NaY, making it less favorable for ion exchange with paraquat.

On photocatalytic degradation of paraquat, photocatalysts were prepared by grafting TiO_2 on rice husk silica (RHS) and zeolite NaY. The amount of TiO_2 was 10 and 30 wt. % and the phase was anatase. The adsorption on TiO_2/NaY was higher than TiO_2/RHS. The adsorption on TiO_2/NaY decreased when the TiO_2 loading increased whereas that on TiO_2/RHS decreases with the TiO_2 loading. In the photocatalytic testing, TiO_2/NaY-supported catalysts were not active probably due to high adsorption of paraquat. For TiO_2/RHS catalysts, the degradation ability was in the following order: 30 %TiO_2/RHS > un-supported TiO_2 > 10 %TiO_2/RHS. Base on

the same TiO_2 content, the photocatalytic degradation of paraquat on 30 %TiO_2/RHS was similar to P25, completed in 180 min.

On the removal of imidacloprid from aqueous solution, RHS, NaY and Al-MCM-41 synthesized by hydrothermal method with 10, 15 and 25 wt. % content was used as an adsorbent. Concentration of imidacloprid decreased with Al loading and reached the maximum in 30 min, then returned to the solution. Thus, the adsorption method was not suitable for imidaclroprid removal. In the photocatalytic degradation, TiO_2/NaY and TiO_2/RHS with 30 wt. % of TiO_2 were used as photocatalysts which compared with P25. Photolysis was tested before the photocatalysis. Imidacloprid was degraded by light without photocatalysts. TiO_2/NaY and TiO_2/RHS showed similar activity giving around 30% degradation. Both catalysts were less active the P25. Although, photocatalytic degradation was slow to remove imidacloprid, it was better than adsorption and photolysis.

Other organic pollutants were studied for photocatalytic degradation by using reduced graphene oxide (rGO) with P25. The study was divided into two parts. In the first part, 1 wt. % of rGO with P25 was investigated by the photocatalytic degradation via oxidation including anionic, cationic and neutral pollutants. The adsorption of all compounds on P25 and rGO/P25 was low at both of pH 3 and pH 6. The photocatalytic degradation of all between compounds on P25 and rGO/P25 was higher activity at pH 3 than pH 6. However, P25 exhibited higher performance than rGO/P25 for the photocatalytic degradation of organic pollutants in three ion groups. Thus, the charge of the pollutions had no influence on the activity of rGO on P25. In the second part, rGO/P25 at the 1, 2, 4, 6, 8 and 10 wt. % rGO content was studied by using the photocatalytic reduction and oxidation. For the reduction, the catalyst with 2

%rGO/P25 was the best for CCl_4 degradation and that with 1 %rGO/P25 was the best for H_2 production. All rGO/P25 catalysts exhibited higher performance than P25 for the reduction process. For the oxidation, all rGO/P25 catalysts were not superior to P25 in the degradation of methylene blue at high concentration. However, rGO/P25 had a better activity than P25 at low concentration of methylene blue. The enhancement for the reductive processes in photocatalysis is ascribed to the ability of rGO as a good electron transfer mediator, whereas in the oxidation process rGO might hinder the activity of TiO_2 for organic pollutants which were degraded with the produced OH•. Since rGO could react with OH•, at high concentration of methylene blue, a competition of OH• using between rGO and methylene blue degradation was suggested.

Recommendation for further work

Interesting topics for further study are as follows:

(i) To find a suitable ratio of NaY and RHS for adsorption of commercial paraquat because both paraquat and blue dye could be removed effectively.

(ii) To study effect of electron or hole scavenger on TiO_2/NaY for photocatalytic degradation of paraquat.

APPENDICES

APPENDIX A

LINEAR EQUATION OF ADSORPTION ISOTHERM FROM LANGMUIR AND FREUNDLICH MODEL

A 1 Adsorption

An adsorption process involves an accumulation of molecule called an adsorbate on a solid surface called an adsorbent. Adsorption can be divided into 2 types which are physical and chemical adsorption. In physical adsorption, the adsorbate interacts with the adsorbent via weak intermolecular force. For chemical adsorption, the adsorbate chemically bonds to the surface of the adsorbent (Do, 1998).Binding behavior of the adsorbate to the adsorbent at a constant temperature can be expressed as a curve called an adsorption isotherm. Adsorption isotherm is plot between the apparent adsorption of the adsorbate and the equilibrium concentration. Langmuir and Freundlich models are commonly applied to explain the adsorption behavior.

A 2 Langmuir model

Langmuir adsorption isotherm is applicable to chemisorptions to form a monolayer. In this model, the adsorbent surface composed of equivalent and dependent sites for adsorption. The rate of adsorption depends on concentration of adsorbate and fraction of bare sites. The rate of desorption depends on activation

energy of adsorption. At equilibrium the rate of adsorption equals to that of desorption. It is assumed that there is no adsorbate – adsorbate interaction. In the Langmuir adsorption isotherm, a plateau is generally obtained.

The Langmuir adsorption isotherm is defined by equation (1).

$$q = q_m K_A X_e/(1+ K_A X_e) \quad \ldots(1)$$

where, q (mg/g) is the amount of the adsorbate adsorbed per gram of the adsorbent;

q_m (mg/g) is the amount of the adsorbate adsorbed to form a monolayer coverage;

K_A (L/mg) is the Langmuir adsorption equilibrium constant;

X_e (mg/L) is the amount of the adsorbate in a solution at equilibrium

Adsorption data can be fitted to the Langmuir isotherm in its linear form as in equation (2).

$$X_e/q = X_e/q_m + 1/K_A q_m \quad \ldots(2)$$

It is possible that there are deviations from Langmuir isotherm.

Adsorption data of paraquat on all adsorbents was fitted to the Langmuir model and give linear equation which can calculate maximum capacity. Figure A 1 – 9 show the linear equation from Langmuir model of all adsorbents.

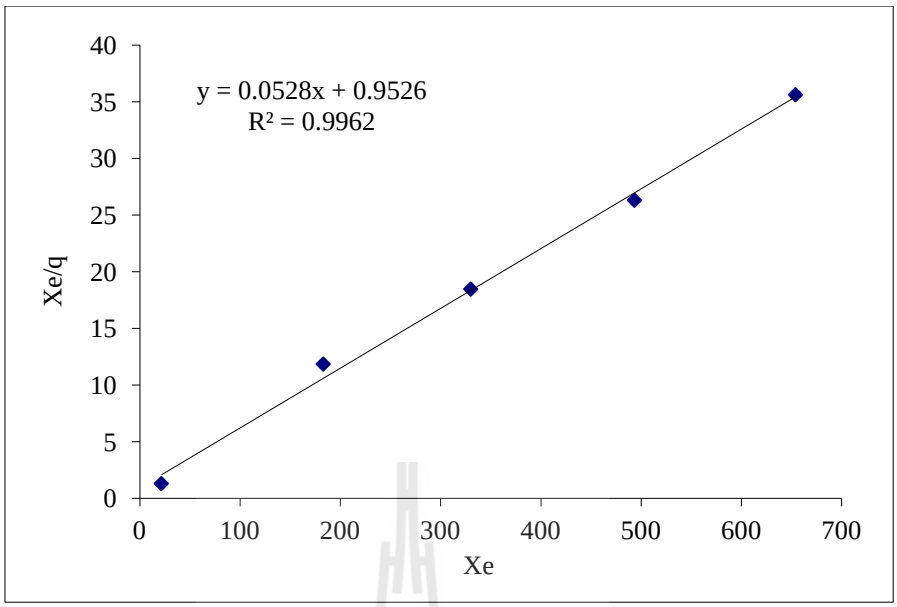

Figure A 1 Adsorption data of RHS was fitted to the Langmuir model.

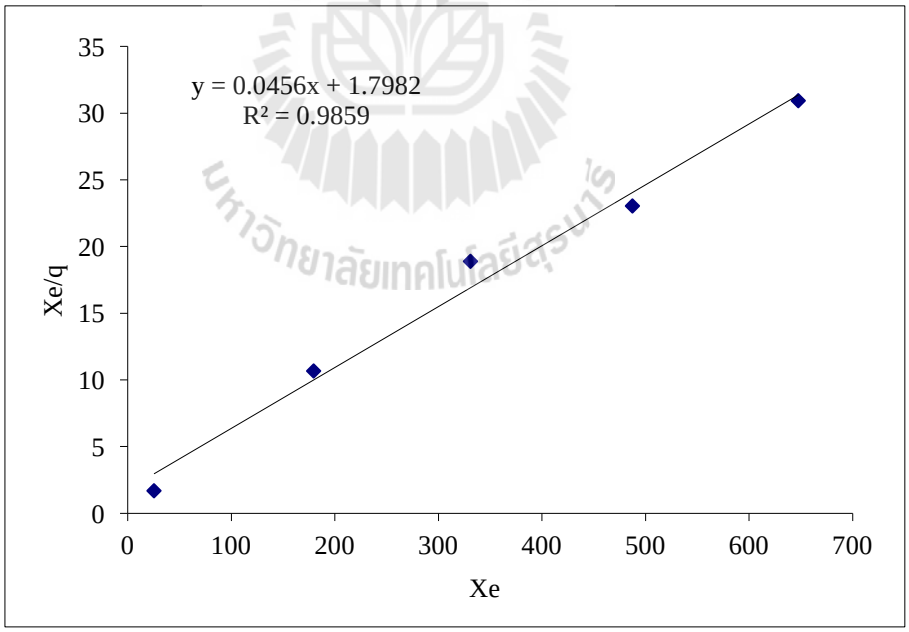

Figure A 2 Adsorption data of MCM-41 was fitted to the Langmuir model.

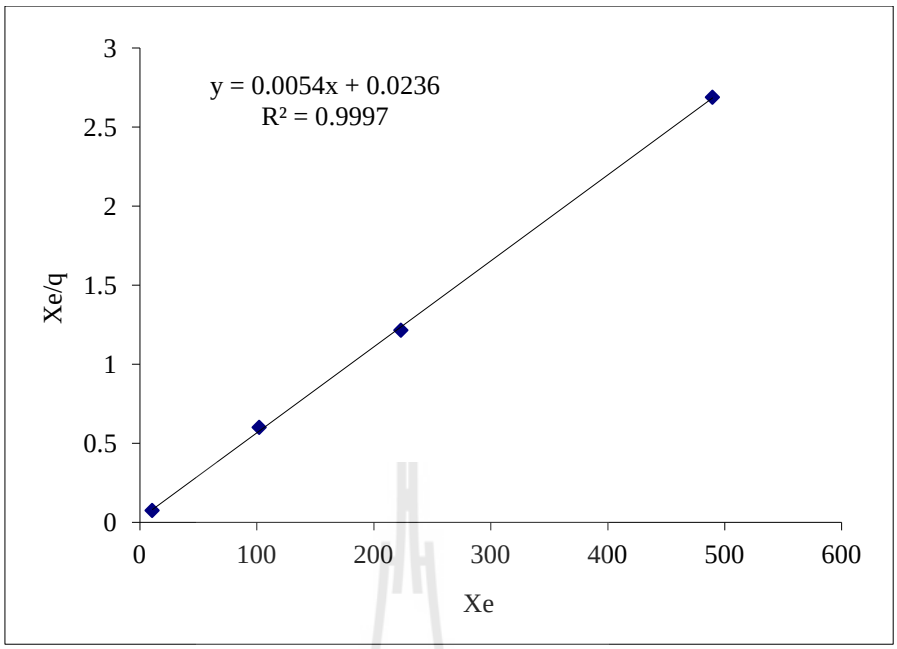

Figure A 3 Adsorption data of NaY was fitted to the Langmuir model.

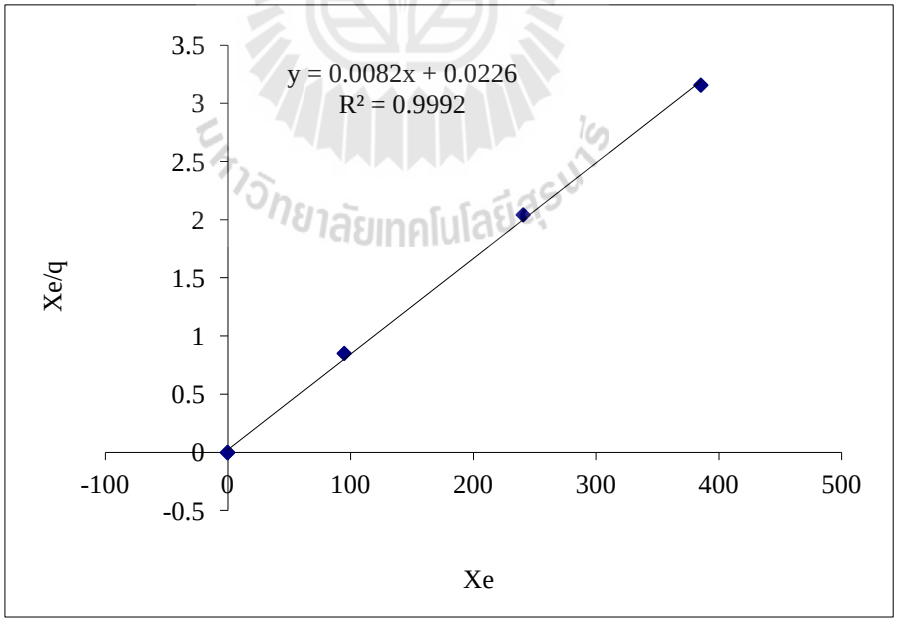

Figure A 4 Adsorption data of NaBEA was fitted to the Langmuir model.

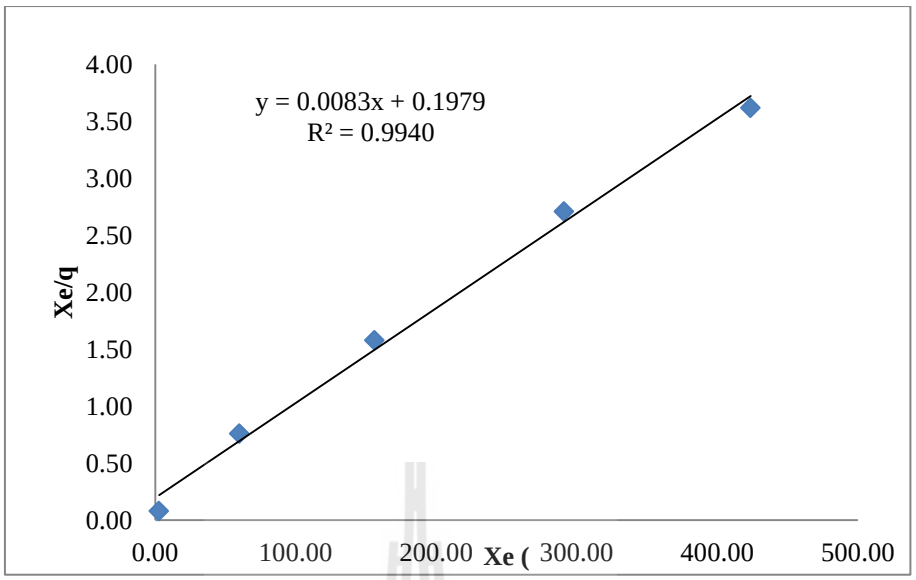

Figure A 5 Adsorption data of NaX was fitted to the Langmuir model.

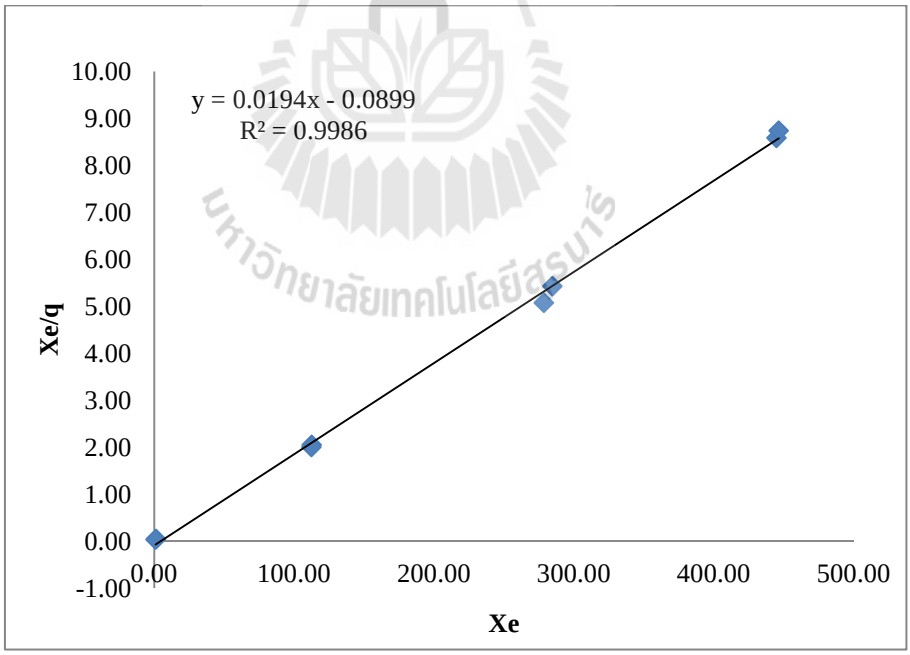

Figure A 6 Adsorption data of 10%Al-MCM-41 was fitted to the Langmuir model.

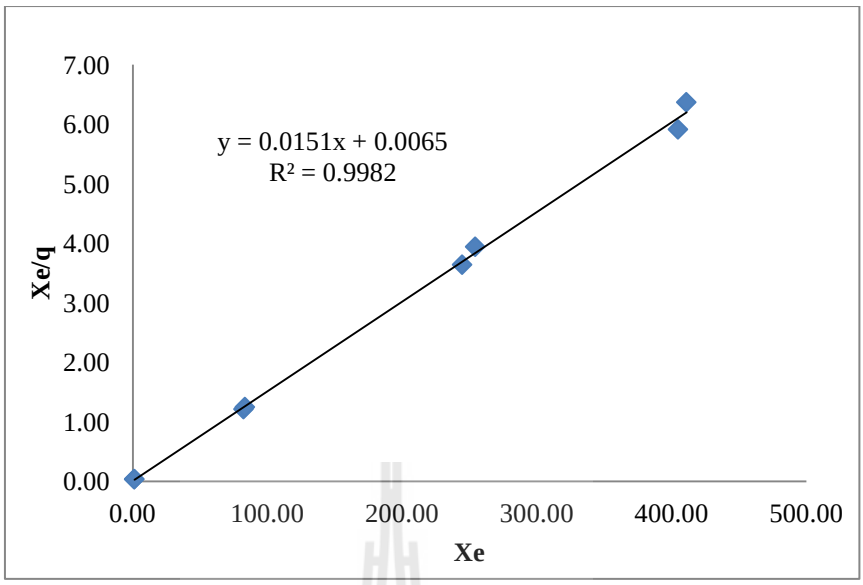

Figure A 7 Adsorption data of 15%Al-MCM-41 was fitted to the Langmuir model.

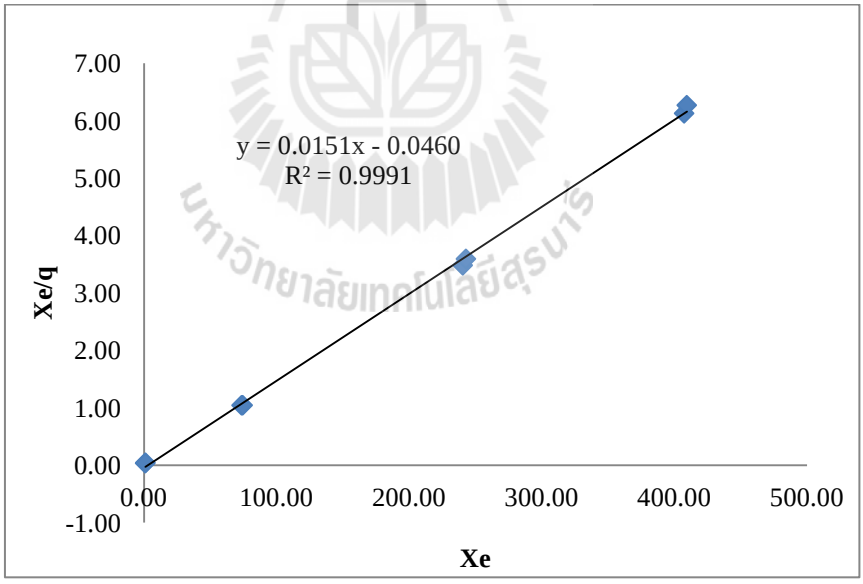

Figure A 8 Adsorption data of 20%Al-MCM-41 was fitted to the Langmuir model.

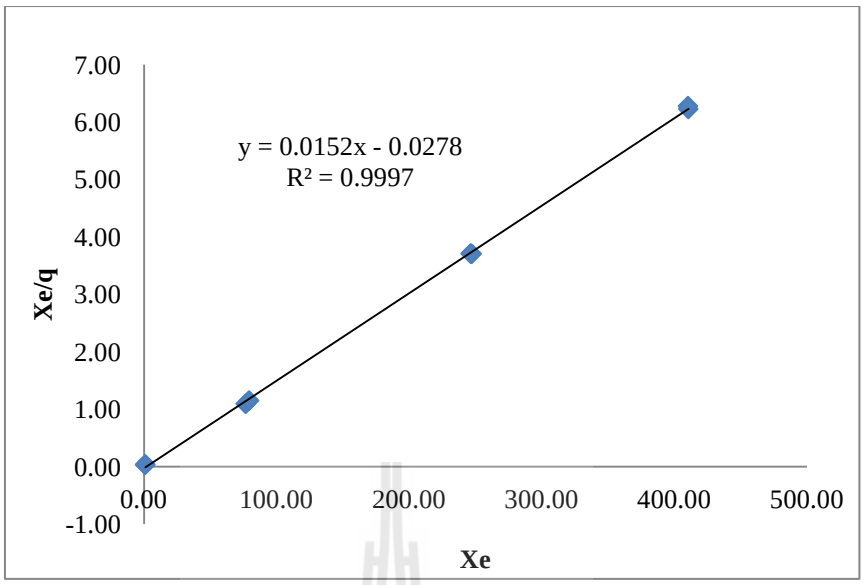

Figure A 9 Adsorption data of 25%Al-MCM-41 was fitted to the Langmuir model.

A 3 Freundlich model

Other types of isotherm can be used to explain the adsorption behavior. For example, Freundlich adsorption isotherm is used for adsorbents with multisites.

The Freundlich adsorption isotherm is defined as shown in equation (3).

$$q = K_F * X_e^{1/n} \quad \ldots(3)$$

where, K_F and n are both Freundlich constant.

Adsorption data can be fitted to the Freundlich isotherm in its linear form as:

$$\log q = \log K_f + 1/n(\log X_E) \quad \ldots(4)$$

Figure A 10-18 showed the linear equation from Freundlich model of all adsorbents.

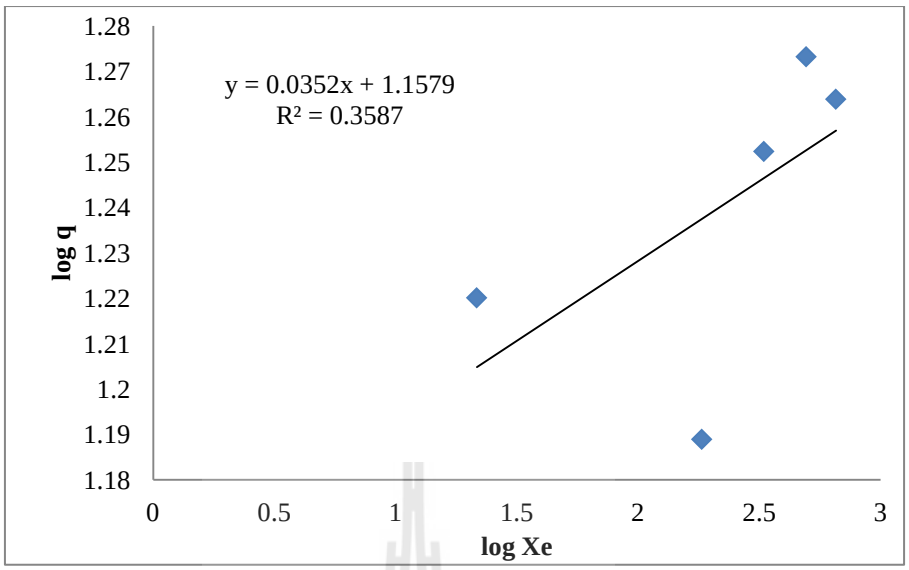

Figure A 10 Adsorption of RHS was fitted to the Freundlich model.

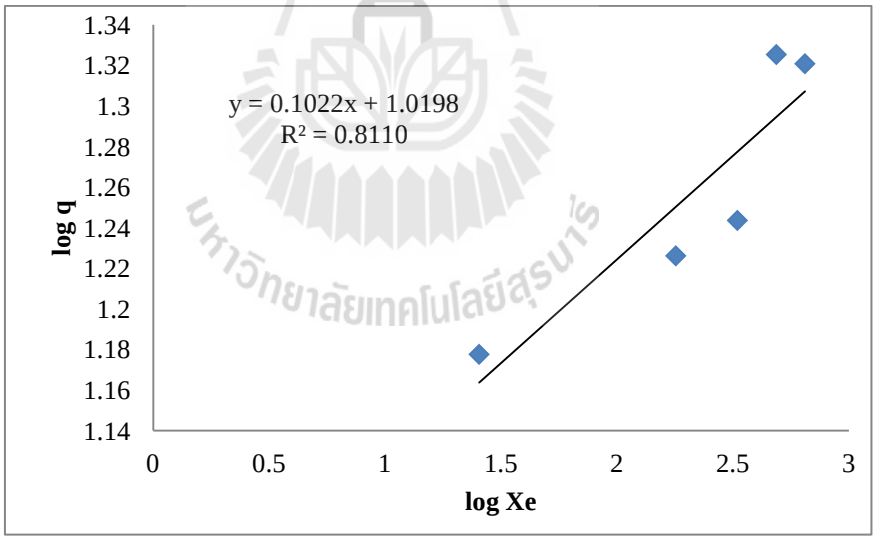

Figure A 11 Adsorption data of MCM-41 was fitted to the Freundlich model.

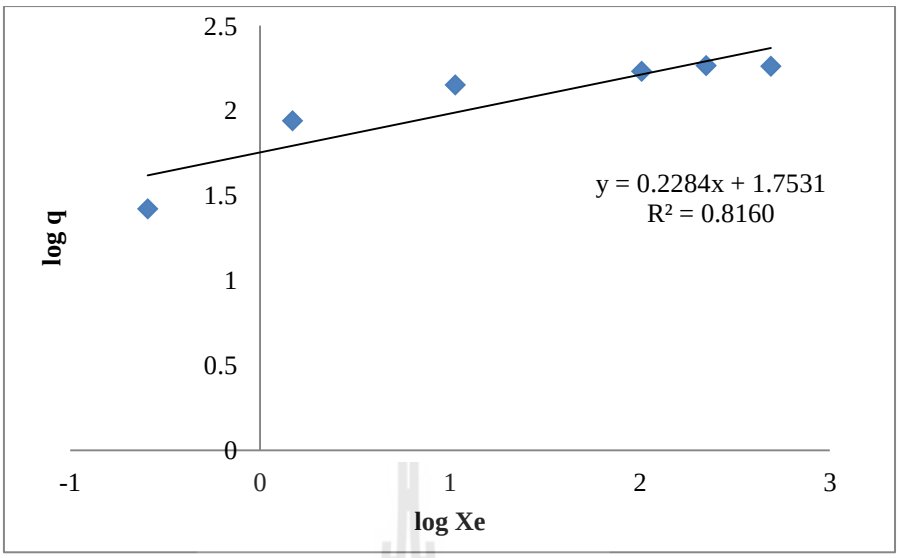

Figure A 12 Adsorption data of NaY was fitted to the Freundlich model.

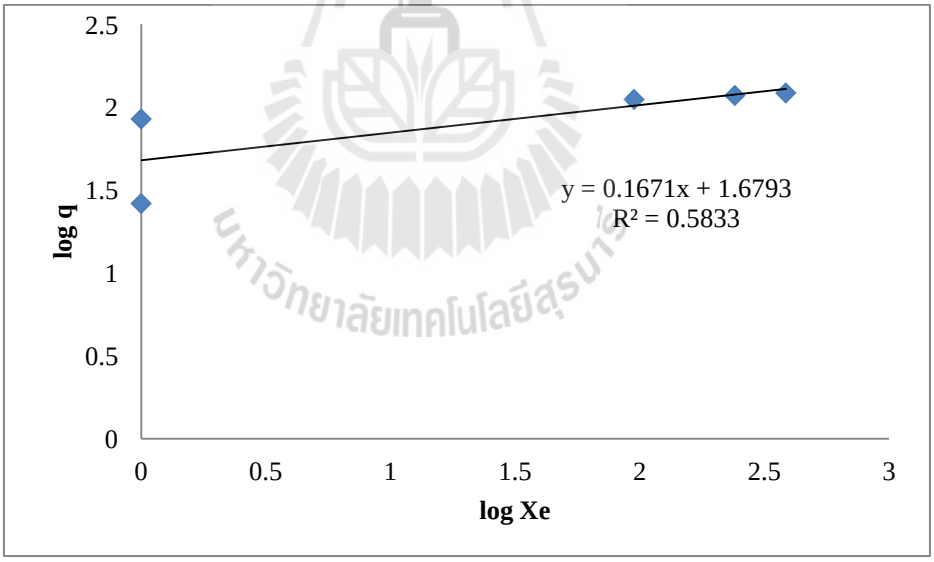

Figure A 13 Adsorption data of NaBEA was fitted to the Freundlich model.

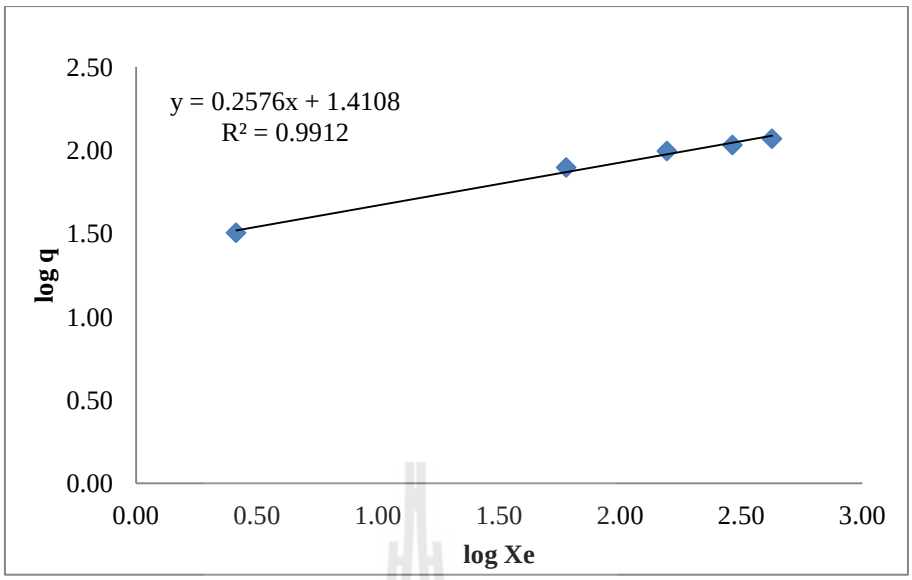

Figure A 14 Adsorption data of NaX was fitted to the Freundlich model.

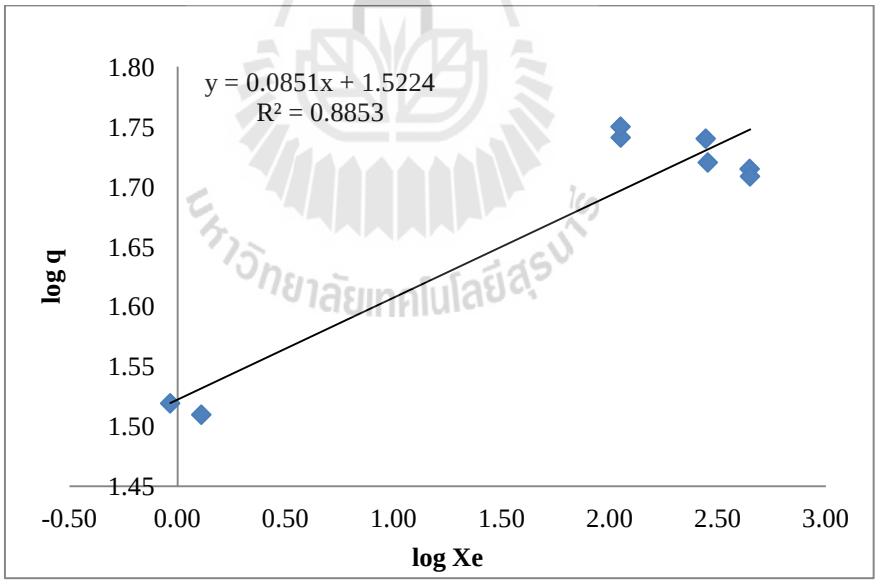

Figure A 15 Adsorption data of 10%Al-MCM-41 was fitted to the Freundlich model.

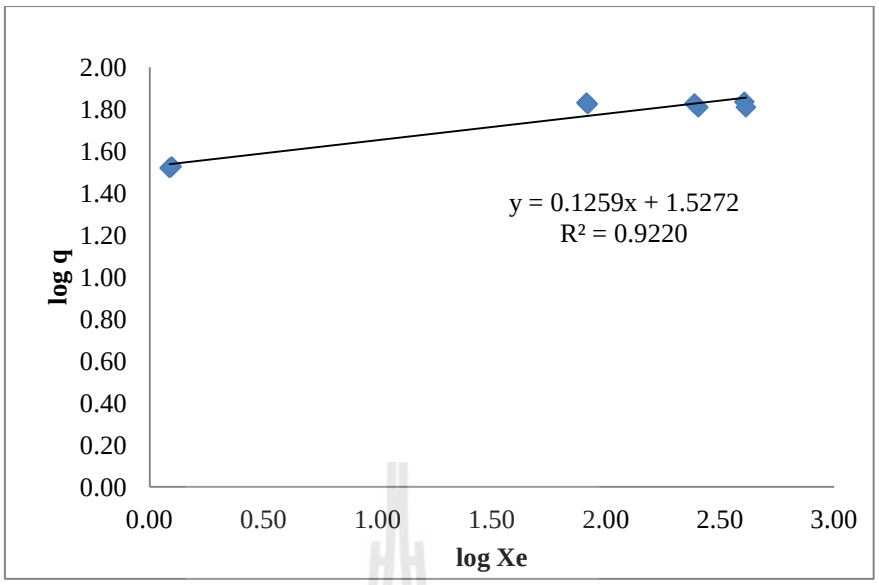

Figure A 16 Adsorption data of 15%Al-MCM-41 was fitted to the Freundlich model.

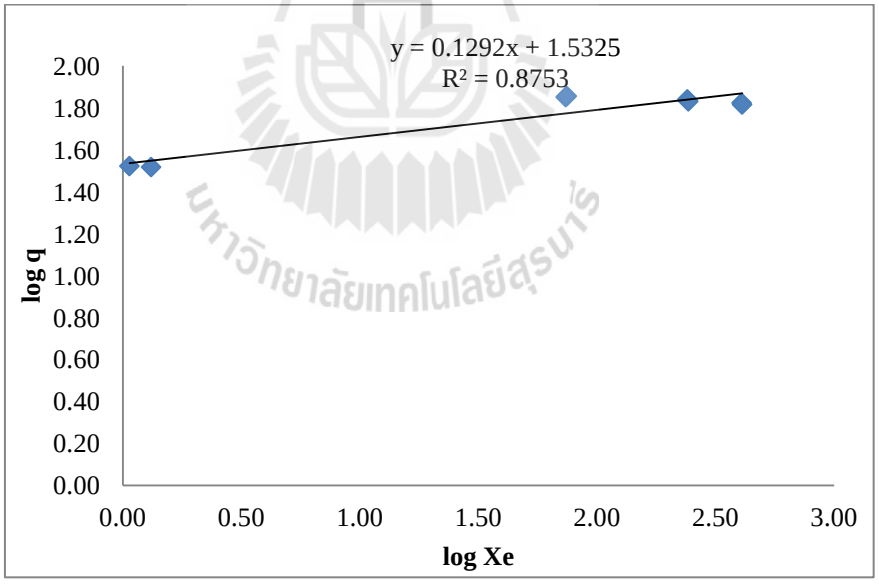

Figure A 17 Adsorption data of 20%Al-MCM-41 was fitted to the Freundlich model.

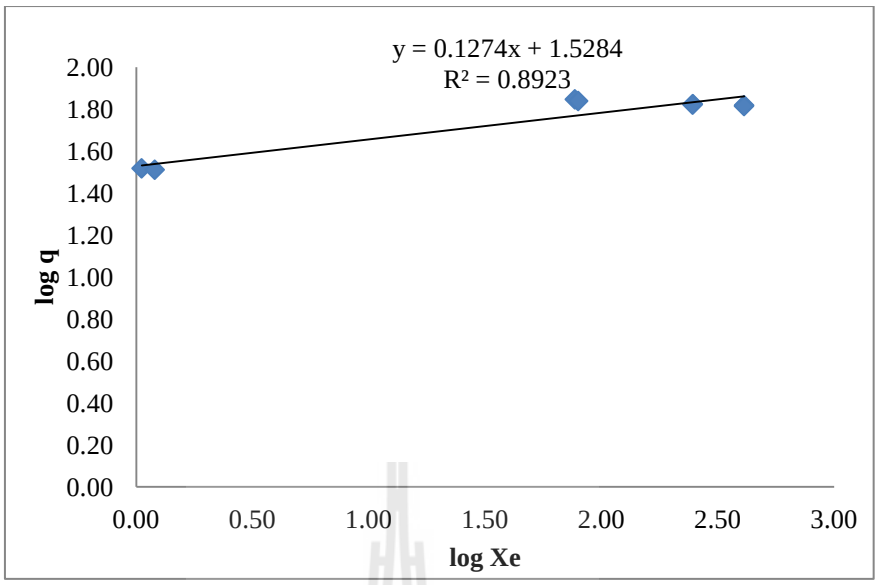

Figure A 18 Adsorption data of 25%Al-MCM-41 was fitted to the Freundlich model.

A 4 Reference

Do, D. D. (1998). **Adsorption analysis: equilibria and kinetic**. Vol.1. London: Imperial College Press.

APPENDIX B

PHOTOCATALYTIC ACTIVITY OF REDUCED GRAPHENE OXIDE WITH P25 FOR DEGRADATION OF VARIOUS POLLUTANTS

B 1 Effect of phosphate with rGO and P25 for Photocatalytic degradation of 2,4-dichlorophenoxyacetic acid (2,4-D)

The photocatalytic degradation of 2,4-D adsorbed on P25 surface is most favorably initiated by the direct hole transfer to the adsorbate, which leads to the generation of 2,4-DCP as an intermediate (Figure B 1). Kim and Choi (2011) reported that P-P25/Pt could completely remove of 2,4-D and 2,4-DCP. In this part we studied cooperation of phosphate and rGO to degrade both of 2,4-D and 2,4-DCP. Moreover, all samples were studied under O_2 or/and Fe^{3+} condition.

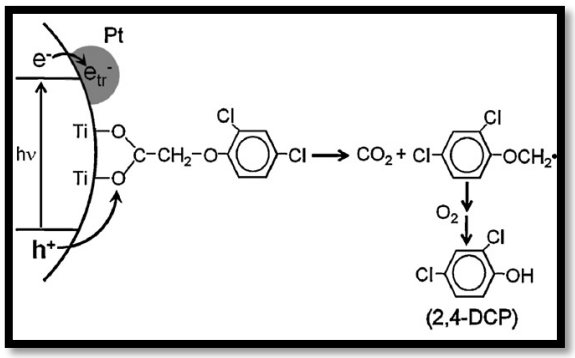

Figure B 1 Problem of 2,4-D photocatalytic degradation (Kim and Choi, 2011).

B 1.1 Experimental

1.1.1 Preparation of surface phosphation

P25, rGO-P25 or 8rGO-P25catalyst (0.1 g) was dispersed in 100 mL of 30 mM phosphoric acid solution and the suspension was stirred for 5 h for the adsorption of phosphate on the surface of catalyst. Phosphate-modified catalyst (P/P25, P/rGO-P25 or P/8rGO-P25) was collected by filtration and then dried at room temperature.

1.1.2 Photocatalytic activity

Catalyst powder (15 mg) was dispersed in 15 mL of distilled water by ultra-sonication. The concentration of 2,4-D was fixed 500 μM via the addition of 15 mL of 1000 μM 2,4-D stock solution. The pH of the suspension was adjusted with 0.1 M $HClO_4$ solution for pH 3 or 1 M NaOH solution for pH 11, and then the suspension was stirred in dark for 30 min to reach the adsorption equilibrium of substrates on the photocatalyst. A 300-W Xe arc lamp was used as a light source, 10-cm IR water filter and a cutoff filter ($\lambda > 320$ nm) were used to light cutoff and focused onto a cylindrical Pyrex reactor (30 mL) with a quartz window. The reactor was open to the ambient air to prevent the depletion of dissolved dioxygen, and stirred magnetically during irradiation. For study of Fe^{3+} and/or O_2 effect, 1 mL of 15 mM Iron(III)perchlorate hydrate ($Fe(ClO_4)_3 .xH_2O$) was add in reactor to give concentration of Fe^{3+} at 0.5 mM and /or oxygen gas dispersed to reactor. Sample aliquots were withdrawn from the reactor intermittently during the illumination and filtered through a 0.45 μm PTFE syringe filter to remove photocatalyst particles.The degradation of 2,4-D and the concurrent production of 2,4-dichlorophenol (2,4-DCP) as an intermediate from the degradation of 2,4-D were monitored using a high

performance liquid chromatograph (HPLC: Agilent 1100 series) equipped with a diode array detector and a ZORBAX 300SB C18 column (4.6 mm ×150 mm). The eluent consisted of a binary mixture of 0.4% acetic acid solution and acetonitrile for the analysis of 2,4-D and 2,4-DCP (7:3 by volume).

B 1.2 Results

Results of various conditions at pH 3 are shown in figure B 2 – 5. Figure B 2 show photocatalytic degradation of 2,4-D and generation of intermediate 2,4-DCP at ambient condition. The results showed that the 2,4-D degradation activity of bare catalysts (without phosphate) were better than P/catalysts. The 2,4-D degradation ability was in the following order: P25 > rGO/P25 > 8%rGO/P25 > P/P25 > P/rGO/P25 > P/8%rGO/P25. Figure B 3 show photocatalytic degradation of 2,4-D and generation of intermediate 2,4-DCP with continually flowed O_2. In the O2 condition photocatalytic activity of all catalysts were improved. This result indicated that O_2 can improve both of 2,4-D degradation activity. Fe^{3+} can decrease 2,4-DCP production. Figure B 4 and 5 show photocatalytic degradation of 2,4-D with Fe^{3+} at ambient and O_2condition, respectively. The 2,4-D degradation ability at various conditions was in the following order: O_2 > Ambient air > Fe^{3+}/O_2 > Fe^{3+} O_2. The results indicated that Fe^{3+} can not improve the activity of rGO on P25 and the activity decrease with rGO loading increase.

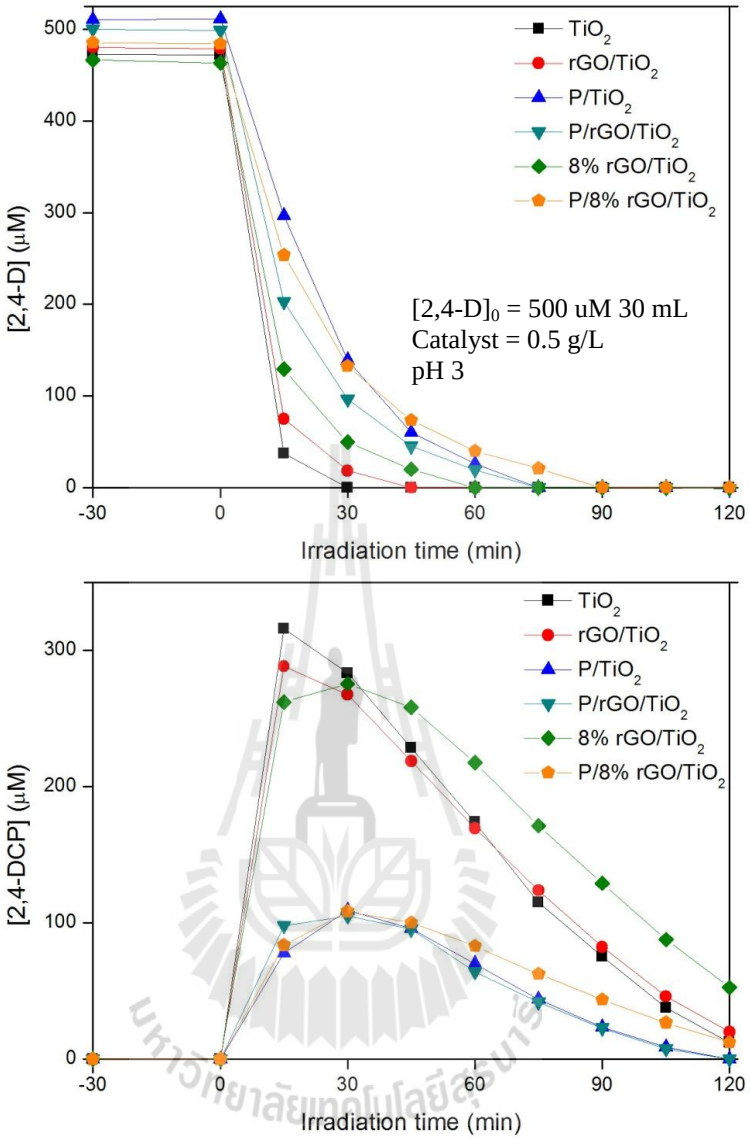

Figure B 2 Photocatalytic degradation of 2,4-D (top) and generation of intermediate 2,4-DCP (bottom) at pH 3.

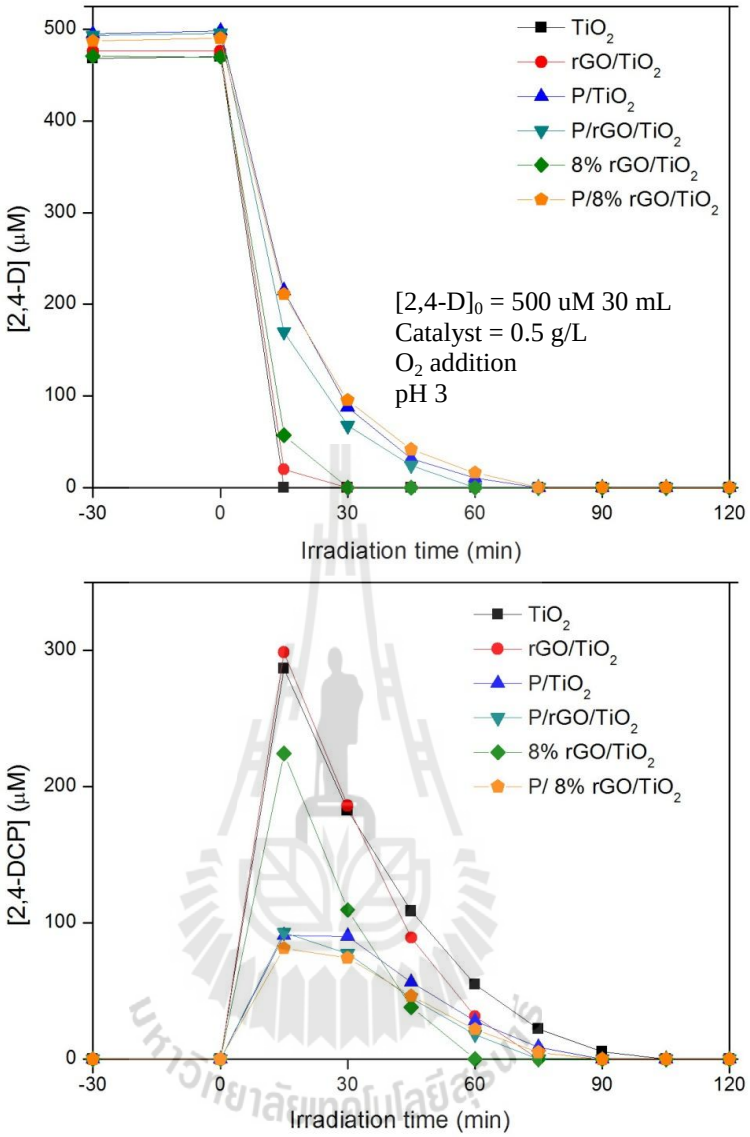

Figure B 3 Photocatalytic degradation of 2,4-D (top) and generation of intermediate 2,4-DCP (bottom) at pH 3 with O_2.

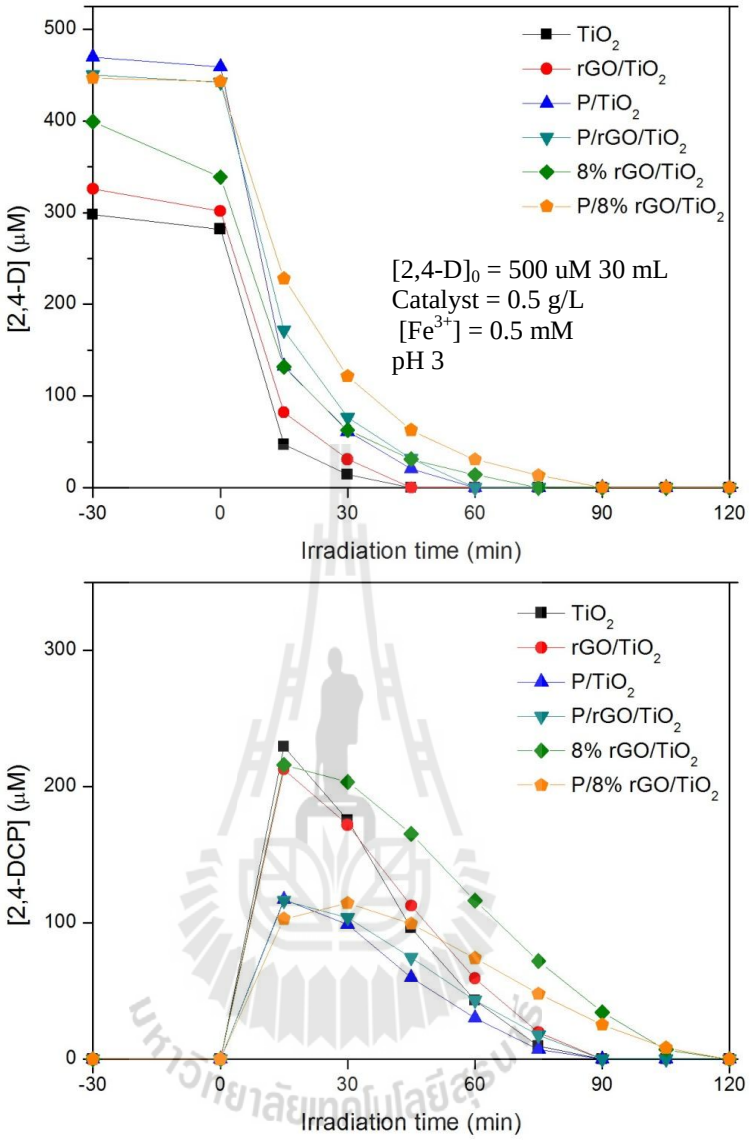

Figure B 4 Photocatalytic degradation of 2,4-D (top) and generation of intermediate 2,4-DCP (bottom) at pH 3 with Fe^{3+}.

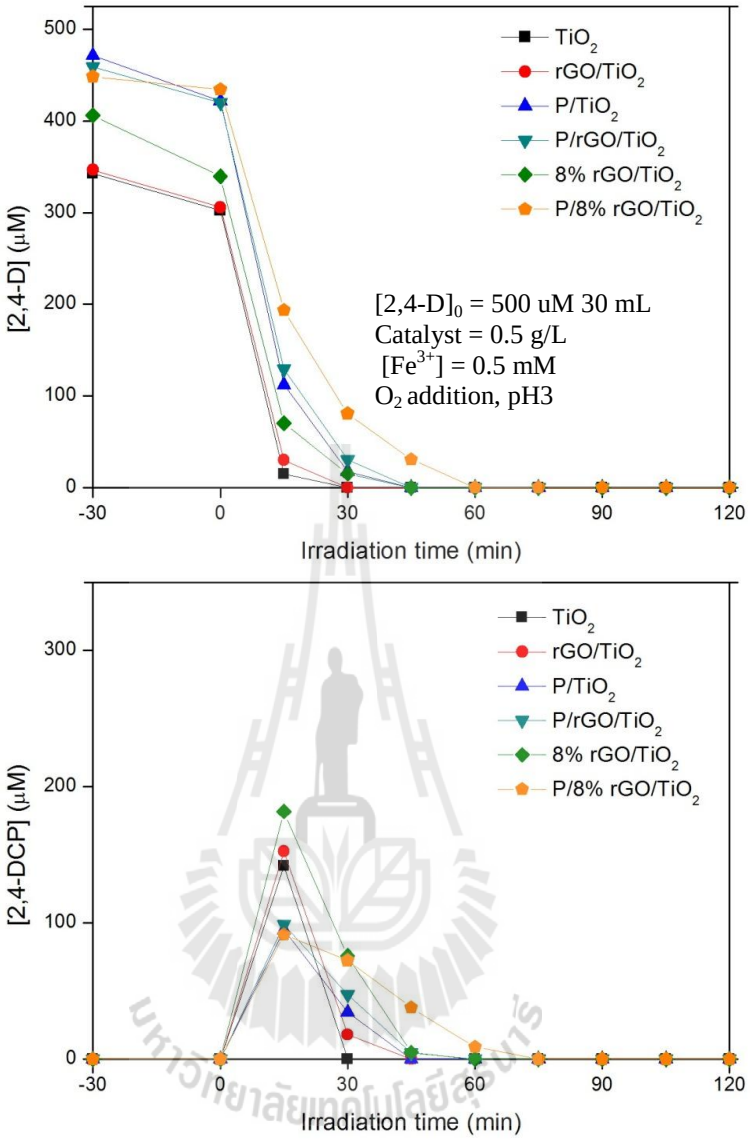

Figure B 5 Photocatalytic degradation of 2,4-D (top) and generation of intermediate 2,4-DCP (bottom) at pH 3 with O_2 and Fe^{3+}.

B 2 Study of rGO activity on P25 in oxidative process via degradation of benzoic acid and coumarin

From the photocatalytic degradation of organic pollutants via oxidation was mentioned in Chapter VIII and IX. The activity of rGO/P25 was investigated with varying the rGO content (1, 2, 4, 6, 8 and 10 wt%) for the degradation of benzoic acid (BA) and coumarin via oxidation. Reaction benzoic acid and coumarin degradation are shown below this paragraph. The results were shown in Figure B 6 – 9.Similarly, all rGO/P25 catalysts were not superior to P25. Thus, rGO may hinder the activity of TiO_2 for oxidation because the produced hydroxyl radical could react with rGO.

- Benzoic acid degradation

- Coumarin degradation

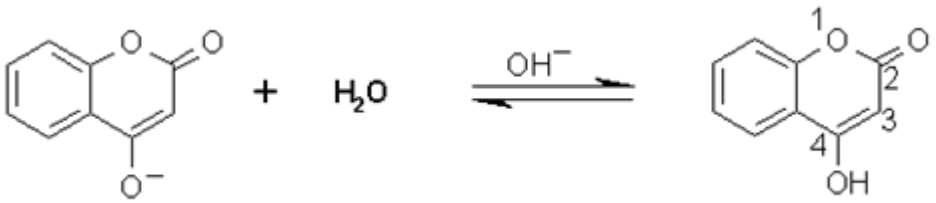

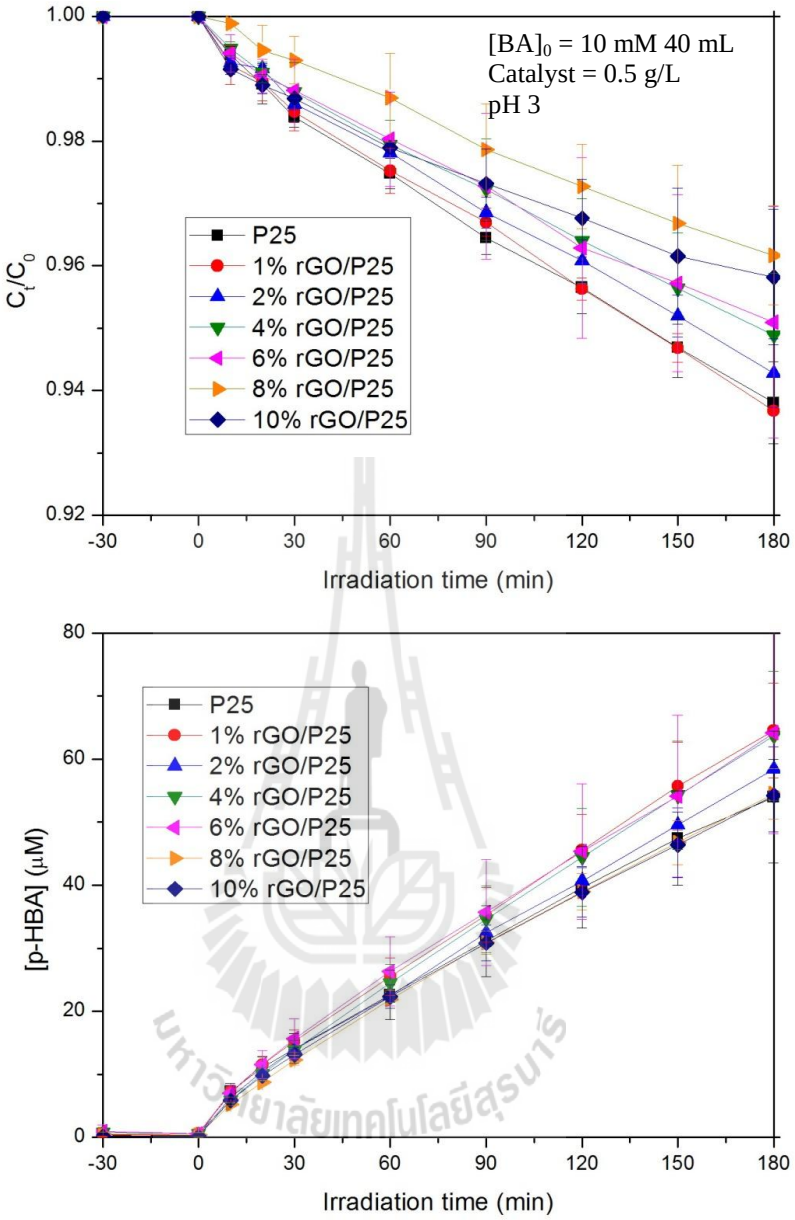

Figure B 6 Photocatalytic degradation of BA (top) and generation of intermediate p-HBA (bottom) at pH 3.

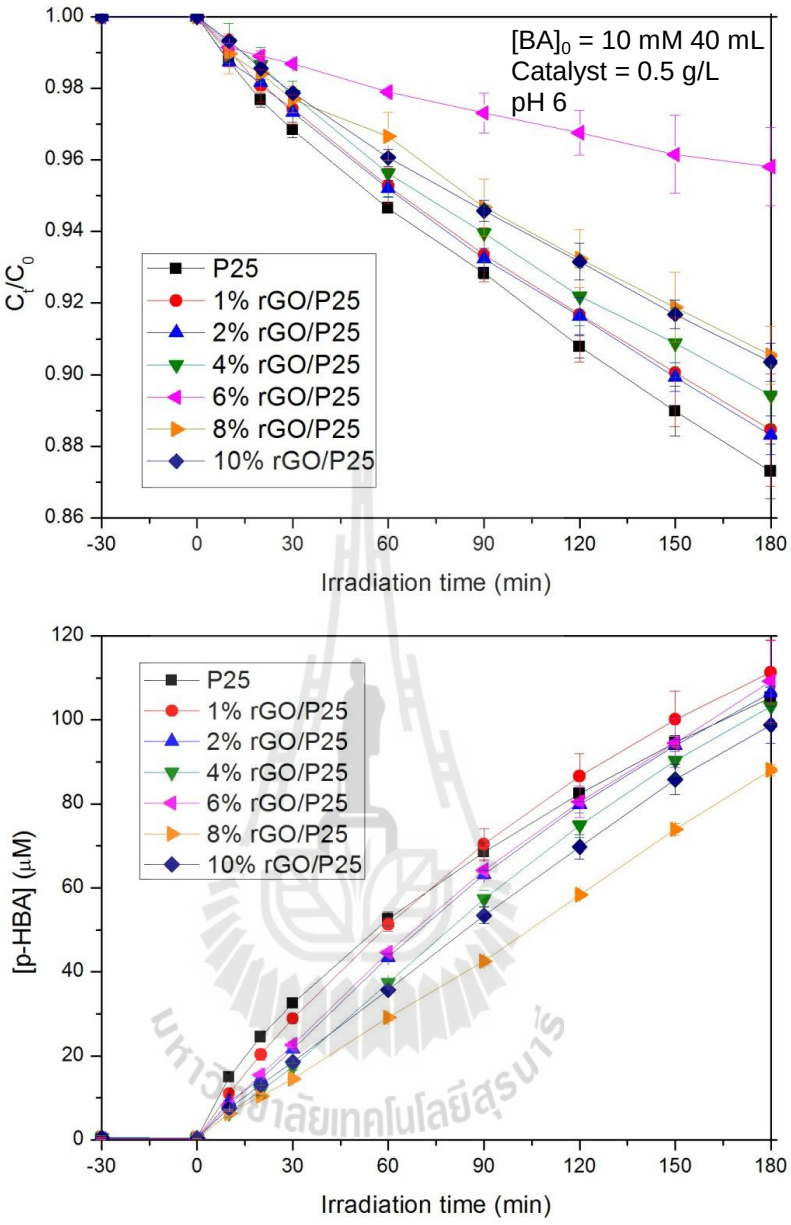

Figure B 7 Photocatalytic degradation of BA (top) and generation of intermediate p-HBA (bottom) at pH 6.

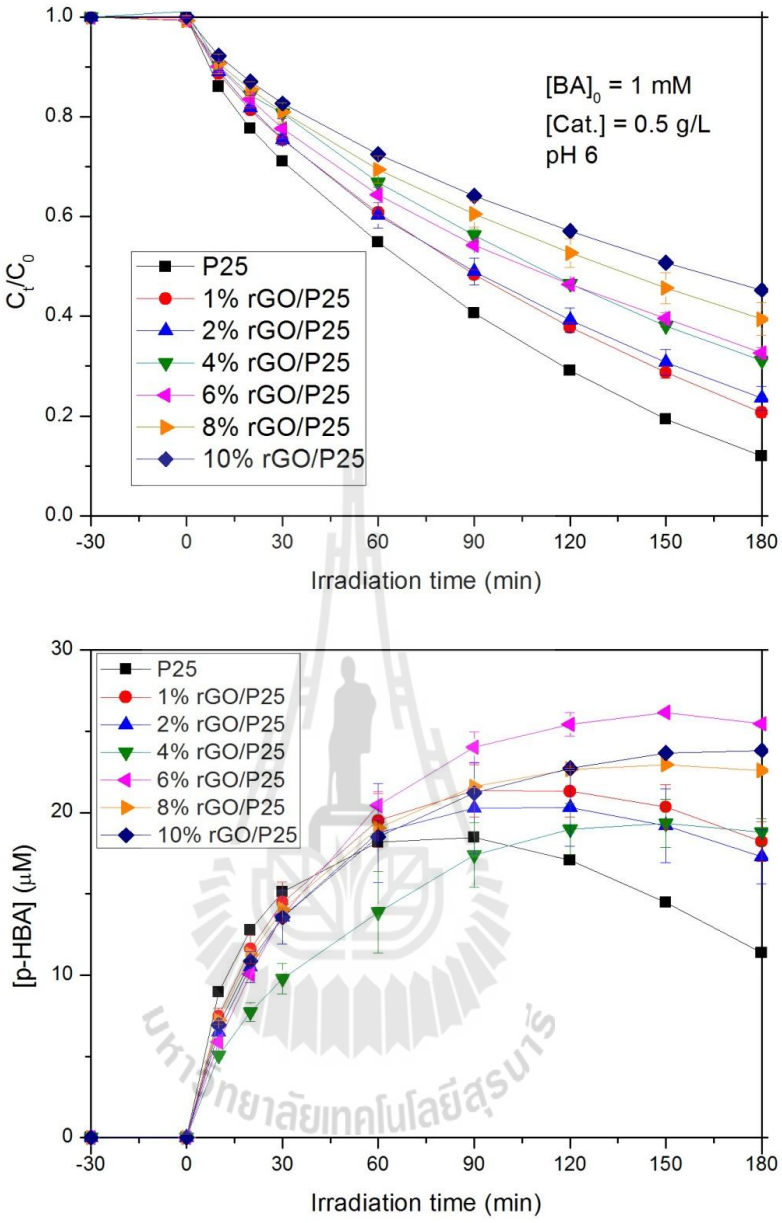

Figure B 8 Photocatalytic degradation of low concentration BA (top) and generation of intermediate p-HBA (bottom) at pH 6.

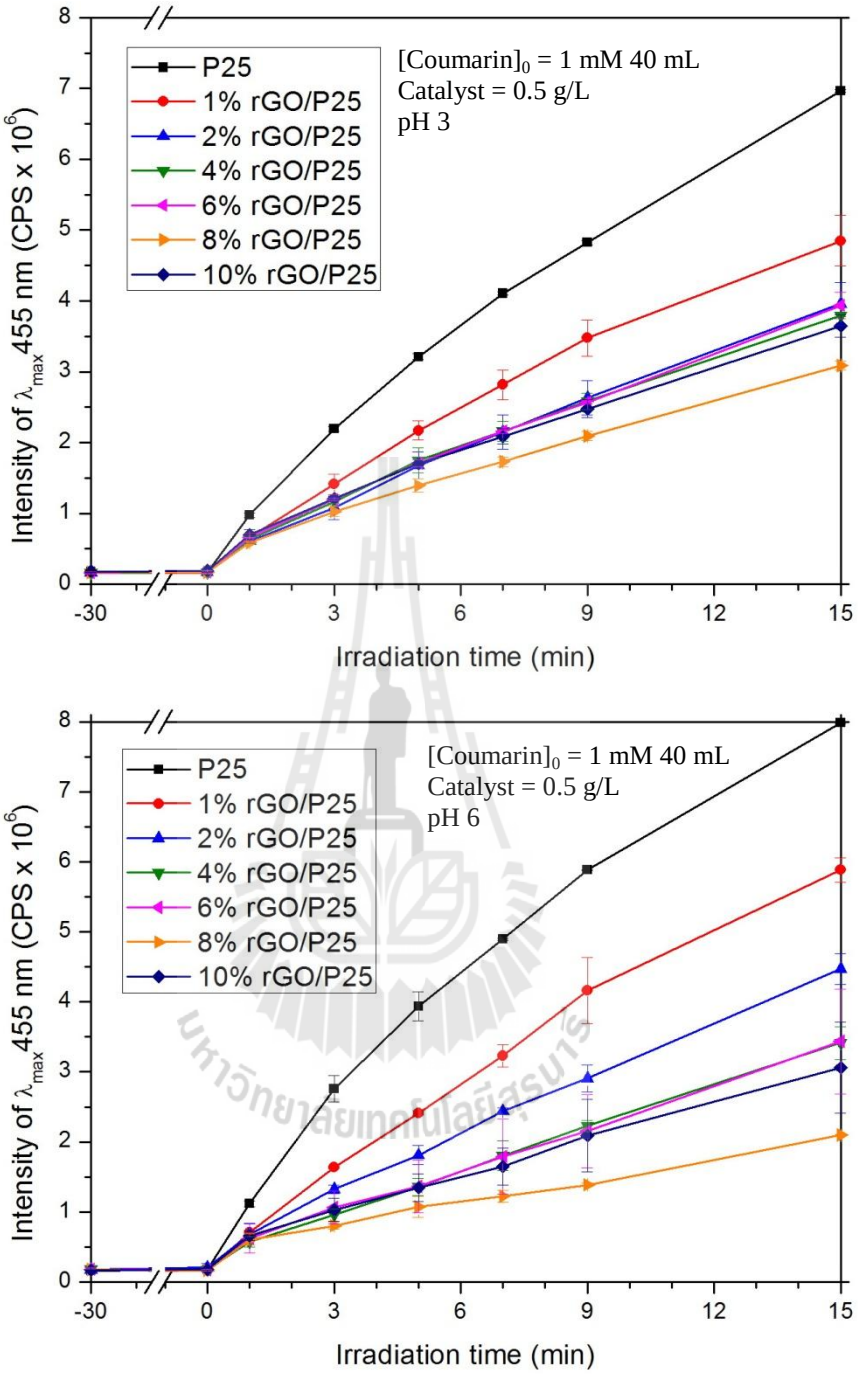

Figure B 9 Photocatalytic degradation of coumarin at pH 3 (top) and pH 6 (bottom).

B 3 Reference

Kim, J., and Choi, W. (2011). TiO_2 modified with both phosphate and platinum and its photocatalytic activities. **Applied Catalysis B: Environmental**. 106: 39-45.

CURRICULUM VITAE

Ms. WINA RONGCHAPO

Education

2008	B.Sc. (1st Class Honors) (Environmental Health), Suranaree University of Technology (SUT), Thailand
2009-2015	Ph.D. candidate (Chemistry), SUT

Research exchange experience

2012	Department of Chemical Engineering at Thammasat University, Thailand (5 months)
2014-2015	School of Environmental and Science at Pohang University of Science and Technology, South Korea (11 months)
2015	Faculty of Chemistry and Pharmacy at Sofia University "St. Kliment Ohridski", Bulgaria (2 months)

International Publications

Rongchapo, W., Sophiphun, O., Rintramee, K., Prayoonpokarach, S., and Wittayakun, J. (2013). Paraquat adsorption on porous materials synthesized from rice husk silica. Water Science and Technology, 68, 863-869. (Impact factor (2014): 1.106)

Rongchapo, W., Deekamwong, K., Loiha, S., Prayoonpokarach, S., and Wittayakun, J. (2015). Paraquat adsorption on NaX and Al-MCM-41. Water Science and Technology, 71, 1347-1353. (Impact factor (2014): 1.106)